NASA CONTRACTOR REPORT

NASA CR-2329

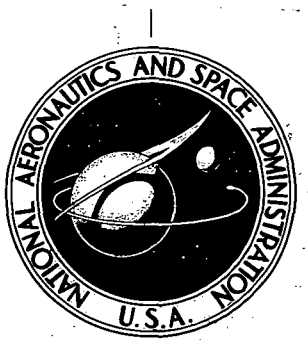

NASA CR-2329

A THEORY OF MICROWAVE APPARENT TEMPERATURE OVER THE OCEAN

by S. T. Wu and A. K. Fung

Prepared by
THE UNIVERSITY OF KANSAS CENTER FOR RESEARCH, INC.
Lawrence, Kans. 66044
for Langley Research Center

NATIONAL AERONAUTICS AND SPACE ADMINISTRATION • WASHINGTON, D. C. • NOVEMBER 1973

1. Report No.	2. Government Accession No.	3. Recipient's Catalog No.
NASA CR-2329		

4. Title and Subtitle	5. Report Date
A Theory of Microwave Apparent Temperature Over the Ocean	November 1973
	6. Performing Organization Code

7. Author(s)	8. Performing Organization Report No.
S. T. Wu and A. K. Fung	Technical Report 186-7

9. Performing Organization Name and Address	10. Work Unit No.
University of Kansas Center for Research, Inc. 2291 Irving Hill Road - Campus West Lawrence, Kansas 66044	11. Contract or Grant No. NAS 1-10048
	13. Type of Report and Period Covered Contractor Report
12. Sponsoring Agency Name and Address National Aeronautics and Space Administration Washington, D.C. 20546	14. Sponsoring Agency Code

15. Supplementary Notes

This is a topical report.

16. Abstract

In the microwave region combined active (scatterometer) and passive (radiometer) remote sensors over the ocean show promise of providing surface wind speeds and weather information to the oceanographer and meteorologist. This has aroused great interest in the investigation of the scattering of waves from the sea surface. Several approaches to the problem are now available, but none satisfactorily predict both the scattering and emission characteristics of the sea surface. The disagreement may be accounted for at least in part by the use of an improper surface model. A composite surface scattering theory is investigated as a more realistic approach.

The two-scale scattering theory proposed by Semyonov has been specifically extended to compute the emission and scattering characteristics of ocean surfaces. The effect of the small irregularities upon the scattering characteristics of the large undulations is included by modifying the Fresnel reflection coefficients; the effect of the large undulations upon those of the small irregularities is accounted for by averaging the scattering cross sections of the small irregularities over the surface normals of the large undulations. The wind dependent parameters of the theory are established by comparing the emission characteristic with measurement and by using measured sea slope data. Improved agreement with measured scattering and emission results over a single-surface theory is demonstrated by the composite theory.

The effects of clouds and rain on the radiometer and scatterometer observations are also investigated using horizontally stratified model atmospheres with rough sea surfaces underneath. Various cloud and rain model proposed by meteorologist have been employed to determine the rise in the microwave temperature when viewing downward through these model atmospheres. For heavy rain-fall rates the effects of scattering on the radiative transfer process are included. It is found that clouds and rains cause the radiometer to lose contact with the surface when clouds or rain intervene. However, the rise of apparent temperature can be used to compute the atmospheric attenuation and the scatterometer measurement corrected accordingly.

17. Key Words (Selected by Author(s))	18. Distribution Statement
Microwave Emission Theory Ocean Surface Atmospheric Effects Remote Sensing	Unclassified - Unlimited

19. Security Classif. (of this report)	20. Security Classif. (of this page)	21. No. of Pages	22. Price*
Unclassified	Unclassified	150	Domestic, $4.50 Foreign, $7.00

*For sale by the National Technical Information Service, Springfield, Virginia 22151

TABLE OF CONTENTS

TABLE OF CONTENTS (CONTINUED)

LIST OF FIGURES

LIST OF FIGURES (CONTINUED)

CHAPTER 1

INTRODUCTION

The microwave apparent temperature over the ocean measured by a radiometer includes contributions from (a) the surface, (b) the intervening atmosphere between the surface and the radiometer, and (c) radiation from the atmosphere above the surface and any signal source that might be present, which upon reflection by the surface falls within the beam of the radiometer antennas. If the atmosphere consists of scattering particles such as the precipitating raindrops with size comparable to radiation wavelength, this will further complicate the problem. A complete understanding of the microwave apparent temperature from the ocean, therefore, requires to know the sea surface characteristics and the atmospheric conditions that account for the total apparent temperature.

The apparent temperature contribution from the sea surface, or the microwave brightness temperature of the sea surface as usually called, depends on the surface temperature and the surface emissivity. The surface emissivity, in general, is related to the surface roughness and the percentage sea foam coverage. The sea foam coverage especially at high wind speed, say 20 m/s, should be properly treated. The investigations of sea foam that affects the surface emissivity can be found elsewhere (Doppleman, 1970; Hollinger, 1971b; Stogryn, 1971, Porter, 1971).

It is our purpose here to pursue only the surface emissivity that relates to surface roughness effect and assume that the sea foam effect is negligible or can be properly accounted for when situation requires. With this perspective, the surface emissivity depends on the differential scattering coefficient of the sea in an integral form defined by Peake (1959). Thus, an assumed scattering model for the rough sea also serves as a model for the surface brightness temperature. A satisfactory sea model will, therefore, be capable of predicting both the scattering and the emission characteristics of the sea surface. This being the case, the roughness parameters of the surface which appear in the model may be studies by examining either the backscattering coefficient measured by a scatterometer (Bradley, 1971) or the microwave apparent temperature measured by a radiometer (Hollinger, 1971a, 1971b) or by both (Claassen, et al., 1971). In the case of apparent temperature

measurement in addition to sea foam effect the atmospheric contribution above the sea surface should also be considered. Since atmospheric contribution under clear sky or even cloudy sky conditions at low frequencies, say below 15 GHz, is relatively small and constant and sea foam effect can also be properly accounted for (Hollinger, 1971b, Stogryn, 1971), both scatterometer and radiometer can be employed to detect sea surface roughness. The sea surface roughness in general depends on the wind blowing over the ocean. Thus scatterometer or radiometer data can be inferred to wind speed over the ocean.

Several investigators have reported radiometric observations over wind driven seas. Hollinger of NRL (1970, 1971a) has conducted radiometric measurements at three microwave frequencies, 1.41, 8.36, and 19.34 GHz, from a tower located in 60 meters of sea. His measurements for horizontally polarized emissions show (1) a linear rising trend with wind speed, over all incident angle (2) an increasing sensitivity to wind speed with frequency, and (3) a small increasing sensitivity to wind speed with incident angle. Vertically polarized emission exhibited little sensitivity to wind speed except at 19.34 GHz, and large incident angles where a declining trend was observed. In processing his data Hollinger removed the effects of foam from the apparent temperature. Atmospheric contributions were also removed from the measurements, so only surface geometry affected the measurements since the surface water temperature was nearly constant. Nordberg et al., (1968, 1969, 1971) have also reported the dependence of brightness temperature on wind speed at 19.34 GHz. Their observations were conducted from an aircraft over the North Sea and the North Atlantic Sea. They report selected data which indicated that the brightness temperature at nadir increases with wind speed from 7 m/s to 25 m/s at a rate of about 1.2° K/m/s.

On the other hand, past theoretical investigations of the microwave brightness temperature from the sea surface either assumed a single surface model for computing the differential scattering coefficient excluding shadowing and multiple scattering (Stogryn, 1967; Fung and Ulaby, 1970) or including these effects but employed one-dimensional model (Lynch and Wagner, 1970) or employed a facet reflection model (Sirounian, 1967; Shifrin, 1969). All these investigations except Fung and Ulaby's physical optics model failed to predict the observed wind dependence at nadir reported by the above measured apparent temperature data. Though the physical optics model proposed by Fung and Ulaby (1970) predicted good

agreement with experimental results, the parameter in this theory appears as a product of the surface parameters which cannot be easily isolated and related to wind speed. For practical applications it is necessary to calibrate this parameter versus wind speed experimentally.

In view of the above deficiency and a closer description of the sea surface consists of small ripples, namely capillary waves, riding on large gravity waves (Pierson et al., 1971), it appears reasonable to consider a two scale model (small irregularities superimposed upon large undulations) for examining the emission and scattering characteristics of the sea. It has already been noted that such a two-scale model allowed closer description of the backscattering cross section of the sea as a function of the incident angle. Its wind dependence remains to be investigated. It is the subject matter of this study to further generalize the two-scale model for predicting both the surface brightness temperature and the backscattering cross section as a function of both wind speed and look angle.

In the following chapter we shall discuss certain aspects of the sea that have significant effects on the differential scattering coefficient. In particular, we shall consider the surface geometry and the electrical properties of sea water. The electrical properties in turn are related to salinity, sea water temperature by the complex relative dielectric constant.

In Chapter 3, a detailed development of two-scale non-coherent scattering theory extended from Semyonov's paper (1966) for computing the differential scattering coefficient is given. Under the non-coherent assumption the differential scattering coefficient can be shown to consist of a sum of two terms: the first term represents the main contribution by the large undulations; and the second term the main contribution by the small irregularities. The theory assumed Gaussian surface height distributions and Gaussian correlation functions for both scales of roughness. The differential scattering coefficient is shown to be dependent on the rms slope of the large undulations, the standard deviation of the small irregularities and the correlation distance of the small irregularities. The wind dependence for the rms slope of the large undulations is treated in accordance with Cox and Munk's measured data. The standard deviation of the small irregularities is correlated to the wind grow capillary wave spectra proposed by Pierson et al. Good agreement with measured characteristics and better agreement than the single surface model are demonstrated.

In Chapter 4, the effect of clouds and rain on the microwave apparent temperature over the ocean is presented. Various cloud and rain models investigated by meteorologist have been employed to determine the rise in the microwave apparent temperature when viewing downward through these model atmospheres. A horizontally uniform stratified model atmospheres is assumed for both cases with or without the scattering term in the solution of radiative transfer equation. The attenuation, absorption and scattering coefficients are computed by using Mie theory for some representative precipitation rate. With the scattering term included the finite difference method proposed by Germogenova (1962) is employed for solving the radiative transfer problem. Comparisons of the computed apparent temperature are also made between the two cases with or without the term when the sky condition is assumed to be under heavy rain. It is found that the apparent temperature contribution by the scattering effect is significant. Hence, for heavy rain case, the apparent temperature computation should include the scattering term. Emphasis has also been placed in correlating the temperature increase resulting from clouds and rain with atmospheric attenuation. Details are given in Section 4.4.

CHAPTER 2

CERTAIN ASPECTS OF THE SEA

2.1 INTRODUCTION

A naturally occuring ocean surface is characterized primarily by the salinity, the temperature of the sea water, the surface roughness, the foam coverage, the white caps, and the sprays. The salinity and temperature of sea water specify its dielectric properties at microwave frequencies in the range 1 to 300 GHz. At frequencies below microwaves, say 100 MHz, sea water is a good conductor with very high conductivity due to its dissociated salts (Neumann and Pierson, 1966). On the other hand the surface roughness, the foam coverage, the white caps, and the sprays are developed, in general, by winds blowing over ocean surface. Since dielectric properties of sea water and sea surface geometry are responsible for the surface emissivity and backscattering cross-section of the sea, it is appropriate to have a brief discussion of the dielectric properties and wind roughened surface characteristics of sea water.

2.2 SALINITY, SURFACE TEMPERATURE, AND DIELECTRIC CONSTANTS OF SEA WATER

The sea water is such a complex solution of salts that it is impossible by direct chemical analysis to determine its total content of dissolved solids. The salinity of the sea water has, therefore, been defined as "the total amount of solid material in grams contained in one kilogram of sea water when all the carbonate has been converted to oxide the bromine and iodine replaced by chlorine, and all organic matter completely oxidized." Since the relative amounts of all the major constituents are virtually constants in the different parts of the oceans, the salinity of a water sample can be computed by determining the amount of only one

of the major components. Chlorine is present in relatively large quantities and can be determined easily and accurately; for this reason the determination of the chlorinity of the sea water has been standardized. The empirical relation between salinity and chlorinity is (Neumann and Pierson, 1966)

$$\text{Salinity} = 0.03 + 1.805 \times \text{chlorinity}. \qquad (2.1)$$

Both salinity and chlorinity are expressed in parts per thousand, or "per mille", for which the symbol "o/oo" is used. Table 2.1 gives the major constituents of sea water (McLelland, 1965).

Table 2.1

PRINCIPAL IONIC CONSTITUENTS OF SEA WATER (34.4 o/oo SALINITY)

Species	Amount (g) per Kg of Solution	Molecular or Atomic Weight	Percentage of Total Salt
cations			
Sodium	10.47	22.997	30.4
Magnesium	1.28	24.32	3.7
Calcium	0.41	40.08	1.2
Potassium	0.38	39.096	0.05
Strontium	0.013	87.63	
Anions			
Chloride	18.97	25.459	55.2
Sulfate	2.65	32.06	7.7
Bromide	0.065	79.916	0.2
Bicarbonate	0.14		0.4
Borste	0.027	10.82	0.08

From Table 2.1 it can be seen that sodium chloride (NaCl) is the major contributor. The specific gravity of a normal solution of NaCl is unity; thus, there are 58.45 grams of sodium chloride in 1,000 grams of solution. With this as a basis, the salinity, S, may be expressed in terms of normality, N, as (Porter and Wentz III, 1971)

$$S = 58.45N \text{ o/oo} \qquad (2.2)$$

Table 2.2 lists surface salinities during the Northern Hemisphere Summer (Sverdrup, et al., 1942).

Sverdrup, et al., (1942) also furnishes data on the average monthly ocean surface temperatures. Table 2.3 lists this information for the months of February and August.

Table 2.2

SURFACE SALINITIES DURING NORTHERN HEMISPHERE SUMMER

Ocean Region	Salinity (o/oo)	
	Minimum	Maximum
North Atlantic	34.0	37.0
South Atlantic	34.0	37.0
Caribbean	35.0	36.5
North Pacific	32.0	35.5
South Pacific	34.0	36.5
Indian Ocean (to Southern Australia)	34.0	36.5

Table 2.3

SMOOTHED AVERAGE MONTHLY OCEAN SURFACE TEMPERATURES

Ocean Region	Temperature (°C)	
	February	August
North Atlantic	-1 to 27	0 to 29
South Atlantic	-1 to 27	-1 to 25
Caribbean	26 to 26	26 to 29
North Pacific	-1 to 27	0 to 28
South Pacific	-1 to 28	-1 to 28
Indian Ocean (to Southern Australia)	20 to 28	15 to 18

On the air-sea boundary three different conditions exist: the stable condition when air is warmer than the sea surface water temperature, the unstable condition when the air is colder and the neutral condition when air and sea temperatures are the same. There are different wind roughned sea surface characteristics under stable, neutral and unstable conditions (Cardone, 1969, Figure 2.4).

Many investigators (Lane and Saxton, 1952, Hasted, et al., 1948, 1958, Grant, et al., 1957) have made measurements of the dielectric properties of ionic solutions of water at various normalities, temperatures and electromagnetic wavelengths. They employed Debye's (1942) formula for comparing theories with measurement. The data of Grant (1957) and Hasted (1958) seemed to indicate that the Debye expressions for the dielectric constant was in slight error. The data could only be explained by a slight spread of relaxation time, as proposed by Cole (1941).

Porter (1971) investigated various parameters that influence the correct expression of Debye formula by summarizing all previous results. Following Porter's result the complex relative dielectric constant, ϵ_r, is expressed in the form

$$\epsilon_r = \epsilon' - j\epsilon'' \tag{2.3}$$

$$\epsilon' = 4.8 + \frac{(\epsilon_s - 4.8)\left[1 + (\lambda_s/\lambda)^{0.98}(\pi \times 10^{-2})\right]}{1 + 2(\lambda_s/\lambda)^{0.98}(\pi \times 10^{-2}) + (\lambda_s/\lambda)^{1.96}} \tag{2.3a}$$

$$\epsilon'' = \frac{(\epsilon_s - 4.8)(\lambda_s/\lambda)^{0.98}}{1 + 2(\lambda_s/\lambda)^{0.98}(\pi \times 10^{-2}) + (\lambda_s/\lambda)^{1.96}} + \frac{18\sigma}{f} \tag{2.3b}$$

Where

$\epsilon_s = 87.8 - 15.3\,N - 0.363\,T \pm \delta_{\epsilon_s}$

$\lambda_s = 3.38 - 0.11T + 0.00147\,T^2 + 0.0173\,TN - 0.52\,N \pm \delta_{\lambda_s}$ cm

$\sigma = 5N + 0.12\,TN + 0.04\,T \pm \delta_\sigma$ mho/meter

λ = wavelength in cm same as λ_s

f = frequency in GHz

N = normality

T= temperature in ^{o}C

δ_{ϵ_s} = 0.1 is the average deviation for corresponding experimental values

δ_{λ_s} = 0.025

δ_{σ} = 0.004

Table 2.4 shows a set of computed dielectric constants at two frequencies, four temperatures and three salinities.

Table 2.4

COMPLEX RELATIVE DIELECTRIC CONSTANTS OF SEA WATER

Fr \ T °K / S		284		288		292		296	
		ϵ'	ϵ''	ϵ'	ϵ''	ϵ'	ϵ''	ϵ'	ϵ''
GHz	33‰	52.75	39.47	55.06	38.16	56.66	36.85	57.53	35.72
9.3	35	52.54	39.60	54.80	38.33	56.34	37.06	57.17	35.99
	37	52.33	39.72	54.53	38.49	56.02	37.28	56.80	36.27
	33	39.93	39.30	43.18	38.93	45.83	38.21	47.70	37.35
13.9	35	39.84	39.33	43.04	38.97	45.62	38.26	47.43	37.43
	35	39.75	39.35	42.89	39.00	45.42	38.31	47.17	37.51

From Table 2.4 it is seen that the change of sea water temperature affects the dielectric constant, while the effect of the change of salinity upon the dielectric constant is insignificant at the above frequency range.

Figure 2.1 illustrates the graphs of the real and the imaginary part of the dielectric constant with respect to varying frequencies ranging from 1 to 20 GHz at 35 o/oo salinity and temperature at 292°K.

Figure 2.2 illustrates the graphs of the real and the imaginary part of the dielectric constant with respect to varying temperature ranging from 276 to 296°K at 35 o/oo salinity and frequencies at 9.3, 13.9 and 19.34 GHz respectively.

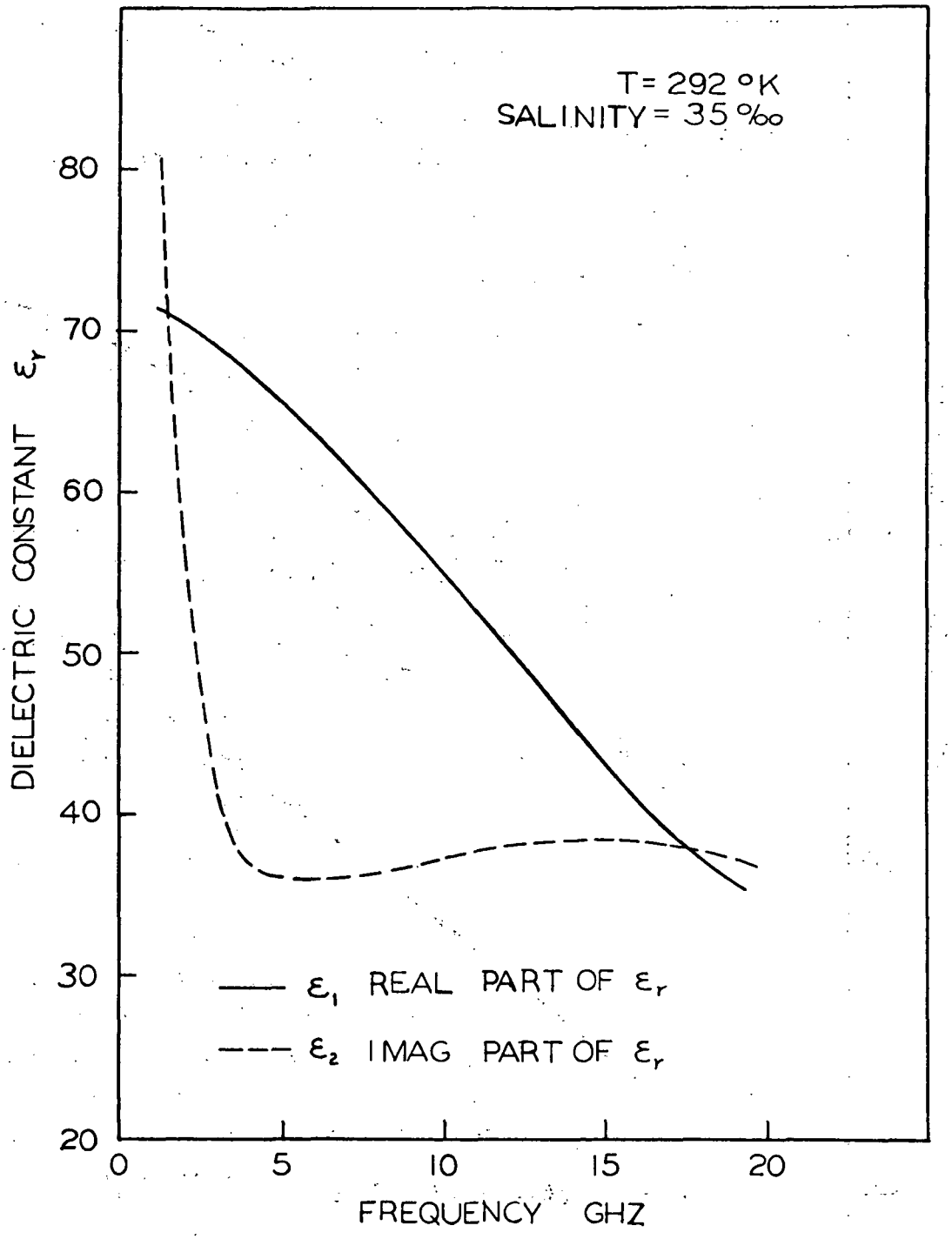

FIG. 2.1 The Dielectric Constant of Sea Water

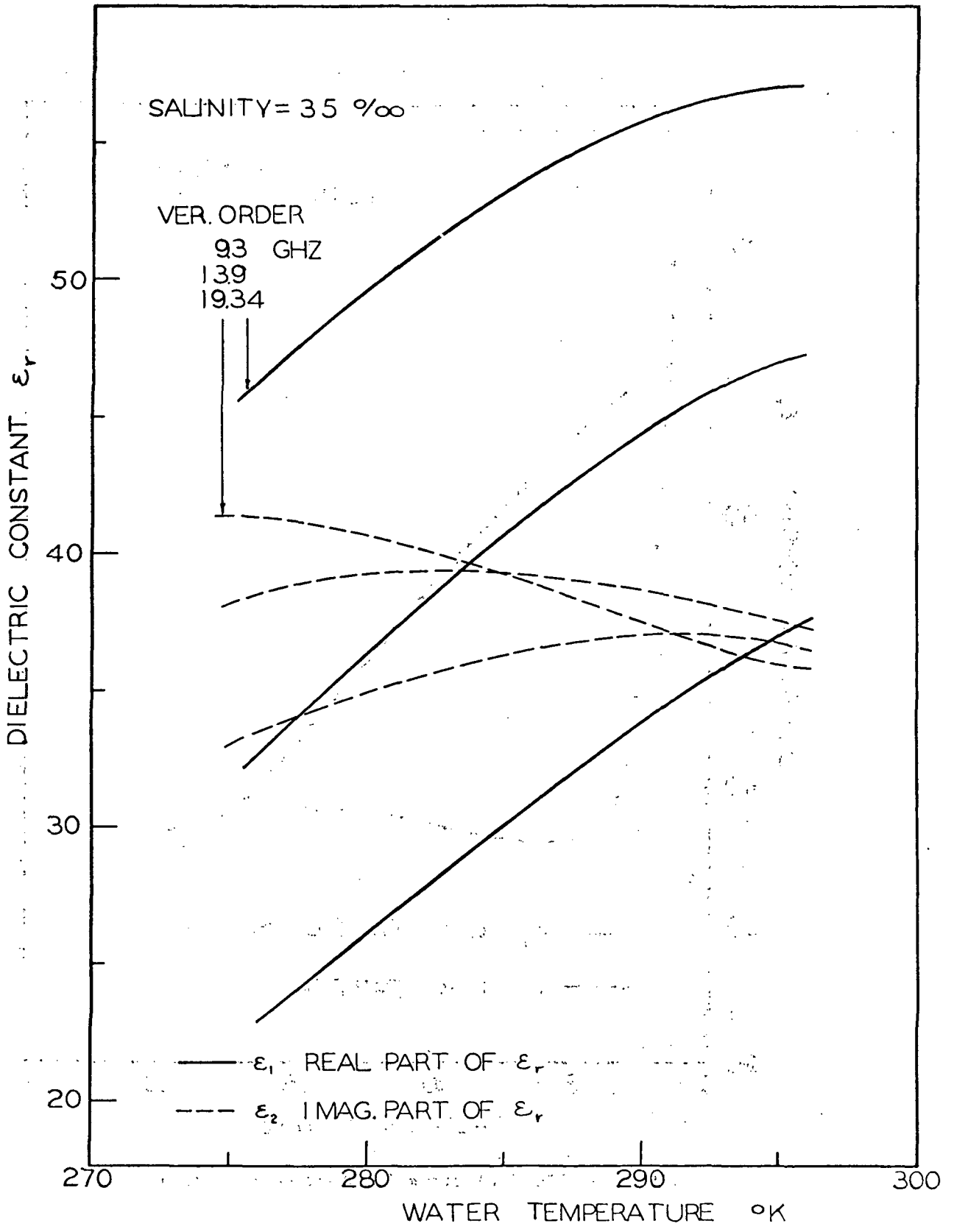

FIG. 2.2 The Dielectric Constant of Sea Water

2.3 WIND ROUGHENED SEA SURFACE CHARACTERISTICS

If the ocean were filled with a completely motionless homogeneous water, the idea sea surface with a boundary adjacent to the atmosphere would be a level surface geologically and a plane conducting surface electrically. The sea surface is, however, not of such a simple ideal nature. It varies all the time due to the changes of the forces of external and internal pressure and mainly of the wind friction stress at the sea surface.

Any given wind structure is, of course, not uniform over an unlimited region of the sea. The length of the path over which a substantially constant wind blows is known as the "fetch". At any given fetch the wave amplitude increases with the length of time that the wind has been blowing. After a certain time a steady state is reached at which the wave height remains constant. It is called the "fully developed" sea. The time that it takes to reach this state of equilibrium, known as the "minimum duration", increases with the length of the fetch and the wind speed. If the wind blows for a time shorter than the minimum duration, the wave height does not depend upon the fetch but only upon the time and wind velocity.

In the case of a fully developed sea there is a unique relationship between wind and sea state. Table 2.5, which is an abstract from a compilation due to Wilbur Mark of the David Taylor Model Basin, shows some useful relationships. Note the wind speed is given in knots in the table (1 knot = 0.5148 m/sec.).

Waves of the actual ocean are very complex phenomena. A detailed description of waves characteristics of ocean can be found elsewhere (Pierson, 1966, Pierson, et al, 1971). Since sea surface characteristics responsible for surface emission and backscattering cross-section from the large structures can be described in good agreement with experiment by using the slope distribution of the sea surface measured by Cox and Munk (1952), the wave spectrum analysis of the large structure gravity wave is not considered. On the other hand, the description of capillary waves, which is also responsible for both surface emission and backscattering characteristics, will follow the wind grow wave numbers spectrum proposed by Pierson (1971)

Table 2.5

WIND AND SEA SCALE FOR A FULLY DEVELOPED SEA

Sea—General		Wind				Sea*				
Sea State	Description	Wind Force (Beaufort)	Description	Range (knots)	Wind Velocity (knots)	Wave Height (Feet) Average	Wave Height (Feet) Significant	Wave Height (Feet) Avg 1/10 Highest	Minimum Fetch (nmi)	Minimum Duration (hours)
0	Sea like a mirror	0	Calm	<1	0	0	0	0	...	...
	Ripples with the appearance of scales are formed; but without foam crests	1	Light Air	1–3	2	0.05	0.08	0.10	5	18 min
1	Small wavelets, still short but more pronounced; crests have a glassy appearance, but do not break	2	Light Breeze	4–6	5	0.18	0.29	0.37	8	39 min
	Large wavelets, crests begin to break. Foam of glassy appearance. Perhaps scattered white horses.	3	Gentle Breeze	7–10	8.5	0.6	1.0	1.2	9.8	1.7 hrs
2					10	0.88	1.4	1.8	10	2.4
	Small waves, becoming larger; fairly frequent white horses	4	Moderate Breeze	11–16	12	1.4	2.2	2.8	18	3.8
					13.5	1.8	2.9	3.7	24	4.8
3					14	2.0	3.3	4.2	28	5.2
					16	2.9	4.6	5.8	40	6.6
4	Moderate waves, taking a more pronounced long form; many white horses are formed. (Chance of some spray.)	5	Fresh Breeze	17–21	18	3.8	6.1	7.8	55	8.3
					19	4.3	6.9	8.7	65	9.2
					20	5.0	8.0	10	75	10
5	Large waves begin to form; the white foam crests are more extensive everywhere (probably some spray).	6	Strong Breeze	22–27	22	6.4	10	13	100	12
					24	7.9	12	16	130	14
					24.5	8.2	13	17	140	15
6					26	9.6	15	20	180	17
	Sea heaps up and white foam from breaking waves begins to be blown in streaks along the direction of the wind. (Spindrift begins to be seen	7	Moderate Gale	28–33	28	11	18	23	230	20
					30	14	22	28	280	23
					30.5	14	23	29	290	24
7					32	16	26	33	340	27
	Moderately high waves of greater length; edges of crests break into spindrift. The foam is blown in well marked streaks along the direction of the the wind. Spray affects visibility.	8	Fresh Gale	34–40	34	19	30	38	420	30
					36	21	35	44	500	34
					37	23	37	46.7	530	37
					38	25	40	50	600	38
					40	28	45	58	710	42

2.3.1 Slope Distribution Statistics of Sea Surface

Cox and Munk (1954a) had made surface slope measurement by optical reflection method on the Hawaiian sea at wind speeds up to 14 m/sec. Due to the method of measurement, the small scale capillary waves, white caps and sprays were ignored in their analysis. To account for such a small scale roughness riding on the large undulating surface a different approach is made and it is presented in the next section.

These authors found the slope distribution of the sea surface to be nearly Gaussian with small corrections expressed by a few terms in a Gram-Charlier series which represents skewness and peakedness. The principal axes, x and y, were found to lie cross wind and parallel to the wind respectively. Cox and Munk expressed the slope distribution function in the form.

$$P(z_x, z_y) = (2\pi \sigma_x \sigma_y)^{-1} \exp\left(-\tfrac{1}{2}(\xi^2+\eta^2)\right) \times \left\{1 - \tfrac{1}{2} C_{21}(\xi^2-1)\eta - \tfrac{1}{6} C_{03}(\eta^3-3\eta) + \tfrac{1}{24} C_{40}(\xi^4-6\xi^2+3) + \tfrac{1}{4} C_{22}(\xi^2-1)(\eta^2-1) + \tfrac{1}{24} C_{04}(\eta^4-6\eta^2+3)\right\} \quad (2.4)$$

Where $\xi = z_x/z_y$ and $\eta = z_y/\sigma_y$, $z_x = \frac{\partial z}{\partial x}$, $z_y = \frac{\partial z}{\partial y}$. The mean square slopes $\sigma_x^2 + \sigma_y^2$ regardless of direction were found to depend linearly on the wind speed (measured at a height of 41 feet above sea level with stable sea condition). The regression lines and correlation coefficient **r** have been computed by the method of least squares:

Clean surface

$$\sigma_x^2 = 0.003 + 1.92 \times 10^{-3} W \pm 0.002 \qquad r = 0.956$$

$$\sigma_y^2 = 0.000 + 3.16 \times 10^{-3} W \pm 0.004 \qquad r = 0.945 \quad (2.5)$$

$$\sigma_x^2 + \sigma_y^2 = 0.003 + 5.12 \times 10^{-3} W \pm 0.004 \qquad r = 0.986$$

Slick surface

$$\sigma_x^2 = 0.003 + 0.84 \times 10^{-3} W \pm 0.002 \qquad r = 0.78$$
$$\sigma_y^2 = 0.005 + 0.78 \times 10^{-3} W \pm 0.002 \qquad r = 0.7 \qquad (2.6)$$
$$\sigma_x^2 + \sigma_y^2 = 0.008 + 1.56 \times 10^{-3} W \pm 0.004 \qquad r = 0.77$$

Where W is the wind speed in meter per second. The indicated error refers to the standard deviation of observed values from the regression lines. Actual values of the ratio σ_x^2/σ_y^2 were found to vary from 1.0 to 1.8 with a mean value of 1.34. These variations are due to fluctuations in the wind direction. Values of this ratio close to 1 are expected for gusty winds while steady winds lead to higher values.

The regression lines for the skewness coefficients C_{21} and C_{03} are given by

$$C_{21} = 0.01 - 0.0086\ W \pm 0.03$$
$$C_{03} = 0.04 - 0.0033\ W \pm 0.12 \qquad (2.7)$$

A large scatter in the data is evident from the indicated standard deviations.

The peakedness coefficients were found to have the values

$$C_{40} = 0.40 \pm 0.23$$
$$C_{22} = 0.12 \pm 0.06 \qquad (2.8)$$
$$C_{04} = 0.23 \pm 0.41$$

independent of the wind speed. Cox and Munk state that the measured peakedness is barely above the limit of experimental error. The observed values may be due to either a variability in wind speed or to systematic errors in their experiment.

This data shows that deviations from a Gaussian distribution are not large. Therefore, the sea surface will be assumed to be Gaussian. Because of this assumption, only the mean square slope $\sigma_o^2 = \sigma_x^2 + \sigma_y^2$ given in Equation (2.5) or (2.6) is needed in the application that follow this chapter.

2.3.2 Empirical Wave Spectrum of Capillary Waves on the Ocean

The Capillary waves are presumably caused by very local eddies in the wind. They are comparable in size to the radar wavelength. Recent investigation in radar return and microwave emission from the ocean surface confirm that these ripples are responsible for both backscattering and emission from the sea.

Oceanographers have been interested in the longer wavelength parts of the spectrum, for these are the ones that represent sizable energy transfer, and affect ships. Published spectra for the sea almost always are based strictly on the gravity wave region. Only recently interest has been generated about the capillary waves since their growth has been found to be related to the wind speed.

Measurements of capillary waves on the open sea are extremely difficult since they are riding on swells many orders of magnitude larger. Consequently our knowledge of capillary waves is based on both theory and measurements in a wind tunnel. Recent work by Pierson et. al. (1971) has combined the data from several investigators so that the variation in the capillary spectrum with wind speed can be determined. The empirical wave spectrum of capillary waves, following Pierson's (1971) proposed model, may be written in the form

$$S(K) = \frac{4.05 \times 10^{-3} D}{K^4} \tag{2.9}$$

Where K is the wave number of capillary waves, D is the wind dependent constant. The wind dependency of D is carried by the friction velocity, U_* defined by (wind stress/water density)$^{1/2}$, in the form

$$D(U_*) = \left[1.247 + 0.0268\, U_* + 6.03 \times 10^{-5} U_*^2\right]^2 \tag{2.10}$$

when U_* is larger than 12 cm/sec.

The results of comparing wind-wave tank data by Toba (1970), Sutherland (1967) and Pierson et. al. (1971) are shown in Figure 2.3. The equation shown there is a best fit to the observations and indicates an increasing rate of spectral growth with increasing friction velocity. Scales are shown both the U_* and $U_{19.5}$, the wind speed measured at anemometer height of 19.5 m for a neutrally stratified atmosphere. For friction velocity below 12 cm/sec. the capillary waves die away extremely rapidly and is of no importance for both radar return and surface emissivity.

The relation between the wind velocity measured at z m above the mean sea surface and the friction velocity at the sea surface is expressed in the form (Pierson 1971)

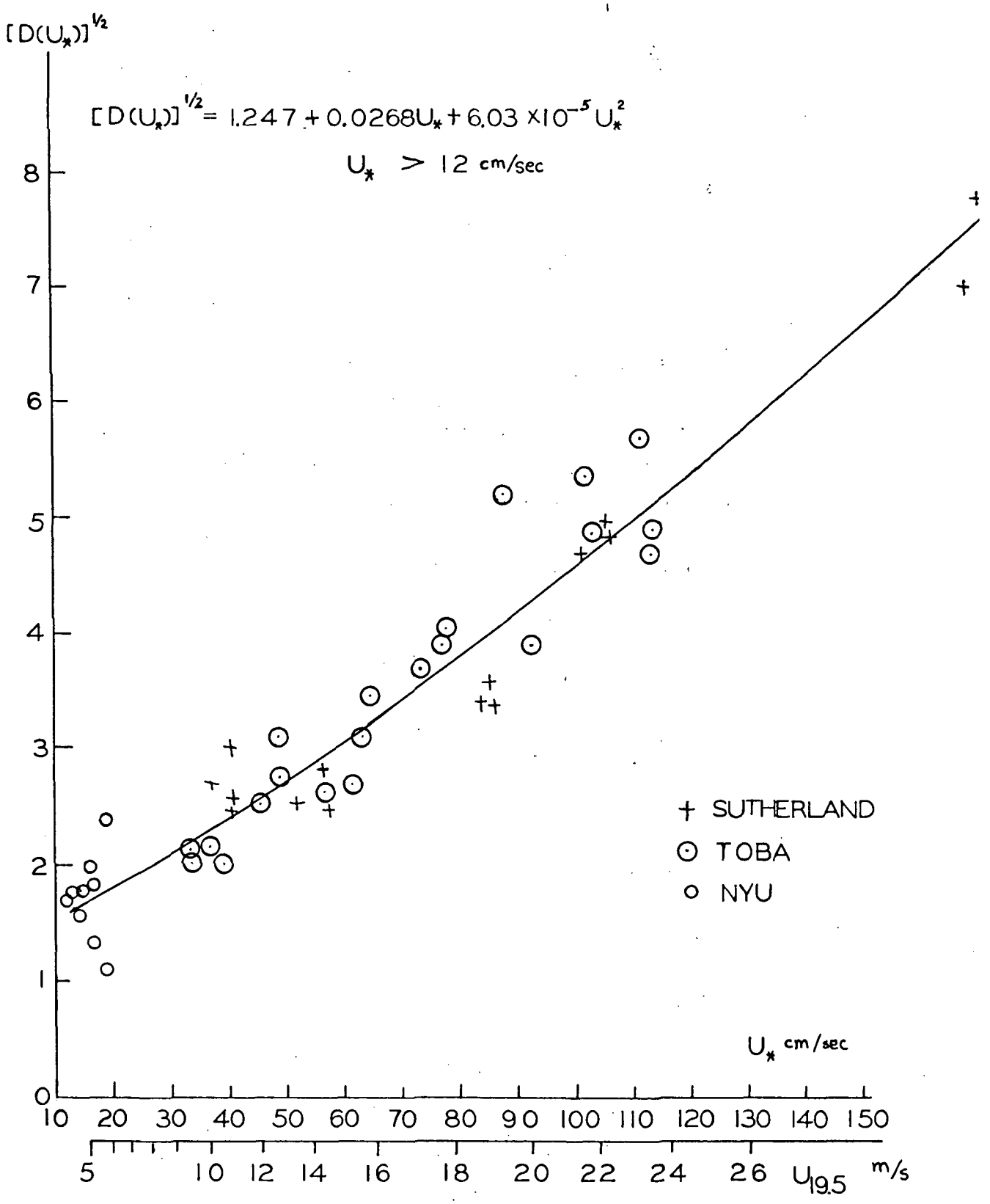

FIG. 2.3 The Wind Dependent Constant,D, of Capillary Waves

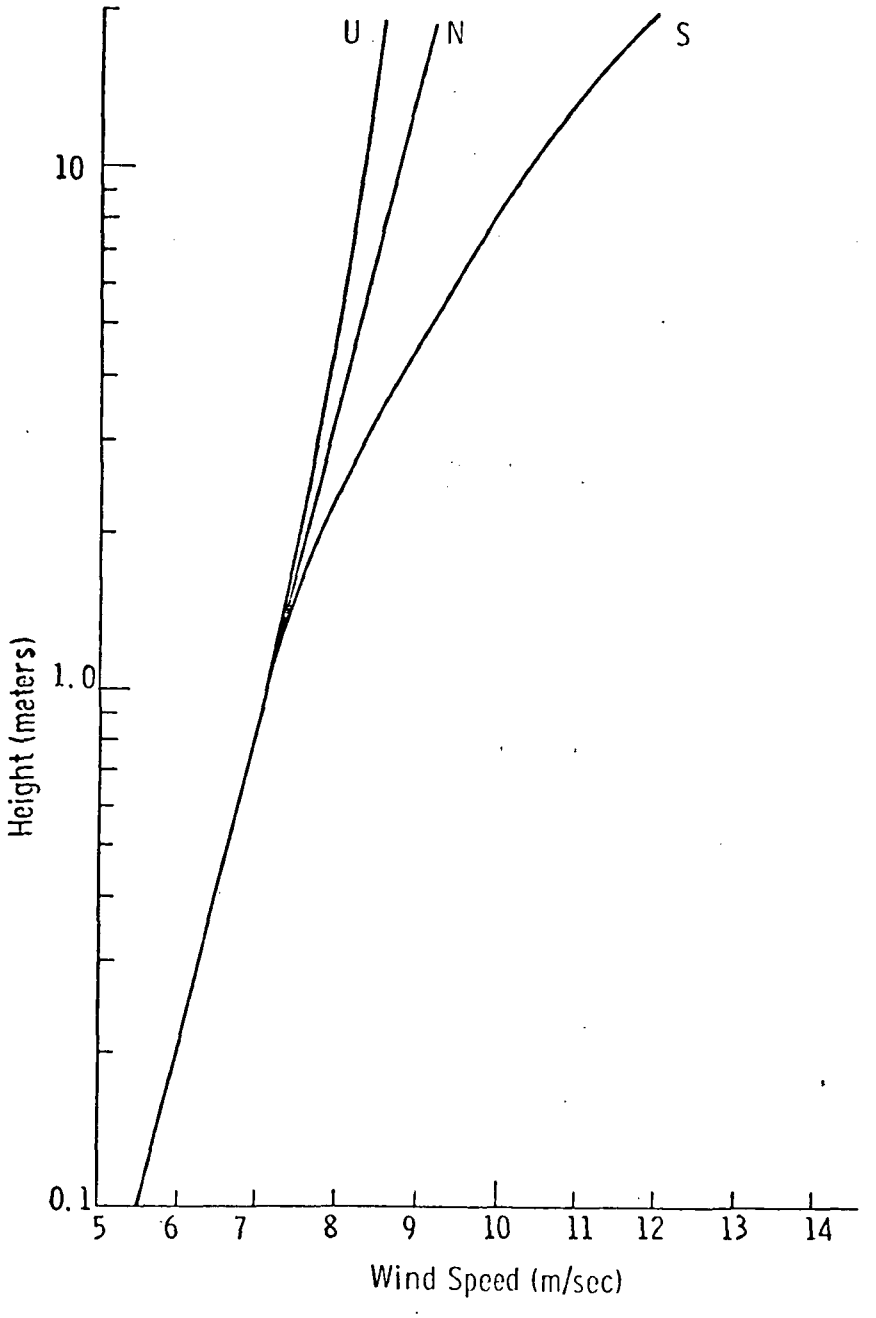

FIG. 2.4 Theoretical wind profiles in the marine surface boundary layer for a surface stress of 1 dyne/cm^2 and neutral (N), unstable (U), and stable (S) stratification.

$$W(U_*) = U_* / 0.4 \log z/z_o \tag{2.11a}$$

$$z_o = \frac{0.684}{U_*} + 4.28 \times 10^{-5} U_*^2 - 4.43 \times 10^{-2} \tag{2.11b}$$

where both W and U_* are in m per sec.

Cardone (1969) demonstrated that the air-sea temperature conditions influence the wind speed measurement at a specific height, and under the same atmospheric temperature condition the wind speed varies with respect to the height where wind speed is being measured. To make wind speed consistent with real surface roughness, namely friction velocity on the surface, every wind speed measurement is needed to specify the temperature conditions, namely stable, neutral or unstable, and the height of the anemometer. To compare two measured wind speeds of different origin a correction factor is needed to bring two situations consistent with the same surface roughness conditions and the correction factor depends on the anemometer height and temperature conditions.

Figure 2.4 illustrated the graph of wind speed variation with respect to the height of measurement under three atmospheric stratifications.

2.4 SPECULAR EMISSIVITY OF SEA WATER

For a plane sea surface, the specular emissivity, $\epsilon_j^{sp}(\theta)$, is related to the Fresnel reflection coefficient, $R_j(\theta)$, in the form

$$\epsilon_j^{sp}(\theta) = 1 - |R_j(\theta)|^2 \qquad j = h, v \tag{2.12}$$

where θ is the incident angle. The Fresnel reflection coefficient, $R_j(\theta)$, for an air-sea boundary, in turn, is expressed in the form

$$R_h(\theta) = \frac{\cos\theta - \sqrt{\epsilon_r - \sin^2\theta}}{\cos\theta + \sqrt{\epsilon_r - \sin^2\theta}} \tag{2.13a}$$

$$R_v(\theta) = \frac{\epsilon_r \cos\theta - \sqrt{\epsilon_r - \sin^2\theta}}{\epsilon_r \cos\theta + \sqrt{\epsilon_r - \sin^2\theta}} \tag{2.13b}$$

where ϵ_r is the complex relative dielectric constant of sea water.

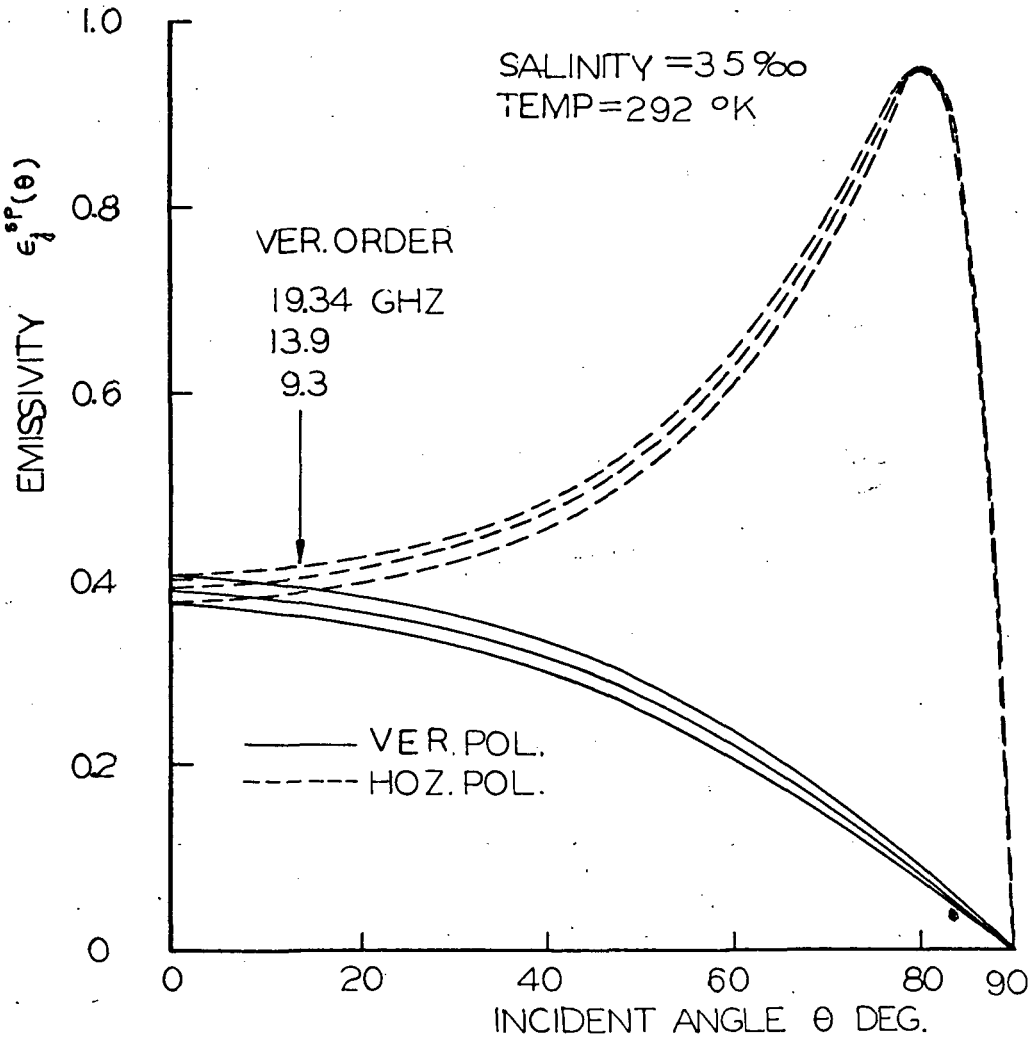

FIG. 2.5 The Plane Sea Surface Emissivity

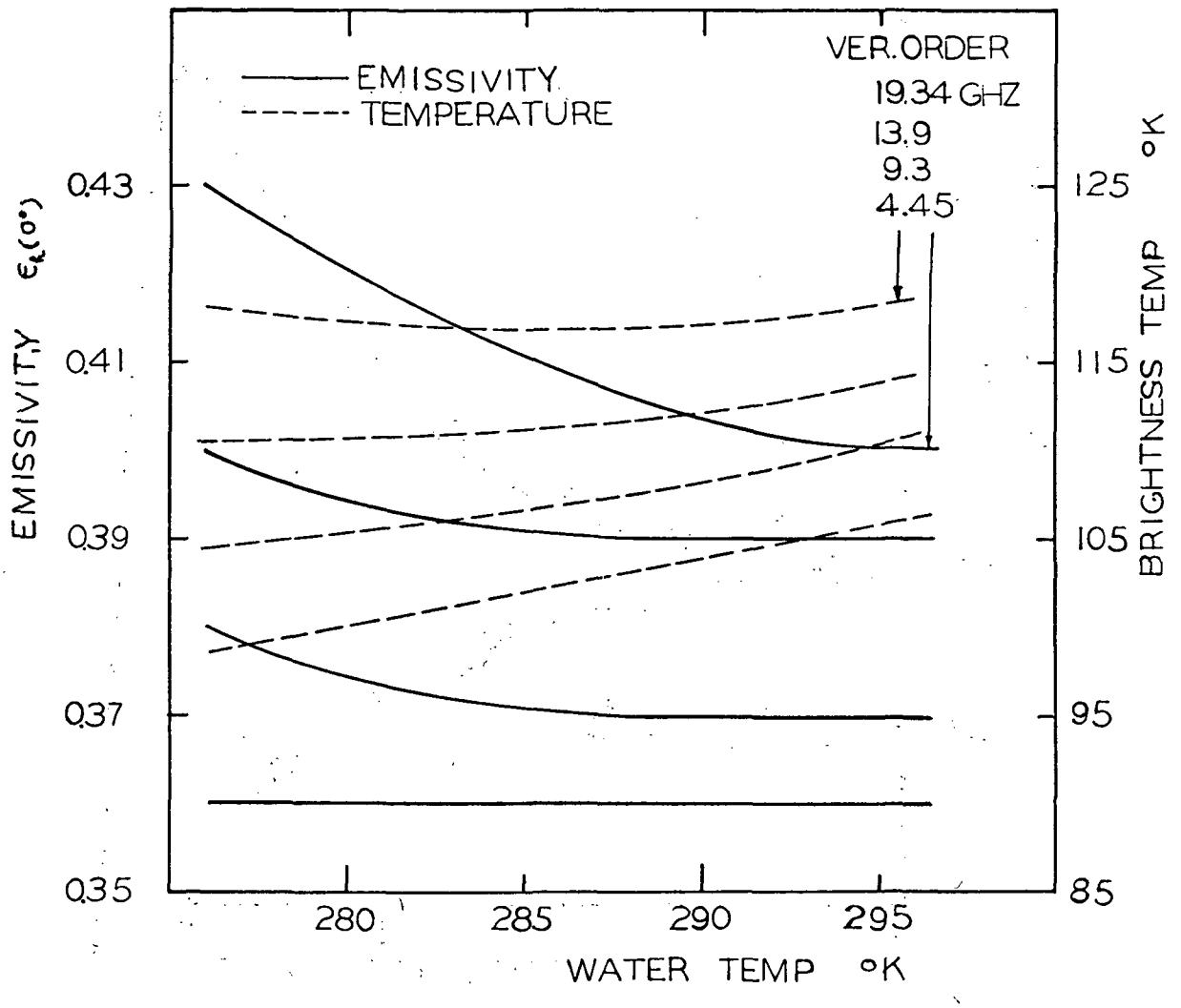

FIG. 2.6 The Plane Sea Surface Emissivity and Brightness Temperature at Nadir

Since the complex relative dielectric constant of sea water has been discussed in the previous subsection, the specular emissivity can be computed by using (2.12) and (2.13). The computed results are shown in Figures 2.5 and 2.6. Also shown in Figure 2.6 is the specular surface brightness temperature which is the product of specular emissivity and surface water temperature. In Figure 2.6 the specular emissivity at 4.455 GHz is almost temperature independent. Such a characteristic may be employed for designing a radiometer as a good sea water temperature sensor once the surface roughness effect and the atmospheric attenuation are removed or compensated.

CHAPTER 3

A THEORY FOR MICROWAVE EMISSIONS FROM THE SEA

3.1 INTRODUCTION

The microwave emission charccteristic of the sea has been measured by several investigators (Nordberg et al., 1969, 1970; Ross et al., 1970; Hollinger 1970, 1971a). These investigators have compared their observations with predictions from the geometric optics theory (Stogryn, 1967b) which uses a single-surface model and found some but not satisfactory agreement between predictions and measurements. The wind dependence of the geometric optics approach was based on measured rms sea slope data presented by Cox and Munk (1954). However, the theory failed to predict the observed emission characteristics near nadir and fitted only loosely for nadir angles of 30 to 70 degrees. The failure of the geometric optics model to account for wind dependence at nadir was first reported by Nordberg, et al. (1969), and was verified by Hollinger (1971a).

In view of the above deficiencies, an investigation is necessary to seek a more adequate model for microwave emissions from the sea. The emphasis in this investigation is oriented towards using a composite-surface model which better reflects the roughness characteristic of the sea. Since several lengthy numerical integrations are required to yield the emissivity, the more adequate model must not be so complicated that it makes numerical calculations prohibitive. With this perspective, a non-coherent scattering theory of the type described by Semyonov (1966) is extended to yield the bistatic scattering coefficient. Since an acceptable scattering coefficient for predicting the microwave emission characteristics must also be acceptable for predicting backscattering, backscattering is examined to provide a cross check on the model.

To compare with experimental observations, an isotropic surface characteristic, although it is not realistic for the ocean surface, is assumed. A justification for this assumption is based on the observed directional insensitivity of emission from the sea (Hollinger, 1971b). The two-scale rough surface model is also assumed to have Gaussian surface height distribution and Gaussian surface correlation for both

scales. The dielectric constant needed in the calculations is based on the data reported in Chapter II.

The wind dependence of the surface parameters in the composite model is introduced in accordance with rms slope data measured by Cox and Munk for the large undulations and Sutherlands (1967) results for the small irregularities. Details for the theory and the choice of surface parameters are given in later sections. Comparisons of the computed brightness temperature and backscattering characteristics at two different wind speeds are made with both measured data and the predictions of a single surface model.

3.2 SURFACE BRIGHTNESS TEMPERATURE THEORY

3.2.1 Formulation of the Problem

The basic theory of apparent surface temperature was developed by Peake (1959). The study that follows concerns only the contribution to the apparent surface temperature due to thermal emission from the sea surface; contributions due to sky radiation reflected from the sea are not considered. The relationship among the surface emissivity, the surface temperature and the apparent surface temperature (or the surface brightness temperature in this case) is as follows:

$$T_{Bj}(\theta) = \epsilon_j(\theta)\, T_g \qquad j = h,\ v$$

where $T_{Bj}(\theta)$ is the brightness temperature; $\epsilon_j(\theta)$ the emissivity; T_g the surface temperature; h is the horizontal polarization and v is the vertical polarization. Note that the azimuthal angle Φ needed together with the nadir angle θ to specify a direction has been chosen to be zero without loss of generality.

The connection between the emissivity and the differential scattering coefficient of the surface, $\gamma_j(\theta, \theta_s, \Phi_s)$ is

$$\epsilon_j(\theta) = 1 - \frac{1}{4\pi}\int_0^{2\pi}\int_0^{\pi/2} \gamma_j(\theta, \theta_s, \Phi_s)\sin\theta_s\, d\theta_s\, d\Phi_s \qquad (3.1)$$

where θ_s, and Φ_s are angles defining the direction of scattering corresponding to a wave incident at an angle θ.

The basic formulation of the problem indicated above shows that the differential scattering coefficient is the quantity that defines the angular characteristics of the brightness temperature of a given surface. Consequently, different brightness temperature theories are also distinguished by the different models assumed for the differential scattering coefficient.

Under the non-coherent assumption $\gamma_j(\theta, \theta_s, \phi_s)$ can be shown (Semyonov, 1966) to consist of two terms,

$$\gamma_j(\theta, \theta_s, \phi_s) = \gamma_j^{\circ}(\theta, \theta_s, \phi_s) + \langle \gamma_j'(\theta, \theta_s, \phi_s) \rangle \qquad (3.2)$$

where $\gamma_j^{\circ}(\theta, \theta_s, \phi_s)$ denotes the main contribution by the large undulations; and $\langle \gamma_j'(\theta, \theta_s, \phi_s) \rangle$ denotes the differential scattering coefficient of the small irregularities averaged over the distribution of the surface normals of the large undulations. Detailed derivations for $\gamma_j^{\circ}(\theta, \theta_s, \phi_s)$ and $\langle \gamma_j'(\theta, \theta_s, \phi_s) \rangle$ are given in the following two sections.

Since the backscattering cross-section is a special case of the differential scattering coefficients, it can be obtained from the known differential scattering coefficients, (see Figure 3.1) i.e.

$$\sigma_{Bj}^{\circ}(\theta) = \cos\theta \cdot \gamma_j(\theta, \theta_s, \phi_s)\Big|_{\substack{\theta_s = \theta \\ \phi_s = \pi}}$$

or equivalently

$$\sigma_{Bj}^{\circ}(\theta) = \sigma_{Bjo}^{\circ}(\theta) + \langle \sigma_{Bj1}^{\circ}(\theta) \rangle \qquad (3.3a)$$

with

$$\sigma_{Bj}^{\circ}(\theta) = \cos\theta \cdot \gamma_j^{\circ}(\theta, \theta_s, \phi_s)\Big|_{\substack{\theta_s = \theta \\ \phi_s = \pi}} \qquad (3.3b)$$

$$\langle \sigma_{Bj1}^{\circ}(\theta) \rangle = \cos\theta \cdot \langle \gamma_j'(\theta, \theta_s, \phi_s) \rangle\Big|_{\substack{\theta_s = \theta \\ \phi_s = \pi}} \qquad (3.3c)$$

Detailed derivations of $\sigma_{Bj}^{\circ}(\theta)$ are given in the section on backscattering cross sections.

3.2.2 Derivation of $\gamma_j^o(\theta, \theta_s, \phi_s)$

To derive $\gamma_j^o(\theta, \theta_s, \phi_s)$ we begin with the vector-scattered field due to a plane wave incident on an undulating surface to which the tangent plane approximation is assumed applicable. Such a field expression is, in general, rather complicated. To simplify results, the stationary phase technique will be employed. An expression for $\gamma_j^o(\theta, \theta_s, \phi_s)$ not indicating explicitly the effect of the small irregularities will be derived first. This expression is then clarified to reflect the small structure effects by computing the explicit forms of the modified Fresnel reflection coefficients. As pointed out by Semyonov, such a computation may be performed for the more general finitely conducting surface in accordance with the work of Rice (1951).

(i) The Scattered Field

The far zone scattered field in the direction $\underline{n}_2$ due to a plane wave polarized along $\underline{a}$ impinging on an undulating surface $z(x, y)$ can be shown to be (Fung, 1967)

$$\underline{E}_{as} = K\underline{n}_2 \times \int\Big\{\Big[(1+\langle R_h\rangle)(\underline{a}\cdot\underline{t})(\underline{n}\times\underline{t}) + (1-\langle R_v\rangle)(\underline{a}\cdot\underline{d})(\underline{n}\cdot\underline{n}_1)\underline{t}\Big] + \underline{n}_2 \times \Big[(1+\langle R_v\rangle)(\underline{a}\cdot\underline{d})(\underline{n}\times\underline{t}) + (1-\langle R_h\rangle)(\underline{a}\cdot\underline{t})(\underline{n}\cdot\underline{n}_1)\underline{t}\Big]\Big\} \cdot E_o \exp\Big[-jk(\underline{n}_2 - \underline{n}_1)\cdot\underline{r}\Big]\, ds. \tag{3.4}$$

where a time factor of the form $e^{j\omega t}$ has been suppressed; $K = -jk e^{-jkR}/(4\pi R)$, R is the distance from the origin to the field point, k is the wave number; $\langle R_h\rangle, \langle R_v\rangle$ are the modified Fresnel reflection for horizontal and vertical polarization respectively; E_o is the magnitude of incident field, and $\underline{n}$ is the normal to the surface $z(x, y)$.

The set of orthogonal unit vectors $(\underline{n}_1, \underline{t}, \underline{d})$ serving as the local coordinates for evaluating the local field on surface is illustrated in Figure 3.2. The unit vectors, $\underline{t}$ and $\underline{d}$ relate to $\underline{n}$ and $\underline{n}_1$ as follows

$$\underline{t} = (\underline{n}_1 \times \underline{n}) / |\underline{n}_1 \times \underline{n}|$$
$$\underline{d} = \underline{n}_1 \times \underline{t} \tag{3.5}$$

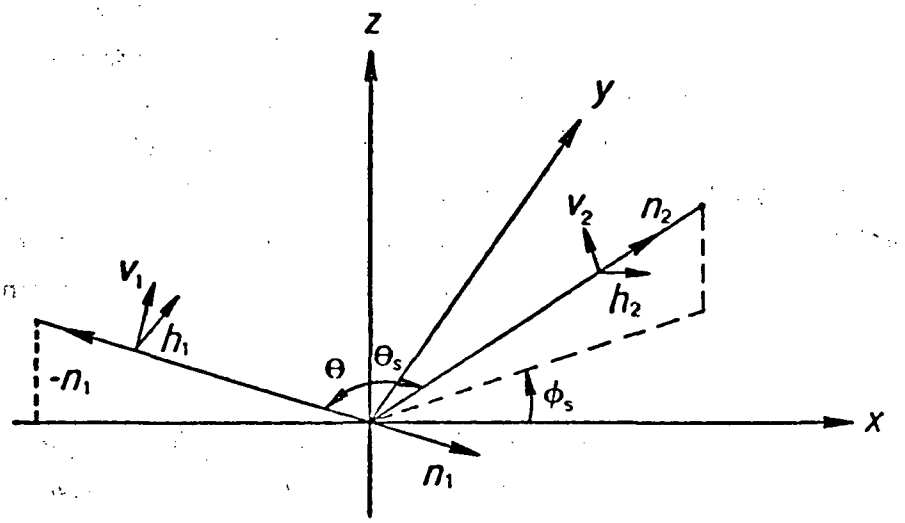

Figure 3.1 The sets of orthogonal unit vector ($-\underset{\sim}{n}_1$, $\underset{\sim}{h}_1$, $\underset{\sim}{v}_1$) and ($\underset{\sim}{n}_2$, $\underset{\sim}{h}_2$, $\underset{\sim}{v}_2$) for expressing the polarization states of the incident and the scattered field.

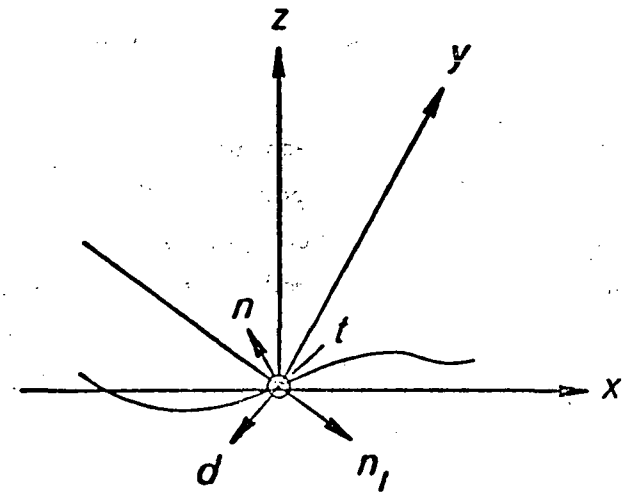

Figure 3.2 A set of orthogonal unit vectors ($\underset{\sim}{n}_1$, $\underset{\sim}{t}$, $\underset{\sim}{d}$) serving as the local coordinates for evaluating the local field on the surface.

where $\underline{n}$ may be written in terms of the partial derivaties, Z_x, Z_y of $Z(x, y)$ along x and y axes as follows

$$\underline{n} = (-\underline{i}\, Z_x - \underline{j}\, Z_y + \underline{k}) \,/\, (1 + Z_x^2 + Z_y^2)^{1/2},$$

($\underline{i}$, $\underline{j}$, $\underline{k}$) are the unit coordinate vectors.

To simplify (3.4) by the stationary phase approximation, let $\underline{q} = \underline{n}_2 - \underline{n}_1$ and q_x, q_y, q_z be the vector components of $\underline{q}$. Then the phase factor in (3.4) is

$$\underline{q} \cdot \underline{r} = q_x x + q_y y + q_z Z(x, y) \tag{3.6}$$

The stationary phase assumption requires that

$$\frac{\partial}{\partial x}(\underline{q} \cdot \underline{r}) = \frac{\partial}{\partial y}(\underline{q} \cdot \underline{r}) = 0$$

It follows that

$$\begin{aligned} Z_x &= -q_x / q_z \\ Z_y &= -q_y / q_z \\ \underline{n} &= \underline{q} / |\underline{q}| \end{aligned} \tag{3.7}$$

The significant result indicated by (3.7) is that all surface slopes in (3.4) can be written in terms of the incident and scattered propagation vectors. Consequently, the integrand in (3.4) except for the phase factor, $\exp[-jk\,\underline{q} \cdot \underline{r}]$ can be moved outside of the integral sign; i.e.,

$$\underline{E}_{as} = E_0 K\, \underline{n}_2 \times \left\{ (\underline{A} - \underline{B}) + \underline{n}_2 \times (\underline{C} + \underline{D}) \right\} \int_{A_0} \exp[jk(\underline{n}_2 - \underline{n}_1) \cdot \underline{r}]\, dS \tag{3.8}$$

with

$$\begin{aligned} \underline{A} &= (1 + \langle R_h \rangle)(\underline{a} \cdot \underline{t})(\underline{n} \times \underline{t}) \\ \underline{B} &= (1 - \langle R_v \rangle)(\underline{a} \cdot \underline{d})(\underline{n} \cdot \underline{n}_1)\, \underline{t} \\ \underline{C} &= (1 + \langle R_v \rangle)(\underline{a} \cdot \underline{d})(\underline{n} \times \underline{t}) \\ \underline{D} &= (1 - \langle R_h \rangle)(\underline{a} \cdot \underline{t})(\underline{n} \cdot \underline{n}_1)\, \underline{t} \end{aligned} \tag{3.9}$$

The local coordinate vectors, two other vector products in (3.9) and the differential surface element in (3.8) can all be written in terms of the propagation vectors,

$$\underset{\sim}{t} = (\underset{\sim}{n}_1 \times \underset{\sim}{n}_2) / |\underset{\sim}{n}_1 \times \underset{\sim}{n}_2|$$

$$\underset{\sim}{d} = \frac{(\underset{\sim}{n}_1 \cdot \underset{\sim}{n}_2)\,\underset{\sim}{n}_1 - \underset{\sim}{n}_2}{|\underset{\sim}{n}_1 \times \underset{\sim}{n}_2|}$$

$$\underset{\sim}{n} \times \underset{\sim}{t} = \frac{|\underset{\sim}{n}_2 - \underset{\sim}{n}_1|\,(\underset{\sim}{n}_1 + \underset{\sim}{n}_2)}{2\,|\underset{\sim}{n}_1 \times \underset{\sim}{n}_2|}$$

$$\underset{\sim}{n} \cdot \underset{\sim}{n}_1 = \frac{-|\underset{\sim}{n}_2 - \underset{\sim}{n}_1|}{2} \qquad (3.10)$$

$$ds = (|\underset{\sim}{n}_2 - \underset{\sim}{n}_1| / q_3)\, dx\, dy$$

To express the polarization states of both the incident and the scattered field, it is convenient to introduce a set of orthogonal unit vectors ($-\underset{\sim}{n}_1$, $\underset{\sim}{v}_1$, $\underset{\sim}{h}_1$) for the incident field and another set ($\underset{\sim}{n}_2$, $\underset{\sim}{v}_2$, $\underset{\sim}{h}_2$) for the scattered field (see Figure 3.1). In view of Figure 3.1, explicit expressions for these unit vectors may be written as

$$\begin{aligned} -\underset{\sim}{n}_1 &= -\sin\theta\, \underset{\sim}{i} + \cos\theta\, \underset{\sim}{k} \\ \underset{\sim}{v}_1 &= \cos\theta\, \underset{\sim}{i} + \sin\theta\, \underset{\sim}{k} \\ \underset{\sim}{h}_1 &= \underset{\sim}{j} \end{aligned} \qquad (3.11)$$

$$\begin{aligned} \underset{\sim}{n}_2 &= \sin\theta_s \cos\phi_s\, \underset{\sim}{i} + \sin\theta_s \sin\phi_s\, \underset{\sim}{j} + \cos\theta_s\, \underset{\sim}{k} \\ \underset{\sim}{v}_2 &= -\cos\theta_s \cos\phi_s\, \underset{\sim}{i} - \cos\theta_s \sin\phi_s\, \underset{\sim}{j} + \sin\theta_s\, \underset{\sim}{k} \\ \underset{\sim}{h}_2 &= \sin\phi_s\, \underset{\sim}{i} - \cos\phi_s\, \underset{\sim}{j} \end{aligned} \qquad (3.12)$$

For horizontally polarized incident wave, ($\underset{\sim}{a} = \underset{\sim}{h}_1$), the polarized and cross polarized scattered fields are given respectively by

$$E_{hh} = \underline{h}_2 \cdot \underline{E}_{h_1 s}$$
$$= E_o K \left[\underline{h}_2 \cdot \underline{n}_2 \times \left\{ (\underline{A}_h - \underline{B}_h) + \underline{n}_2 \times (\underline{C}_h + \underline{D}_h) \right\} \right] \int_{A_o} \exp[-jk(\underline{n}_2 - \underline{n}_1)\cdot \underline{r}]\, ds \tag{3.13}$$

$$E_{hv} = \underline{v}_2 \cdot \underline{E}_{h_1 s}$$
$$= E_o K \left[\underline{v}_2 \cdot \underline{n}_2 \times \left\{ (\underline{A}_h - \underline{B}_h) + \underline{n}_2 \times (\underline{C}_h + \underline{D}_h) \right\} \right] \int_{A_o} \exp[-jk(\underline{n}_2 - \underline{n}_1)\cdot \underline{r}]\, ds$$

where

$$\underline{A}_h = -|f|\,(1 + \langle R_h \rangle)(\underline{v}_1 \cdot \underline{n}_2)(\underline{n}_1 + \underline{n}_2)$$

$$\underline{B}_h = |f|\,(1 - \langle R_v \rangle)(\underline{h}_1 \cdot \underline{n}_2)(\underline{n}_1 \times \underline{n}_2)$$

$$\underline{C}_h = -|f|\,(1 + \langle R_v \rangle)(\underline{h}_1 \cdot \underline{n}_2)(\underline{n}_1 + \underline{n}_2)$$

$$\underline{D}_h = |f|\,(1 - \langle R_h \rangle)(\underline{v}_1 \cdot \underline{n}_2)(\underline{n}_1 \times \underline{n}_2)$$

$$|f| = |\underline{n}_2 - \underline{n}_1| / 2\,|\underline{n}_1 \times \underline{n}_2|^2$$

Similarly, for a vertically polarized incident wave ($\underline{a} = \underline{v}_1$), the polarized and depolarized scattered fields are

$$E_{vh} = \underline{h}_2 \cdot \underline{E}_{v_1 s}$$
$$= E_o K \left[\underline{h}_2 \cdot \underline{n}_2 \times \left\{ (\underline{A}_v - \underline{B}_v) + \underline{n}_2 \times (\underline{C}_v + \underline{D}_v) \right\} \right] \cdot$$
$$\cdot \int_{A_o} \exp[\, jk(\underline{n}_2 - \underline{n}_1)\cdot \underline{r}\,]\, dS$$

(3.14)

$$E_{vv} = \underline{v}_2 \cdot \underline{E}_{v_1 s}$$
$$= E_o K \left[\underline{v}_2 \cdot \underline{n}_2 \times \left\{ (\underline{A}_v - \underline{B}_v) + \underline{n}_2 \times (\underline{C}_v + \underline{D}_v) \right\} \right]$$
$$\cdot \int_{A_o} \exp[\, jk(\underline{n}_2 - \underline{n}_1)\cdot \underline{r}\,]\, dS$$

where

$$\underset{\sim}{A}_v = |f|\,(1 + \langle R_h \rangle)(\underset{\sim}{h}_1 \cdot \underset{\sim}{n}_2)(\underset{\sim}{n}_1 + \underset{\sim}{n}_2)$$

$$\underset{\sim}{B}_v = |f|\,(1 - \langle R_v \rangle)(\underset{\sim}{v}_1 \cdot \underset{\sim}{n}_2)(\underset{\sim}{n}_1 \times \underset{\sim}{n}_2)$$

$$\underset{\sim}{C}_v = -|f|\,(1 + \langle R_v \rangle)(\underset{\sim}{v}_1 \cdot \underset{\sim}{n}_2)(\underset{\sim}{n}_1 + \underset{\sim}{n}_2)$$

$$\underset{\sim}{D}_v = -|f|\,(1 - \langle R_h \rangle)(\underset{\sim}{h}_1 \cdot \underset{\sim}{n}_2)(\underset{\sim}{n}_1 \times \underset{\sim}{n}_2)$$

These field expressions can be simplified further by using the vector identifies

$$\underset{\sim}{h}_2 \cdot \underset{\sim}{n}_2 \times (\underset{\sim}{M} + \underset{\sim}{n}_2 \times \underset{\sim}{N}) = \underset{\sim}{v}_2 \cdot \underset{\sim}{M} - \underset{\sim}{h}_2 \cdot \underset{\sim}{N}$$

$$\underset{\sim}{v}_2 \cdot \underset{\sim}{n}_2 \times (\underset{\sim}{M} + \underset{\sim}{n}_2 \times \underset{\sim}{N}) = -\underset{\sim}{h}_2 \cdot \underset{\sim}{M} - \underset{\sim}{v}_2 \cdot \underset{\sim}{N}$$

Thus,

$$\begin{aligned} E_{hh} &= C_o\,(-\langle R_h \rangle bc + \langle R_v \rangle df)\,I \\ E_{hv} &= C_o\,(\langle R_h \rangle bf + \langle R_v \rangle dc)\,I \\ E_{vh} &= C_o\,(-\langle R_h \rangle df + \langle R_v \rangle bc)\,I \\ E_{vv} &= C_o\,(\langle R_h \rangle dc + \langle R_v \rangle bf)\,I \end{aligned} \qquad (3.15)$$

where

$$C_o = \frac{-jk E_o a_1 e^{-jkR}}{2\pi R q_z |\underset{\sim}{n}_2 \times \underset{\sim}{n}_1|^2}$$

$$I = \int_{A_o} \exp(jk\,\underset{\sim}{q} \cdot \underset{\sim}{r})\,dx\,dy$$

$$q_x = \sin\theta_s \cos\phi_s - \sin\theta$$

$$q_y = \sin\theta_s \sin\phi_s$$

$$q_z = \cos\theta + \cos\theta_s$$

$$b = (\underset{\sim}{v}_1 \cdot \underset{\sim}{n}_2) = \sin\theta \cos\theta_s + \cos\theta \sin\theta_s \cos\phi_s$$

$$c = (\underset{\sim}{v}_2 \cdot \underset{\sim}{n}_1) = -\sin\theta \cos\theta_s \cos\phi_s - \cos\theta \sin\theta_s$$

$$d = (\underset{\sim}{h}_1 \cdot \underset{\sim}{n}_2) = \sin\theta_s \sin\phi_s$$

$$f = (\underset{\sim}{h}_2 \cdot \underset{\sim}{n}_1) = \sin\theta \sin\phi_s$$

$$a_1 = |\underset{\sim}{n}_2 - \underset{\sim}{n}_1|^2/2 = 1 + \cos\theta \cos\theta_s - \sin\theta \sin\theta_s \cos\phi_s$$

$$|\underset{\sim}{n}_2 \times \underset{\sim}{n}_1|^2 = (c^2 + f^2) = (b^2 + d^2)$$

Note that by expressing $\underset{\sim}{n}_2$ in terms of the orthogonal set ($\underset{\sim}{n}_1$, $\underset{\sim}{v}_1$, $\underset{\sim}{h}_1$) it can be shown that $|\underset{\sim}{n}_2 \times \underset{\sim}{n}_1|^2 = b^2 + d^2$. Similarly, by expressing $\underset{\sim}{n}_1$, in terms of the orthogonal set ($\underset{\sim}{n}_2$, $\underset{\sim}{v}_2$, $\underset{\sim}{h}_2$) it follows that $|\underset{\sim}{n}_1 \times \underset{\sim}{n}_2|^2 = c^2 + f^2$.

(ii) The Differential Scattering Coefficients

The differential scattering coefficients related to the scattered fields computed in the previous section (Peake, 1959 and Storgryn, 1967a) are of the form

$$\gamma_{j,i}(\theta, \theta_s, \phi_s) = \frac{4\pi R^2 \langle E_{j,i} E_{j,i}^* \rangle}{E_o^2 A_o \cos\theta} \qquad (3.16)$$

where the symbol $*$ denotes complex conjugate, and $\langle \text{---} \rangle$ the ensemble average. The subscripts j, i denote the polarization states of the incident and the scattered fields respectively. A_o is the illuminated area.

Upon substituting (3.15) into (3.16) it follows that

$$\gamma_h^o(\theta, \theta_s, \phi_s) = \gamma_{hh}^o(\theta, \theta_s, \phi_s) + \gamma_{hv}^o(\theta, \theta_s, \phi_s)$$
$$= \frac{k^2 a_1^2}{\pi A_o \cos\theta\, g_j^2} \left[\frac{|\langle R_h \rangle|^2 b^2 + |\langle R_v \rangle|^2 d^2}{b^2 + d^2} \right] \langle |I|^2 \rangle \qquad (3.17a)$$

$$\gamma_v^o(\theta, \theta_s, \phi_s) = \gamma_{vh}^o(\theta, \theta_s, \phi_s) + \gamma_{vv}^o(\theta, \theta_s, \phi_s)$$
$$= \frac{k^2 a_1^2}{\pi A_o \cos\theta\, g_j^2} \left[\frac{|\langle R_v \rangle|^2 b^2 + |\langle R_h \rangle|^2 d^2}{b^2 + d^2} \right] \langle |I|^2 \rangle \qquad (3.17b)$$

For an isotropically rough surface with Gaussian height distribution, $\langle |I|^2 \rangle$ simplifies to

$$\langle |I|^2 \rangle = 2\pi A_o \int_0^\infty J_o \left[k \xi \left(g_x^2 + g_y^2 \right)^{1/2} \right] \exp \left[- k^2 g_z^2 \sigma^2 \left(1 - \rho(\xi) \right) \right] \xi \, d\xi \qquad (3.18)$$

where $J_o(\ )$ is the zero order Bessel function of the first kind; σ^2 and $\rho(\xi)$ are the variance and the autocorrelation coefficient of the surface respectively.

An approximate solution for (3.18) consistent with the stationary phase approximation is

$$\langle |I|^2 \rangle = 2\pi A_o / \left(k^2 g_z^2 m^2 \right) \exp \left[- \left(g_x^2 + g_y^2 \right) / \left(2 g_z^2 m^2 \right) \right] \qquad (3.19)$$

where $m = \left[\sigma^2 |\rho''(o)| \right]^{1/2}$ is the rms slope of the surface.

3.2.3 Derivation of $\langle \gamma_j^i(\theta, \theta_s, \Phi_s) \rangle$

The scattered field due only to the small irregularities has been derived by many investigators (Rice, 1951, Valenzuela, 1967, and Barrick and Peake, 1967). As was indicated in the previous section, when the scattered field expression is known, the scattering coefficient can be computed. To account for the interaction between the small irregularities and the large undulations, the expression for the scattering coefficient of the small irregularities is averaged with respect to the slope distribution of the large undulations. The resulting expression is the desired scattering coefficient, $\langle \gamma_j^i(\theta, \theta_s, \Phi_s) \rangle$.

(i) Differential Scattering Coefficients

The far zone scattered field of i-polarization along the direction defined by the angles θ_s' and Φ_s' due to a plane wave of j-polarization with unit amplitude impinging on an irregular surface $s(x, y)$ along the direction defined by the angles θ' and Φ' has been derived by using the method of small perturbation (Barrick and Peake, 1967). The ensemble average of the magnitude square of the scattered field, $\langle |E_{ji}(\theta', \Phi', \theta_s', \Phi_s')|^2 \rangle$ can be shown to be (Barrick and Peake, 1967)

$$\langle |E_{ji}(\theta', \Phi', \theta_s', \Phi_s')|^2 \rangle = \frac{k^4 A_o}{R^2} \cos^2\theta' \cos^2\theta_s' \, |M_{ji}|^2 \, W(P, q) \qquad (3.20)$$

where

j, i = incident and scattered polarization respective, either horizontal or vertical polarizations,

A_o = illuminated area,

R = distance from the field point to the surface, and

$$M_{hh} = \frac{(\epsilon_r - 1)\cos(\phi_s' - \phi')}{\left[\cos\theta' + (\epsilon_r - \sin^2\theta')^{1/2}\right]\left[\cos\theta_s' + (\epsilon_r - \sin^2\theta_s')^{1/2}\right]}$$

$$M_{vh} = \frac{(\epsilon_r - 1)\sin(\phi_s' - \phi')(\epsilon_r - \sin^2\theta_s')^{1/2}}{\left[\cos\theta' + (\epsilon_r - \sin^2\theta')^{1/2}\right]\left[\epsilon_r\cos\theta_s' + (\epsilon_r - \sin^2\theta_s')^{1/2}\right]} \qquad (3.21)$$

$$M_{hv} = \frac{-(\epsilon_r - 1)\sin(\phi_s' - \phi')(\epsilon_r - \sin^2\theta_s')^{1/2}}{\left[\epsilon_r\cos\theta' + (\epsilon_r - \sin^2\theta')^{1/2}\right]\left[\cos\theta_s' + (\epsilon_r - \sin^2\theta_s')^{1/2}\right]}$$

$$M_{vv} = \frac{-(\epsilon_r - 1)\left[\cos(\phi_s' - \phi')(\epsilon_r - \sin^2\theta')^{1/2}(\epsilon_r - \sin^2\theta_s')^{1/2} - \epsilon_r\sin\theta_s'\sin\theta'\right]}{\left[\epsilon_r\cos\theta' + (\epsilon_r - \sin^2\theta')^{1/2}\right]\left[\epsilon_r\cos\theta_s' + (\epsilon_r - \sin^2\theta_s')^{1/2}\right]}$$

in which ϵ_r is the complex relative dielectric constant,

$W(p, q)$ = surface roughness spectral density,

$$p = k\left[\sin\theta_s'\cos(\phi_s' - \phi') - \sin\theta'\right]$$

$$q = k\sin\theta_s'\sin(\phi_s' - \phi')$$

Note that the surface roughness spectral density $W(p, q)$, is related to its correlation function $R(x, y)$ by

$$R(x, y) = \frac{1}{4}\int_{-\infty}^{\infty}\int_{-\infty}^{\infty} W(p, q)\exp(jpx + jqy)\,dp\,dq$$

For an isotropically rough surface, it reduces to

$$R(r) = \frac{\pi}{2}\int_0^{\infty} W(t)\,J_0(tr)\,t\,dt$$

and

$$W(t) = \frac{2}{\pi}\int_0^{\infty} R(r)\,J_0(tr)\,r\,dr$$

For a Gaussian spectral density, it is expressed in the form

$$W(t) = \frac{\sigma_i^2 l^2}{\pi}\exp\left[-\left(\frac{lt}{2}\right)^2\right] \qquad (3.22)$$

where $t = (p^2 + q^2)^{1/2}$

σ_1, ℓ = standard deviation and correlation length of the small irregularities respectively.

From (3.16) and the relation

$$\gamma_j^1(\theta', \phi', \theta_s', \phi_s') = \gamma_{jh}^1(\theta', \phi', \theta_s', \phi_s') + \gamma_{jv}^1(\theta', \phi', \theta_s', \phi_s')$$

we get

$$\gamma_j^1(\theta', \phi', \theta_s', \phi_s') = 4k^4\sigma_1^2\ell^2 \cos\theta' \cos^2\theta_s' \left[|M_{jh}|^2 + |M_{jv}|^2\right] \exp\left[-\left(\frac{\ell t}{2}\right)^2\right]$$

$$j = h, v \qquad (3.23)$$

(ii) Averaging Procedure

To account for the tilting effect of the small irregularities by the large undulations it is necessary to average $\gamma_j^1(\theta', \phi', \theta_s', \phi_s')$ with respect to the slope distribution of the large undulations (Semyonov, 1966). That is

$$\langle \gamma_j^1(\theta, \theta_s, \phi_s) \rangle = \int_{-\infty}^{\infty}\int_{-\infty}^{\infty} \gamma_j^1(\theta', \phi', \theta_s', \phi_s')\, P(z_x, z_y)\,(1 + z_x^2 + z_y^2)^{1/2}\, dz_x\, dz_y \qquad (3.24)$$

where θ is the incident angle and θ_s and ϕ_s are the scattering angles.

To evaluate the above integral, connecting relations between the surface slopes z_x, z_y and the local angles, θ', ϕ', θ_s', ϕ_s' are needed. To find these relations let us first express z_x and z_y in terms of the azimuth and the elevation angles, ϕ_n and θ_n, which represent the tilting effect:

$$z_x = \cos\phi_n \tan\theta_n$$
$$z_y = \sin\phi_n \tan\theta_n \qquad (3.25)$$

From (3.25) it follows that

$$(1 + z_x^2 + z_y^2)^{1/2} = \sec\theta_n$$

$$dz_x\, dz_y = \left|\frac{\partial(z_x, z_y)}{\partial(\theta_n, \phi_n)}\right| d\theta_n\, d\phi_n \qquad (3.26)$$

$$= \sec^3\theta_n \sin\theta_n\, d\theta_n\, d\phi_n$$

The local angles (θ', ϕ', θ_s' , ϕ_s') can now be related to the azimuth and the elevation angles ϕ_n and θ_n by connecting relations derived below.

In Figure 3.3, the two sets of coordinates (x , y , z) and (x', y', z') are related in terms of the angles θ_n and ϕ_n as follows:

$$\begin{bmatrix} x' \\ y' \\ z' \end{bmatrix} = \begin{bmatrix} \cos\theta_n \cos\phi_n & \cos\theta_n \sin\phi_n & \sin\theta_n \\ -\sin\phi_n & \cos\phi_n & 0 \\ -\sin\theta_n \cos\phi_n & -\sin\theta_n \sin\phi_n & \cos\theta_n \end{bmatrix} \begin{bmatrix} x \\ y \\ z \end{bmatrix} \tag{3.27}$$

Hence, for a scattered field point, P, located at a distance, R , from the origin, the coordinates of P may be expressed either in terms of the angles θ_s' and ϕ_s' or the angles θ_s and ϕ_s ,

$$\begin{aligned} x' &= R \sin\theta_s' \cos\phi_s' \\ y' &= R \sin\theta_s' \sin\phi_s' \\ z' &= R \cos\theta_s' \end{aligned} \tag{3.28a}$$

$$\begin{aligned} x &= R \sin\theta_s \cos\phi_s \\ y &= R \sin\theta_s \sin\phi_s \\ z &= R \cos\theta_s \end{aligned} \tag{3.28b}$$

Substituting equation (3.28) into (3.27) we obtain the connecting equations for the sets of angles as follows:

$$\begin{bmatrix} \sin\theta_s'\cos\phi_s' \\ \sin\theta_s'\sin\phi_s' \\ \cos\theta_s' \end{bmatrix} = \begin{bmatrix} \cos\theta_n\cos\phi_n & \cos\theta_n\sin\phi_n & \sin\theta_n \\ -\sin\phi_n & \cos\phi_n & 0 \\ -\sin\theta_n\cos\phi_n & -\sin\theta_n\sin\phi_n & \cos\theta_n \end{bmatrix} \begin{bmatrix} -\sin\theta_s\cos\phi_s \\ \sin\theta_s\sin\phi_s \\ \cos\theta_s \end{bmatrix} \tag{3.29}$$

If we take the angles with a prime to be local scattering angles, we see from (3.29) that the local scattering angles may be expressed in terms of the scattering angles θ_s , ϕ_s and the tilting angles θ_n, ϕ_n , i.e.

$$\begin{aligned} \cos\theta_s' &= \cos\theta_n\cos\theta_s - \sin\theta_n \sin\theta_s \cos(\phi_s - \phi_n) \\ \sin\phi_s' &= \sin\theta_s \sin(\phi_s - \phi_n)(1 - \cos^2\theta_s')^{-1/2} \end{aligned} \tag{3.30}$$

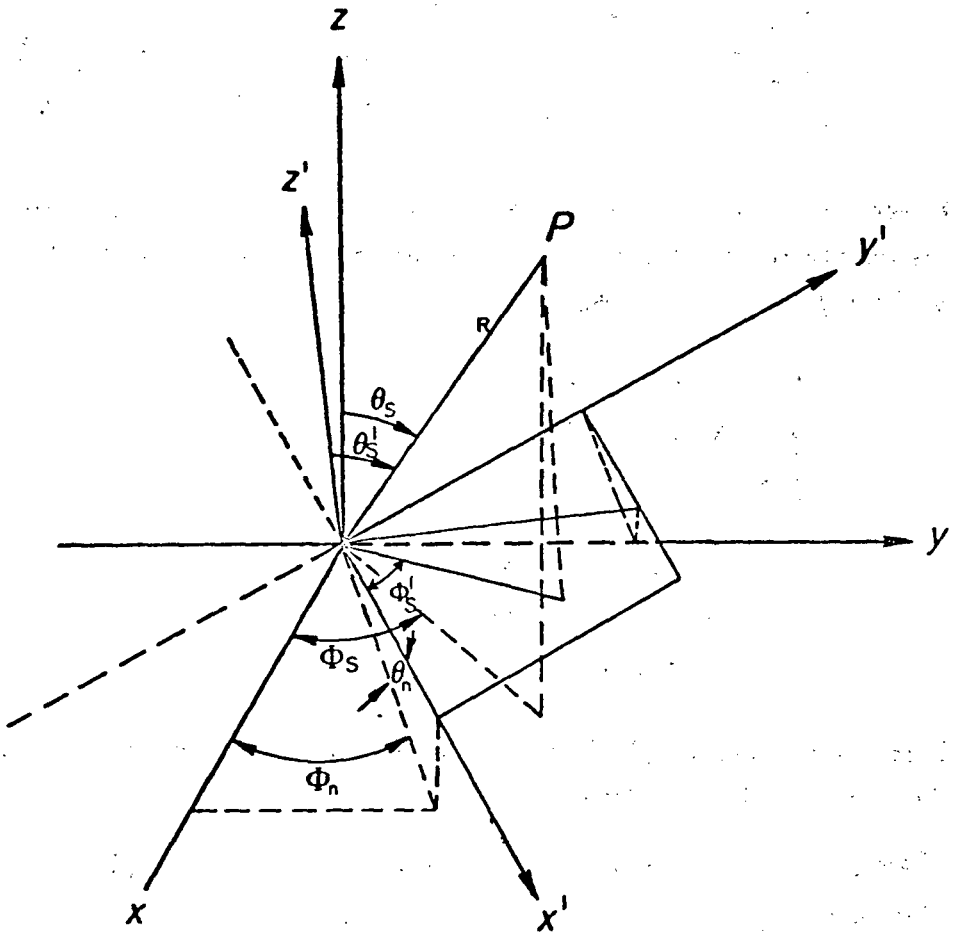

Figure 3.3 The azimuthal and the elevation angles Φ_n and θ_n connecting the two sets of coordinates (x , y , z) and (x', y', z').

In a similar fashion, the local incident angles can also be expressed in terms of the tilting angles θ_n, ϕ_n and the incident angle, θ.

$$\cos\theta' = \cos\theta_n \cos\theta + \sin\theta_n \sin\theta \cos\phi_n$$
$$\sin\phi' = -\sin\theta \sin\phi_n (1 - \cos^2\theta')^{-1/2} \qquad (3.31)$$

When the connecting relations between the local angles and the surface slopes are known, (3.24) can be evaluated by assuming a form of $P(z_x, z_y)$. For a Gaussian surface slope distribution it may be represented as

$$P(z_x, z_y) = \frac{1}{2\pi m^2} \exp\left(-(z_x^2 + z_y^2)/2m^2\right) \qquad (3.32)$$

or equivalently

$$P(\theta_n, \phi_n) = \frac{1}{2\pi m^2} \exp\left(-\tan^2\theta_n/2m^2\right) \qquad (3.33)$$

where m, the rms slope, is assigned according to Cox and Munk's slick sea data.

Since m^2 is usually sufficiently small for the sea and since $\gamma_j^1(\theta', \phi', \theta_s', \phi_s')$ is insensitive to θ_n for small values of θ_n, the integration with respect to θ_n given in (3.24) can be evaluted by the method of steepest decent, the result being expressed as

$$\langle \gamma_j^1(\theta, \theta_s, \phi_s) \rangle = \frac{1}{2\pi} \int_{-\pi/2}^{\pi/2} \left\{ \gamma_j^1(\theta', \phi', \theta_s', \phi_s')\Big|_{\theta_n = \tan^{-1}(m)} + \gamma_j^1(\theta', \phi', \theta_s', \phi_s')\Big|_{\theta_n = -\tan^{-1}(m)} \right\} d\phi_n \qquad (3.34)$$

3.2.4 Modified Fresnel Reflection Coefficients

As was mentioned earlier, the Fresnel reflection coefficient should be modified to account for the presence of the small irregularities (Rice, 1951, Semyonov, 1966). The method for computing these coefficients has been discussed by Rice for horizontally polarized waves. Following Rice's approach Valenzuela (1970) derived the modified reflection coefficient for the vertically polarized waves. However, there appears to be an error in his results, since they differ from Rice's original work by a cosine factor in one of the terms. The corrected modified Fresnel reflection coefficients calculated by Rice's method are

$$\langle R_j \rangle = R_j(\Phi)\left[1 - \tfrac{1}{2} k \cos\Phi \int_{-\infty}^{\infty}\int_{-\infty}^{\infty} W(u - k\sin\Phi, v)\, F_j(u,v)\, du\, dv\right]$$

$$j = h, v \qquad (3.35a)$$

$$F_h(u,v) = k(\epsilon_r - \sin^2\Phi)^{1/2} - (c-b)\left(1 - \frac{v^2}{u^2+v^2+bc}\right)$$

$$F_v(u,v) = \frac{\epsilon_r}{\epsilon_r\cos^2\Phi - \sin^2\Phi}\left[k(\epsilon_r - \sin^2\Phi)^{1/2}\left(1 - \frac{2k\sin\Phi\, u}{u^2+v^2+bc}\right)\right. \qquad (3.35b)$$

$$\left. - \frac{(c-b)}{u^2+v^2+bc}\left(\sin^2\Phi\{bc + u^2/\epsilon_r\} - u^2\right)\right] - (c-b)$$

where

$$R_h(\Phi) = \frac{\cos\Phi - (\epsilon_r - \sin^2\Phi)^{1/2}}{\cos\Phi + (\epsilon_r - \sin^2\Phi)^{1/2}}$$

$$R_v(\Phi) = \frac{\epsilon_r\cos\Phi - (\epsilon_r - \sin^2\Phi)^{1/2}}{\epsilon_r\cos\Phi + (\epsilon_r - \sin^2\Phi)^{1/2}} \qquad (3.36)$$

$$\cos\Phi = \frac{1}{\sqrt{2}}(1 + \cos\theta\cos\theta_s - \sin\theta\sin\theta_s\cos\Phi_s)^{1/2}$$

in which ϵ_r is the complex relative dielectric constant and where

$$c = [k^2\epsilon_r - (u^2+v^2)]^{1/2}$$
$$b = [k^2 - (u^2+v^2)]^{1/2} \qquad (3.37)$$

For the purpose of this paper the surface roughness spectrum in the above formula is chosen to be

$$W(u - k\sin\Phi, v) = \frac{l^2\sigma^2}{\pi}\exp\left[-\frac{l^2}{4}(u^2+v^2 - 2ku\sin\Phi + k^2\sin^2\Phi)\right]$$

(3.38)

3.2.5 Backscattering Cross-Sections

Substituting $\theta_s = \theta$ and $\Phi_s = \pi$ into (3.36) we obtain

$$R_h(0) = R_v(0) = \frac{1 - (\epsilon_r)^{1/2}}{1 + (\epsilon_r)^{1/2}} \qquad (3.39)$$

From (3.17), (3.19) and (3.3b), it follows that

$$\sigma^{\circ}_{Bh_0}(\theta) = \frac{|\langle R_h(0)\rangle|^2}{2m^2\cos^4\theta}\exp\left(-\tan^2\theta/2m^2\right) \tag{3.40a}$$

$$\sigma^{\circ}_{Bv_0}(\theta) = \frac{|\langle R_v(0)\rangle|^2}{2m^2\cos^4\theta}\exp\left(-\tan^2\theta/2m^2\right) \tag{3.40b}$$

To find $\langle \sigma^{\circ}_{Bj1}\rangle$, note the following two points:

(1) Substituting $\theta_s = \theta$ and $\phi_s = \pi$ into (3.30) we obtain

$$\begin{aligned}\cos\theta_s' = \cos\theta' &= \cos\theta_n\cos\theta + \sin\theta_n\cos\phi_n\sin\theta \\ \sin\phi_s' = -\sin\phi' &= \sin(\phi'+\pi)\end{aligned} \tag{3.41}$$

or

$$\theta_s' = \theta' \quad , \qquad \phi_s' = \phi' + \pi$$

(2) Since $\theta_s = \theta$ and $\phi_s = \pi$ imply $\phi_s' = \phi' + \pi$ and $\theta_s' = \theta'$, from (3.34) it follows that

$$\langle \gamma_j^1(\theta, \theta_s, \phi_s)\rangle\Big|_{\substack{\theta_s=\theta\\ \phi_s=\pi}} = \frac{1}{2\pi}\int_{-\pi/2}^{\pi/2}\left\{\gamma_j^1(\theta', \phi', \theta_s', \phi_s')\Big|_{\substack{\theta_n=\tan^{-1}(m)\\ \theta_s'=\theta'\\ \phi_s'=\phi'+\pi}} + \gamma_j^1(\theta', \phi', \theta_s', \phi_s')\Big|_{\substack{\theta_n=\tan^{-1}(m)\\ \theta_s'=\theta'\\ \phi_s'=\phi'+\pi}}\right\} d\phi_n$$

$$j = h, v \tag{3.42}$$

Thus from (3.3c) and (3.42),

$$\langle \sigma^{\circ}_{Bj1}(\theta)\rangle = \frac{1}{2\pi}\int_{-\pi/2}^{\pi/2}\left\{\sigma^{\circ}_{Bj1}(\theta')\Big|_{\theta_n=\tan^{-1}(m)} + \sigma^{\circ}_{Bj1}(\theta')\Big|_{\theta_n=-\tan^{-1}(m)}\right\} d\phi_n \tag{3.43}$$

$$j = h, v$$

where

$$\sigma^{\circ}_{Bh1}(\theta') = \cos\theta'\, \gamma^{1}_{h}(\theta', \phi', \theta_s', \phi_s')\Big|_{\substack{\phi_s' = \phi' + \pi \\ \theta_s' = \theta'}}$$
$$= 4k^4 \sigma_1^2 \ell^2 \cos^4\theta' \left| R_h(\theta') \right|^2 \exp(-k^2\ell^2 \sin^2\theta') \qquad (3.44)$$

and

$$\sigma^{\circ}_{Bv1}(\theta') = \cos\theta'\, \gamma^{1}_{v}(\theta', \phi', \theta_s', \phi_s')\Big|_{\substack{\phi_s' = \phi' + \pi \\ \theta_s' = \theta}}$$
$$= 4k^4 \sigma_1^2 \ell^2 \cos^4\theta' \left| \frac{(\epsilon_r - 1)[(\epsilon_r - 1)\sin^2\theta' + \epsilon_r]}{[\epsilon_r \cos\theta' + (\epsilon_r - \sin^2\theta')^{1/2}]^2} \right|^2 \exp(-k^2\ell^2 \sin^2\theta') \qquad (3.45)$$

The complete backscattering cross-section is, of course, given by (3.3a) that is the sum of (3.40) and (3.43).

3.3 SELECTION OF PARAMETERS

The surface parameters that appear in the above theory are the rms slope of the large structures m, the standard deviation of the small structures σ_1, and the correlation length of the small structures ℓ. This scattering model can be adapted to predict sea returns by noting that the rms slope can be based on measurements by Cox and Munk (1952) and that the assumed Gaussian spectrum for the small irregularities can approximate the high frequency part of the sea spectrum BK^{-4}, where the Bragg scatter condition applies, i.e., $K = 2k \sin\theta$. In view of the requirements of the composite surface theory it is reasonable to choose the oil slick sea measurements by Cox and Munk, since the small irregularities have been suppressed. The value of m is thus assigned. The value of $k\ell$ is assigned so that the correct angular behavoir of the Gaussian spectrum approximated BK^{-4} well over the angular range, $30^\circ \leq \theta \leq 70^\circ$ i.e., BK^{-4} is approximated by $\sigma_1^2 \ell^2/\pi \exp(-K^2\ell^2/4)$ where $K = 2k \sin\theta$, the Bragg scatter condition. This approximation is achieved by noting that when $k\ell = 2$ similar behavoir is realized (see Figure 3.4). The factor 35.3 appears in the Gaussian approximation to bring the levels into agreement at $\theta = 60$ degrees. The value of B must yet be assigned.

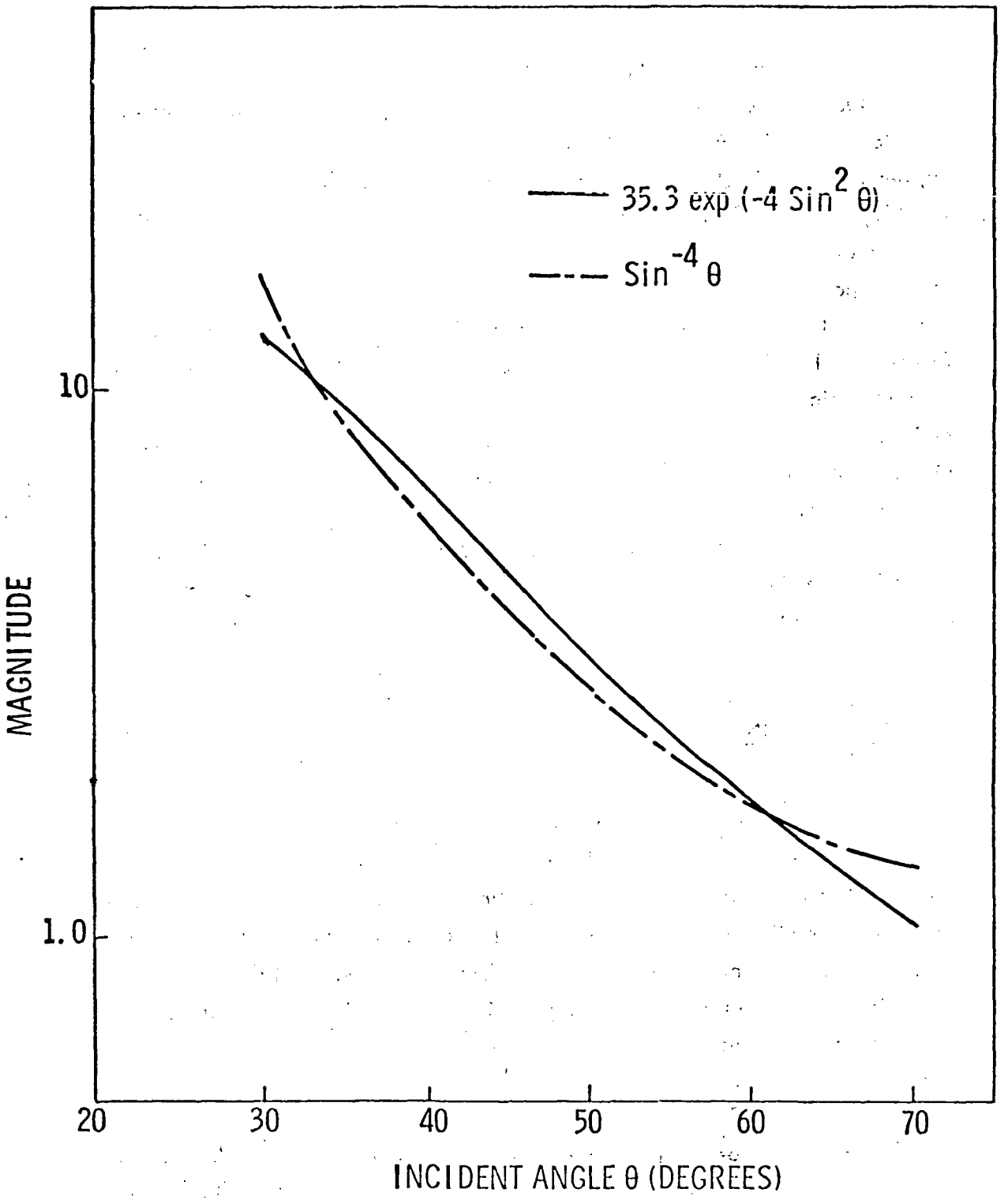

Figure 3.4 Comparison of the angular variations of $\sin^{-4}\Theta$ and 35.3 exp ($-4 \sin^2\Theta$).

Oceanographic investigations indicate values of B in the range from 4.6×10^{-3} to 3.26×10^{-2} (Cox and Munk, 1954, Pierson, 1970, Phillips, 1966). This implies that $k\sigma_1$ should lie in the range from 0.084 to 0.24 when BK^{-4} is equated to $\sigma_1^2 \ell^2/4 \exp(-K^2\ell^2/4)$ at $\theta = 60$ degrees. These values of $k\sigma_1$ are consistent with the assumptions of the small perturbation theory, an encouraging result. The recent reports by Sutherland (1967) and Pierson et al. (1971) indicate that B is a function of the wind speed. Thus, the surface parameter $k\sigma_1$ must also be a function of the wind speed. It is noted that the horizontally polarized emission characteristic for nadir angles from zero to thirty degrees is very sensitive to $k\sigma_1$ and hence the parameter $k\sigma_1$ can be estimated by fitting the predicted emission characteristics to the measured data. (It appears that the wind sensitivity of B may be assigned by this technique.)

With the surface parameters established in the manner described above, both the emission and backscatter characteristics may be computed and compared with reported measurements.

3.4 COMPARISON WITH EXPERIMENTS

The parameter $k\sigma_1$ is estimated from horizontally polarized emission characteristics at 8.36 GHz associated with two distinct wind speeds. The emission characteristics are based on an average of several of Hollinger's experiment runs under similar wind stress conditions (Cardone, 1969). The data reported by Hollinger are in the form of surface brightness temperature. Effects due to foam and the reflected sky radiation have been removed (Hollinger, 1971a). The vertically polarized emission characteristic is computed from the estimated $k\sigma_1$. These results are shown in the graphs of Figures 3.5 and 3.6. The dielectric constant is based on data reported by Saxton and Lane (1952).

Comparison of the predictions of this emission model indicates a significantly improved agreement over that predicted by a single-surface model. Better level and trend agreement is evident for both horizontally and vertically polarized emissions. Sensitivity to wind speed is evident at nadir which is not noted with the single-surface model. The sensitivity at nadir is carried by the modified Fresnel coefficient (see Equation (3.35)).

The adequacy of the composite-surface theory is further demonstrated when the predicted backscatter characteristics are compared with measured characteristics. Data at 8.91 GHz reported by Daley, et al., (1971) at similar wind stress conditions were chosen as a basis for comparision. The dielectric constant is changed to reflect the influence of the slightly different frequency. The comparison of predicted and measured characteristics are shown in Figure 3.7 to 3.10. These results indicate reasonable agreement with measurements and improved agreement over the predictions of the simple geometric optics approach (single-surface model). It is noted that the best agreement with measurements occurs primarily at larger angles and for vertical polarization. There is some uncertainty in the accuracy of the measurements near nadir (Daley et al., 1971) so lack of agreement may be anticipated there. The discrepancy at large angles for horizontally polarized cross sections may be attributable to receiver noise at these small cross sections. This statement is, however, speculative.

The level of NRL data which are based on the statistical median had to be raised by 6 dB to realize the agreement. Valenzuela et al., (1971) indicated that the average cross section was about 4.6 dB above the median based on exponential statistics assumed for the returns. As a consequence, 1.4 dB remains unaccounted for. Perhaps the remaining 1.4 dB may be partially associated with the biases disclosed by Claassen and Fung (1972).

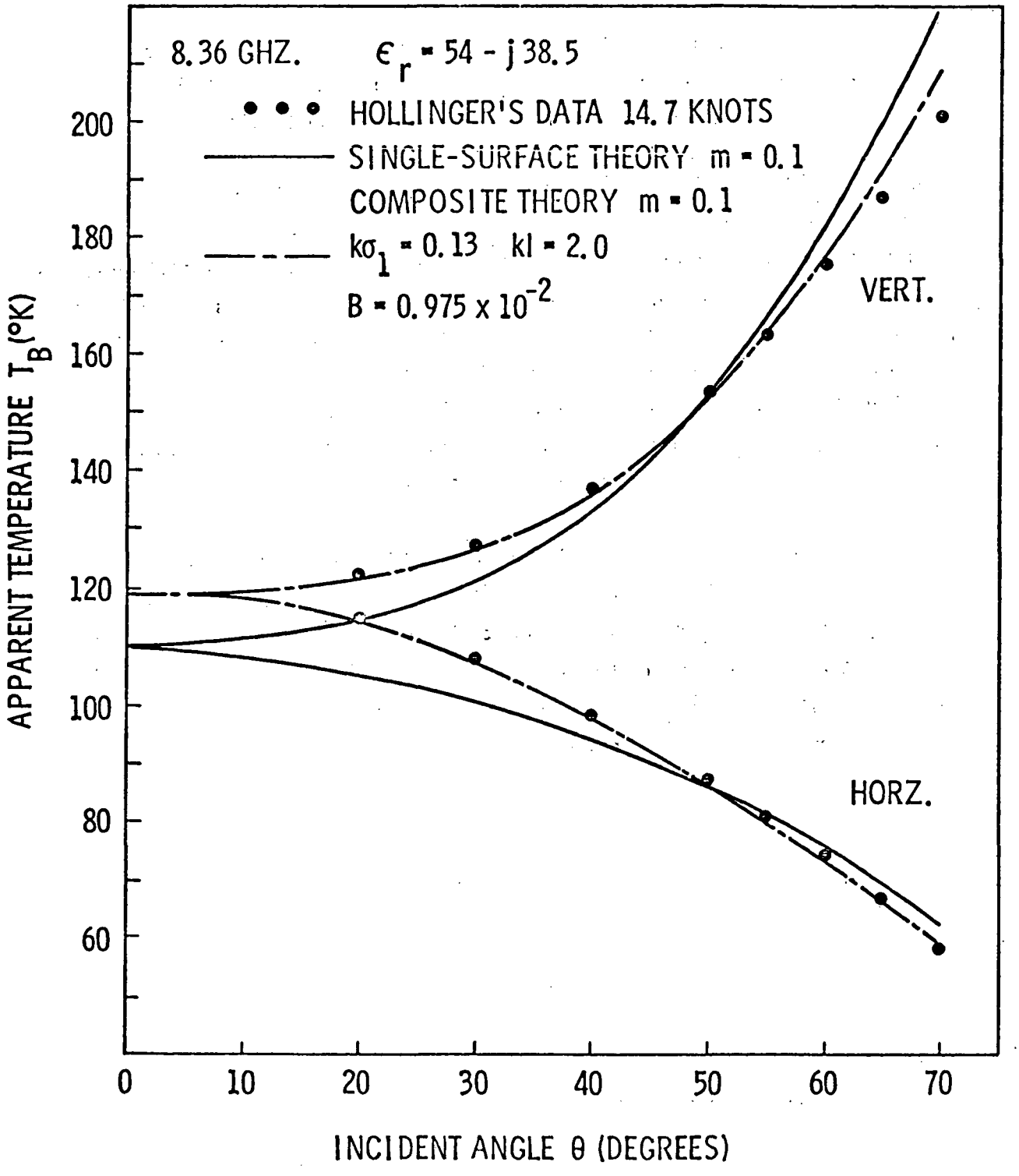

Figure 3.5 Comparison of surface brightness temperature between the measured data and theoretical calculations using the composite-surface theory and the single-surface theory (after Stogryn).

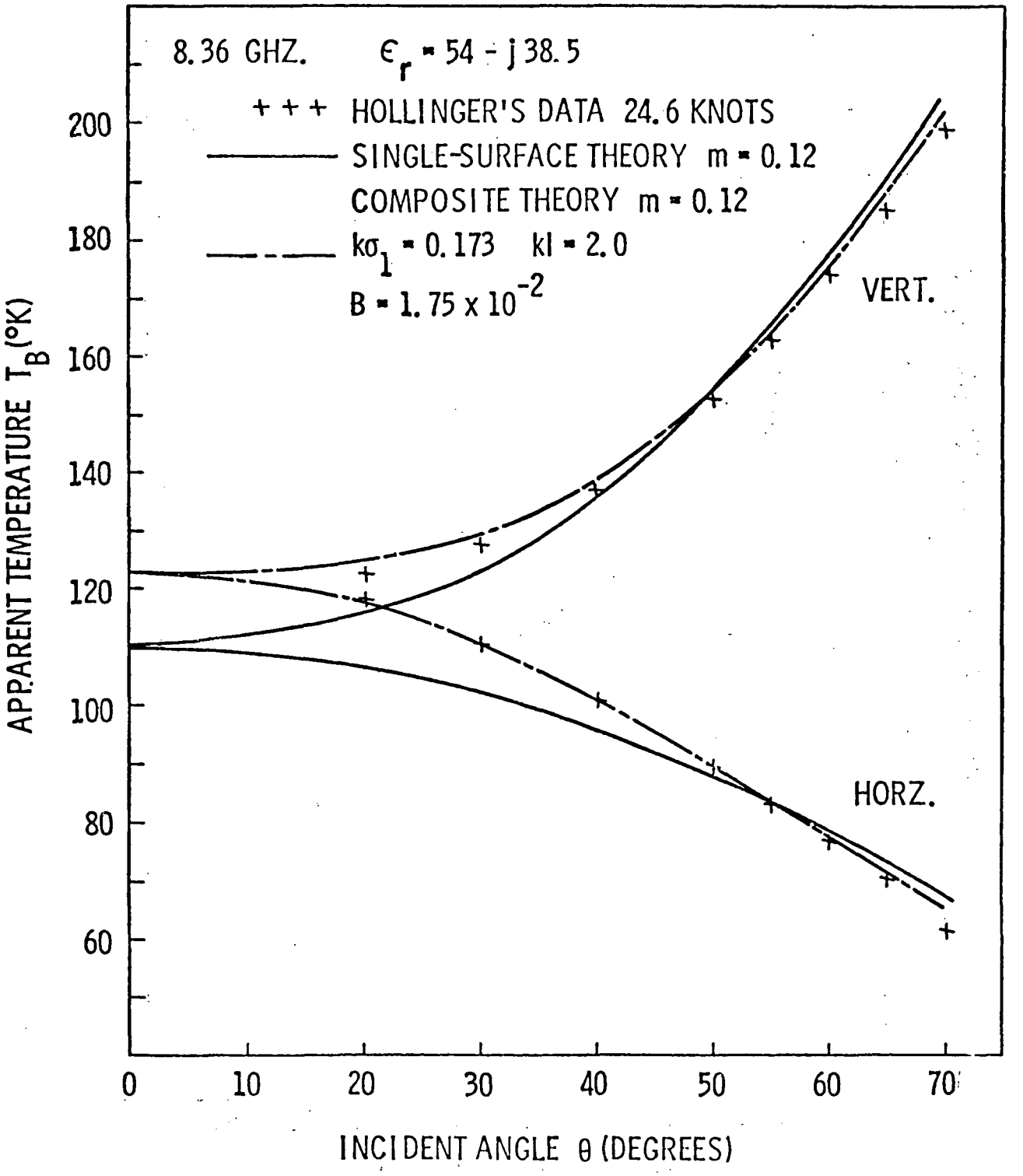

Figure 3.6 Comparison of surface brightness temperature between the measured data and theoretical calculations using the composite-surface theory and the single-surface theory (after Stogryn).

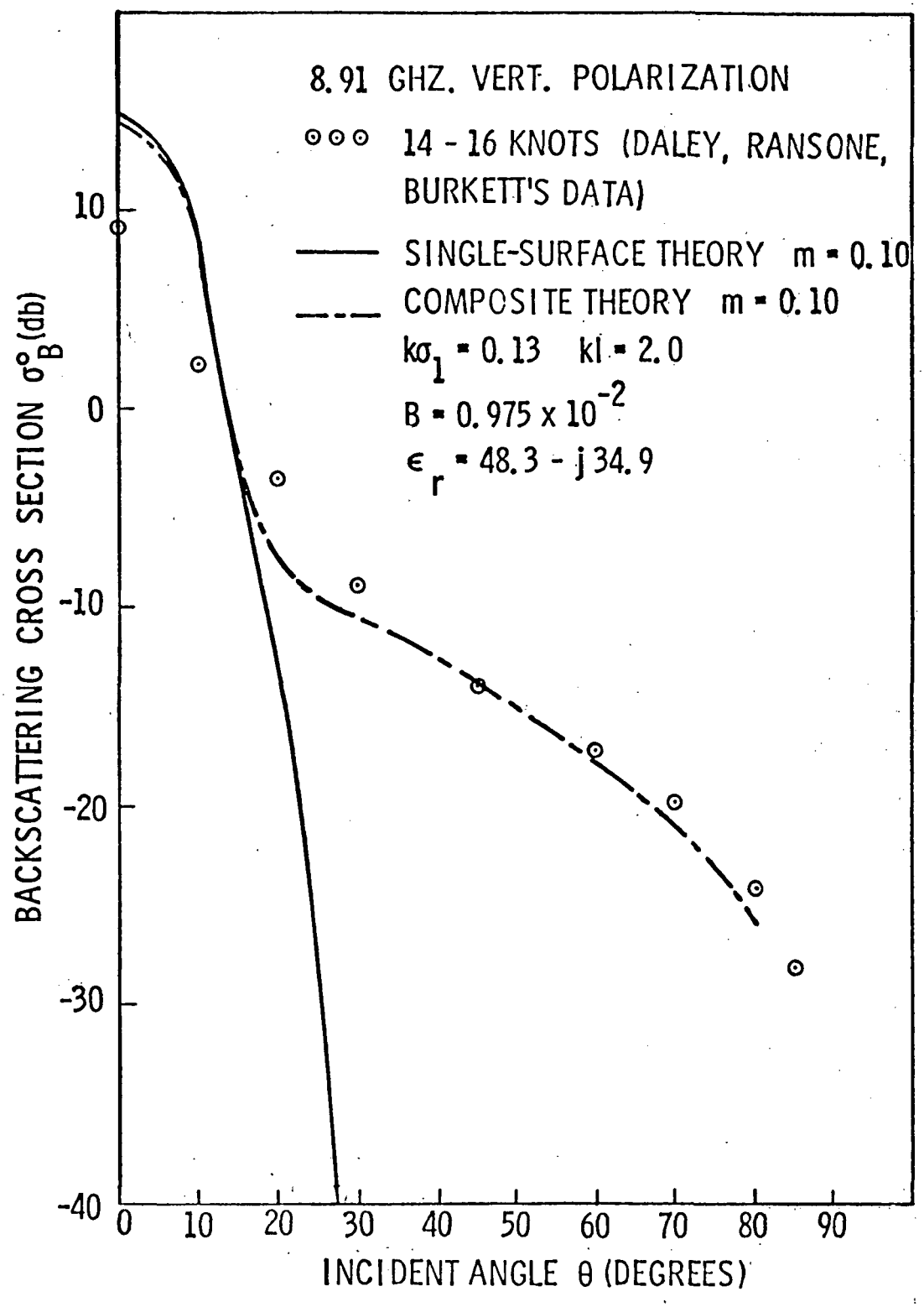

Figure 3.7 Comparison of backscattering cross-section between the measured data and theoretical calculations using the composite-surface theory and the single-surface theory (after Stogryn).

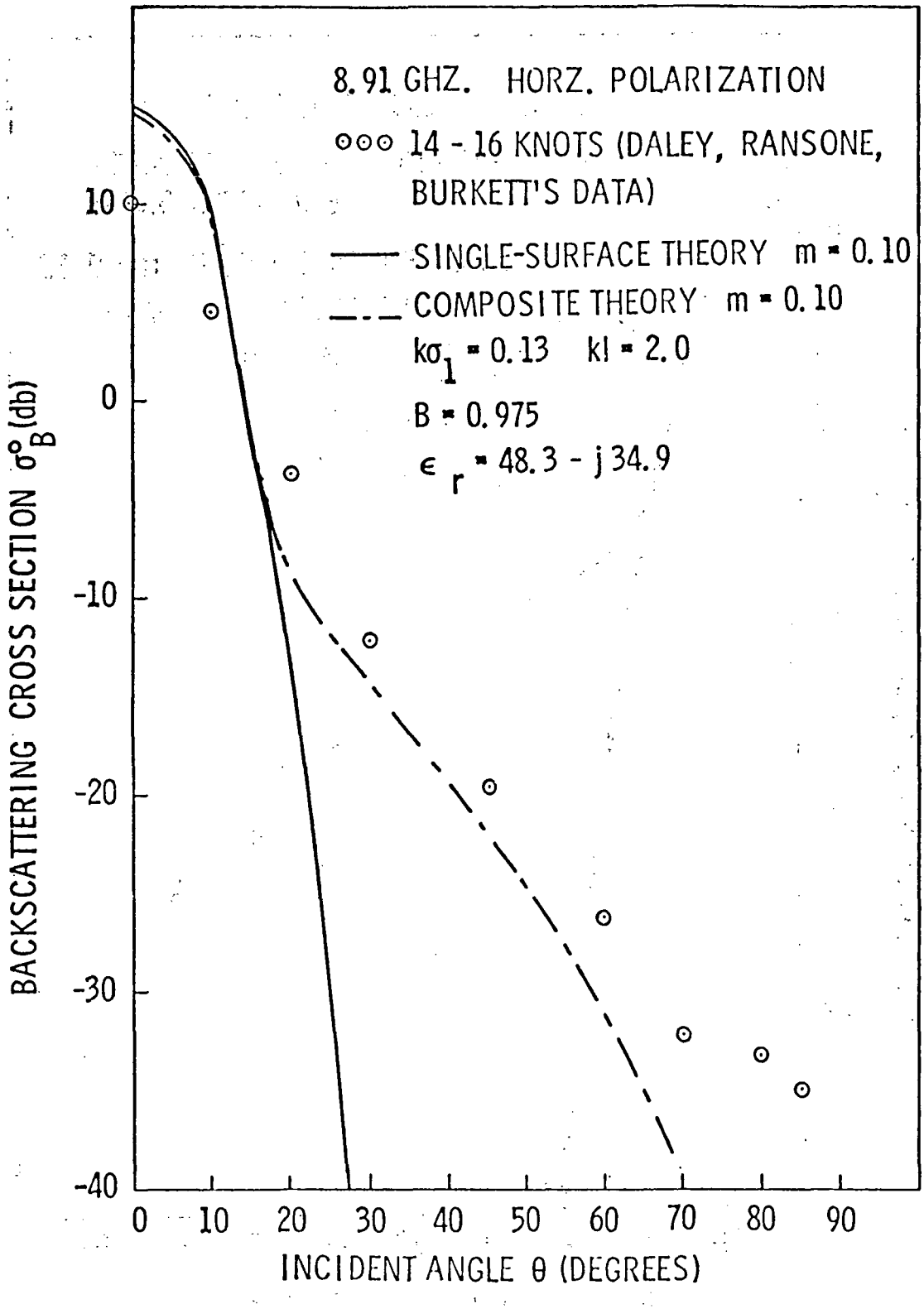

Figure 3.8 Comparison of backscattering cross-section between the measured data and theoretical calculations using the composite-surface theory and the single-surface theory (after Stogryn).

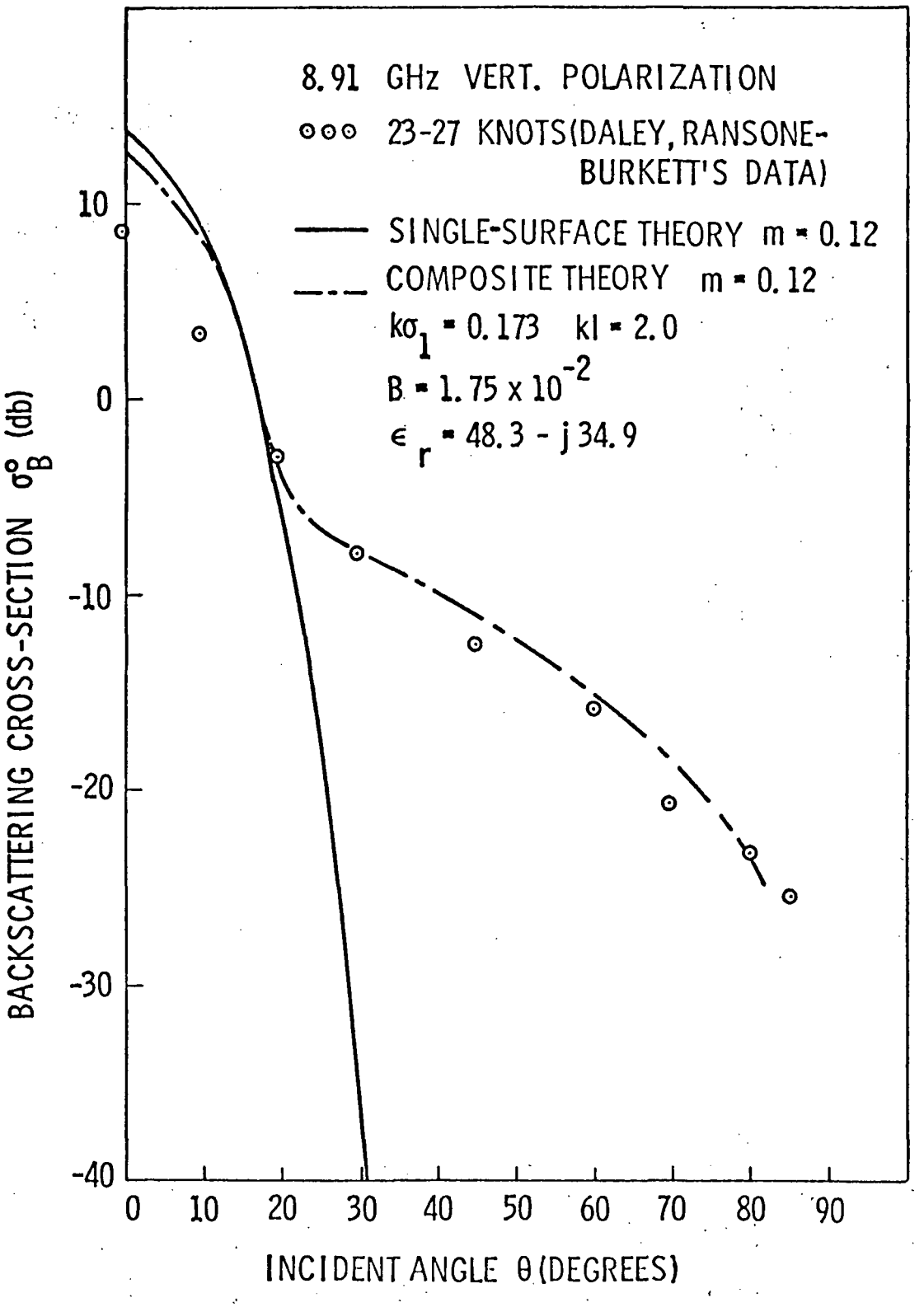

Figure 3.9 Comparison of backscattering cross-section between the measured data and theoretical calculations using the composite-surface theory and the single-surface theory (after Stogryn).[49]

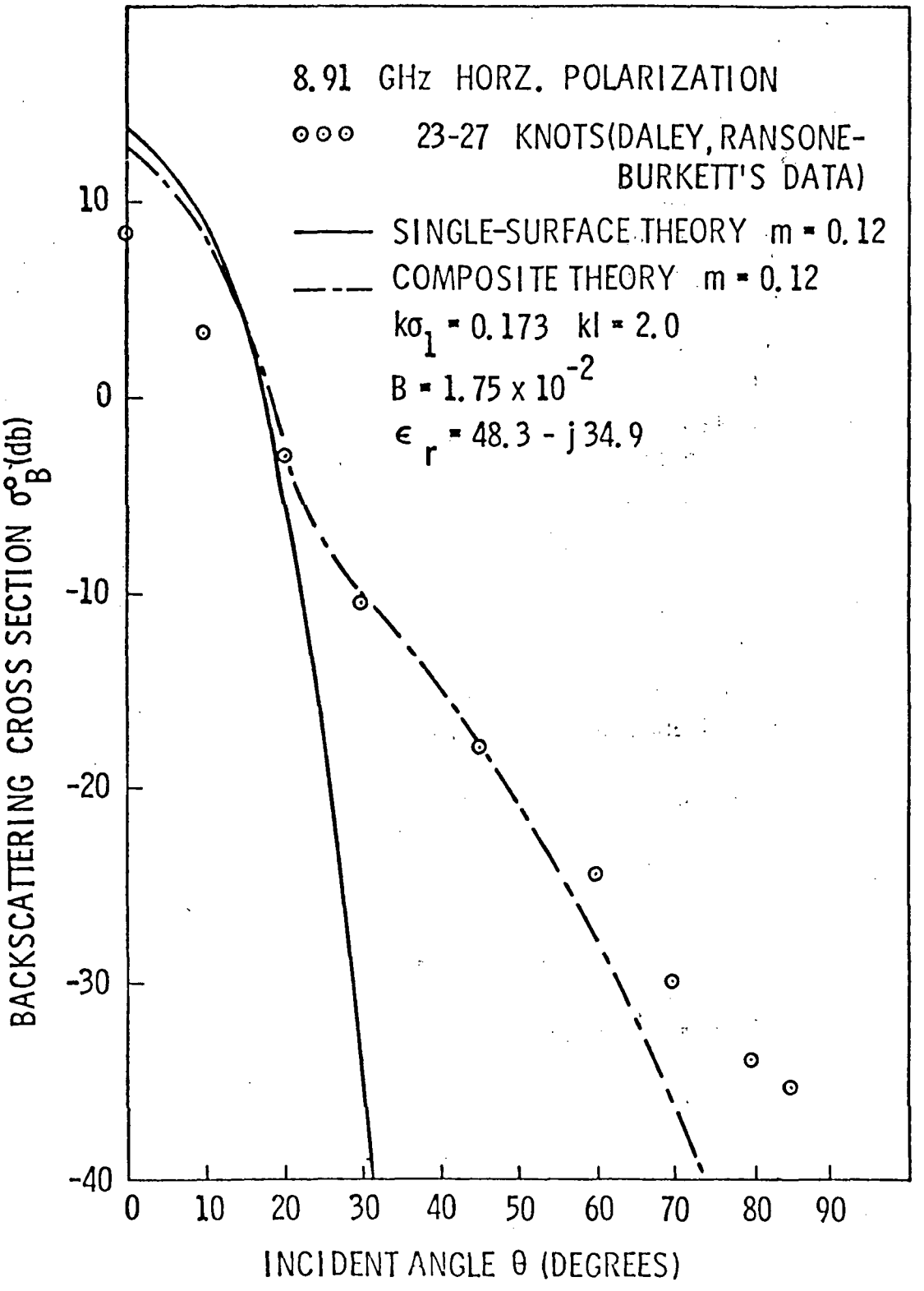

Figure 3.10 Comparison of backscattering cross-section between the measured data and theoretical calculations using the composite-surface theory and the single-surface theory (after Stogryn).

CHAPTER 4

THE EFFECTS OF CLOUDS AND RAIN ON THE MICROWAVE APPARENT TEMPERATURE

4.1 INTRODUCTION

High winds over the ocean are usually accompanied by clouds and rain (Claassen, et al., 1971). These meteorological conditions influence radiometric observations over the ocean primarily because of atmospheric absorption (emission). In the particular case of heavy rain fall, radiometric measurements are affected also be scattering due to rain drops. It is the aim of this chapter to discuss these meteorological effects on the measured or computed apparent temperature as observed by a radiometer.

In clear sky the contributions to the apparent temperature are mainly due to the absorption of the molecular oxygen and water vapor present in the atmosphere. The absorption of these constituents can be calculated by using the well developed formulas (Meeks and Lilley, 1963; Staelin, 1966) and the model atmosphere which describes the temperature, the pressure and the moisture profiles (Valleys, 1965). Hence, in clear sky the apparent temperature due to the atmosphere is reasonably well defined.

In cloudy sky, the liquid water content of the cloud absorbs and hence emits microwave radiation in addition to the effects of the molecular oxygen and water vapor already present under clear sky conditions. Furthermore, different kinds of cloud with various spatial distributions may be present in the atmosphere. Consequently to investigate the cloud effect on the measured apparent temperature is a much more complicated problem than the clear sky case.

In rainy sky the raindrops not only can absorb but also scatter microwave radiation in all directions. If the size of the rain-drop is much smaller than the incident wavelength, it has been shown (Kerr, 1951) that the scattered energy is negligible as compared to the absorbed energy. The terms representing scattering effects in the radiative transfer equation can therefore be ignored. However, when the size of raindrops is comparable to the incident wavelength, the scattered energy

becomes significant and the scattering effect has to be included. In the later case a mathematically involved formulation is needed to solve the problem.

The apparent temperature contribution to the surface brightness temperature by clouds and rain have been reported by Singer and Williams (1968) at 15.89 GHz. Additional observations at 19.45 GHz were reported by Conaway (1969) and Kreiss (1969). On the other hand, theoretical investigations of cloud and rain effects, except for the efforts of Kreiss (1969) and Porter (1971) have largely been limited to cases in which only the sky temperature is computed (Stogryn, 1964; Shifrin, 1969).

Other radiometric measurements have documented the effects of clouds and rain on the sky temperature, i.e. looking upward. For example, Haroules and Brown (1969) in a comprehensive set of measurements have measured sky temperature and inferred atmospheric attenuation. The attenuations and sky temperatures of various cloud and rain conditions shown in Table 4.1 are an excerpt of their data. Other extensive measurements of this type have been reported by Strickland (1970), Crane (1971), and Ippolito (1971) in conjunction with the ATS-V communication satellite experiments. From these results the apparent temperature when looking downward may be qualitatively described.

Radiometric measurements conducted over clouds and rain will experience an attenuated surface brightness temperature plus a cloud or rain contribution in excess of the clear sky temperature. When the attenuation due to clouds and rain is sufficiently large it is possible for the radiometer to lose contact with the surface. The greater sensitivity of the radiometer to clouds and rain can be employed to correlate the increased apparent temperature with attenuation when clouds or rain intervene. This attenuation measured from the excess apparent temperature, in turn, can be used to calibrate scatterometer measurements and to determine when scatterometer data should be discarded due to the presence of heavy rain. Although the relation between atmospheric attenuation and apparent temperature has been studied for upward looking radiometers, and measurements have shown that the expected temperature enhancements do indeed occur for downward looking radiometers, this is believed to be the first study aimed specifically at determining the relationship between brightness temperature and attenuation for the downward looking radiometer. Apparent temperatures for various meteorological conditions are computed by employing the models postulated by meteorologists. Comparison of the apparent temperature with attenuation has justified the general idea of the use of radiometer

TABLE 4.1

ATTENUATION AND BRIGHTNESS TEMPERATURE OF CLOUDS AND RAIN

Cloud Type	One-Way Attenuation		T_{sky}	
	8 GHz dB	15 GHz dB	8 GHz °K	15 GHz °K
High Level	.02-.05	.03-.07	7	15
Medium Level	.03-.12	.08-.13	10	21
Low Level	.10-.25	.17-.40	14	30
Light Rain	.15-.25	.20-.60	16	38
Medium Rain	.80	3.2	20	43
Heavy Rain	1.5	5.4	70	140

to calibrate the scatterometer. The surface roughness model needed in the computation is based on the composite surface model developed in Chapter III.

4.2 THEORETICAL APPROACH

4.2.1 The Radiative Transfer Equation

To study the radiative transfer problem of the planets, astronomers have formulated the equation of radiative transfer. By solving this equation the intensity of radiation from the planets under specific conditions can be obtained. A downward looking radiometer at an altitude z above the ground surface receives the intensity of radiation from the ground surface as well as the intervening atmosphere. Hence the radiative transfer equation can also be applied to compute the intensity of radiation received by the radiometer. The radiative transfer equation for radiometric temperature computation has already been formulated (Stogryn, 1964; Shifrin, 1969). In radiometric temperature computation, the apparent temperature at any point is defined as the temperature of an equivalent blackbody which emits the same intensity as the existing radiation intensity at any point. Thus, at microwave frequency, the apparent temperature $T_{aj}(z, \theta, \phi)$ is related to the radiation intensity $I_j(z, \theta, \phi)$ in the form

$$I_j(z, \theta, \phi) = \frac{K \nu^2}{c^2} T_{aj}(z, \theta, \phi) \tag{4.1}$$

where j represents the polarization state either horizontal (h) or vertical (v) polarization; K is the Beltzman's constant; ν is the propagation frequency; c is the velocity of light, and z, θ, ϕ are the coordinates that specify the point of interest.

In what follows we shall assume a uniform horizontally stratified atmosphere and choose a coordinate system with the z axis normal to the earth surface and the origin at the earth-atmosphere boundary directly below the point in the atmosphere under consideration (Figure 4.1). By expressing the apparent temperature at point z and in the direction θ and ϕ as $T_{aj}(z, \theta, \phi)$, and assuming (1) the mechanism of raindrop scattering to be a random function uniformly distributed from 0 to 4π steradian for both polarizations, and (2) the radiation process to be

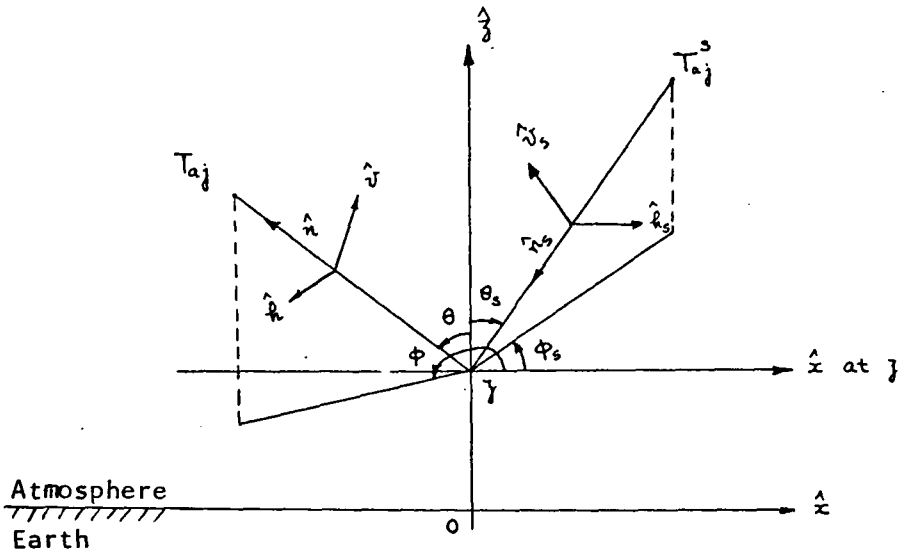

Figure 4.1 The coordinate system in the atmosphere for expressing the incident and scattering of the polarized apparent temperature.

dominated by thermal radiation, the radiative transfer equation may be written in the form (Stogryn, 1964)

$$\cos\theta \frac{dT_{aj}(z,\theta,\phi)}{dz} + [\alpha(z)+\beta_{sc}(z)]\,T_{aj}(z,\theta,\phi) = \alpha(z)\,T_{air}(z) + \beta_{sc}(z)\int_0^{2\pi}\int_0^{\pi}\gamma(\cos\Theta)\,T_{aj}(z,\theta_s,\phi_s)\sin\theta_s\,d\theta_s\,d\phi_s \qquad j = h \text{ or } v \qquad (4.2)$$

where $T_{aj}(z,\theta,\phi)$ is the apparent temperature with j polarization at an altitude of z and in the direction θ and ϕ. The first term on the righthand side of (4.2), namely $\alpha(z)T_{air}(z)$, is the source function due to thermal radiation. $\alpha(z)$ is the total absorption coefficient of the atmosphere, $T_{air}(z)$ is the thermometric temperature profile of the atmosphere. The second term on the righthand side of (4.2) is the source function due to particle scattering (for instance, rain drops) of the incident radiation from all directions into the direction of interest. $\beta_{sc}(z)$ is the scattering coefficient of precipitation per unit volume at an altitude z ; $\gamma(\cos\Theta)$ is the scattering phase function of precipitation per unit volume with

$$\cos\Theta = \cos\theta\cos\theta_s + \sin\theta\sin\theta_s\cos(\phi-\phi_s) \qquad (4.3)$$

θ, Φ = observing angles

θ_s, Φ_s = scattering angles.

A detailed analysis of $\beta_{sc}(z)$ and $\gamma(\cos\Theta)$ will be presented in the following section.

4.2.2 Apparent Temperature Theory with β_{sc} Neglected

Under clear sky, cloudy sky and light to moderate rain conditions the effects of scattering by the atmospheric constituents may be neglected for observation frequencies less than 20 GHz (Porter, 1970). Under these conditions, the source function in (4.2) consists only of the thermal radiation term and (4.2) reduces to the form:

$$\cos\theta \frac{d T_{aj}(z,\theta,\Phi)}{dz} + \alpha(z) T_{aj}(z,\theta,\Phi) = \alpha(z) T_{air}(z) \quad (4.4)$$

For uniformly straitified atmosphere bounded below by an isotropic surface, there is no azimuthal variation. For this case (4.4) becomes

$$\cos\theta \frac{d T_{aj}(z,\theta)}{dz} + T_{aj}(z,\theta)\,\alpha(z) = T_{air}(z)\,\alpha(z) \quad (4.5)$$

Equation (4.5) is a first order differential equation. It can be solved with appropriate boundary conditions. The solution for a downward looking radiometer situated at an altitude z above the ground has been found to be (Stogryn, 1967)

$$T_{aj}(z,\theta) = L(z,\theta)\left[\epsilon_j(\theta) T_g + T_{rj}(\theta)\right] + T_{atm}(z,\theta) \quad (4.6)$$

$$j = h \text{ or } v$$

where $T_{aj}(z,\theta)$ = apparent temperature at an altitude z, and nadir angle θ.

$L(z,\theta)$ = transmittance

$$= \exp\left[-\sec\theta \int_0^z \alpha(u)\,du\right] \quad (4.7a)$$

$\alpha(z)$ = total absorption coefficient of the atmosphere at an altitude z.

$\epsilon_j(\theta)$ = surface emissivity (see explanation in Chapter III)

T_g = surface thermometric temperature

$T_{atm}(z,\theta)$ = atmospheric temperature

$$= \sec\theta \int_0^{z} T_{air}(z')\, \alpha(z') \exp\left[-\sec\theta \int_{z'}^{z} \alpha(u)\, du\right] dz' \quad (4.7b)$$

$T_{air}(z)$ = thermometric temperature profile of the air

$T_{rj}(\theta)$ = reflected sky temperature

$$= \frac{1}{4\pi} \int_0^{2\pi} \int_0^{\pi/2} \gamma_j(\theta, \theta_s, \phi_s)\, T_{sky}(\theta_s) \sin\theta_s\, d\theta_s\, d\phi_s \quad (4.7c)$$

$\gamma_j(\theta, \theta_s, \phi_s)$ = polarized differential scattering coefficients of the surface.

$T_{sky}(\theta_s)$ = sky temperature

$$= \sec\theta_s \int_0^{\infty} T_{air}(z')\, \alpha(z') \exp\left[-\sec\theta_s \int_0^{z'} \alpha(u)\, du\right] dz' \quad (4.7d)$$

As shown in (4.6) and (4.7) the apparent temperature contains the attenuated surface brightness temperature, $\epsilon_j(\theta) T_g$, as well as the direct and reflected temperature contributions from the atmosphere. To compute the apparent temperature $T_{aj}(z, \theta)$, we use the surface roughness model developed in previous chapters and assume sea water temperature to be 290°K. To account for the temperature contribution from the atmosphere the ARDC standard atmosphere which describes the temperature, the pressure and the water vapor profiles and the absorption coefficients of various constituents due to different weather conditions are needed. The weather model proposed by meteorologists that describes the spatial distribution of liquid water content and precipitation rates needed in the apparent temperature computation will be discussed separately in the following section.

For an ARDC standard atmosphere, the temperature, pressure and water vapor profiles with altitude are given by:

$$T_{air}(z) = T_g - 6.5\, z \ ^\circ K \quad \text{for } z \le 11 \text{ km}$$
$$= T_g - 71.5 \ ^\circ K \quad \text{for } z > 11 \text{ km} \quad (4.8a)$$

$$P(z) = P_g \exp[-0.143\, z] \quad (4.8b)$$

$$\rho(z) = \rho_g \exp[-z/2.2] \quad (4.8c)$$

where,

T_g = sea surface temperature in ^oK.

P_g = sea surface pressure in mm of Hg.

ρ_g = sea surface water vapor density in gm/m^3.

ζ = altitude in km.

For multiple constituent atmosphere and by linear superposition, the total absorption coefficient $\alpha(\zeta)$ in (4.5) and (4.7) can be written in the form

$$\alpha(\zeta) = \alpha_{cs}(\zeta) + \alpha_{cld}(\zeta) + \alpha_{rain}(\zeta) \qquad (4.9)$$

where

$\alpha_{cs}(\zeta)$ = clear sky absorption coefficient

$\alpha_{cld}(\zeta)$ = cloud absorption coefficient

$\alpha_{rain}(\zeta)$ = rain absorption coefficient

If there is no cloud or rain, the total absorption coefficient $\alpha(\zeta)$ is due to clear sky absorption only. The same kind of argument can be applied to the other weather conditions.

A) Clear Sky Absorption Coefficient

The two major contributors to the clear sky microwave absorption spectrum are oxygen and water vapor, thus, the clear sky absorption coefficient is

$$\alpha_{cs}(\zeta) = \alpha_{O_2}(\zeta) + \alpha_{H_2O}(\zeta) \qquad \text{neper/km} \qquad (4.10)$$

A.1) Molecular Oxygen

The oxygen molecule absorbs microwave energy through the interaction of its magnetic dipole moment with the electromagnetic field. This phenomena was used by Van Vleck (1947a) to develop expressions for the absorption spectra of molecular oxygen in the microwave region. Oxygen has a series of absorption lines near 60 GHz (often referred to as the oxygen complex) and a single line at 118.75 GHz. Using 60 GHz as a central line, Van Vleck derived an approximate expression for the absorption by the oxygen complex valid for frequencies outside the 50-70 GHz region. The dependence of the oxygen absorption on temperature and pressure was further investigated by many investigators (Hill and Gordy, 1954; Artman and Gordon,

1954; Zimmerer and Mizushima, 1961; and Meeks and Lilley, 1963). The more recent results for calculating the microwave absorption by oxygen (outside the 50-70 GHz region) may be summarized by the following expressions:

$$\alpha_{O_2}(\zeta) = \alpha_{60}(\zeta) + \alpha_{118}(\zeta) \qquad \text{nep/km} \qquad (4.11)$$

where,

$$\alpha_{60}(\zeta) = K_{60}\,\gamma\,\nu^2\left[\frac{\Delta\nu}{(60-\nu)^2+\Delta\nu^2} + \frac{\Delta\nu}{(60+\nu)^2+\Delta\nu^2} + \frac{\Delta\nu}{\nu^2+\Delta\nu^2}\right] \quad (4.12a)$$

$$\alpha_{118}(\zeta) = K_{118}\,\gamma\,\nu^2\left[\frac{\Delta\nu}{(118.75-\nu)^2+\Delta\nu^2} + \frac{\Delta\nu}{(118.75+\nu)^2+\Delta\nu^2}\right] \quad (4.12b)$$

ν = frequency in GHz

$K_{60} = 83.50$

$K_{118} = 1.20$

$$\gamma = \frac{0.21\,P(\zeta)}{[T_{air}(\zeta)]^3}$$

$$\Delta\nu = 1.5\left(\frac{P(\zeta)}{760}\right)\left(\frac{293}{T_{air}(\zeta)}\right)^{1/2} \qquad (4.13)$$

$P(\zeta)$ = atmospheric pressure in mm Hg at altitude ζ.

$T_{air}(\zeta)$ = atmospheric temperature in °K at altitude ζ.

A.2) Water Vapor

Though water vapor has only two absorption lines in the microwave part of the electromagnetic spectrum, at 22.23 GHz and 183.3 GHz, the cumulative effect of the large number of submillimeter water vapor line can be significant. Using a low frequency approximation for the line shape factor, Van Vleck (1947b) derived an approximate expression for the residual effect of all the major water vapor lines whose resonances are higher than 30 GHz (thereby including the 183.3 GHz line). These expressions were later modified by other investigators (Barrett and Chung, 1962; Chung, 1962; and Staelin, 1966) to include the dependence on temperature, pressure and water vapor density using experimentally determined values for the line with parameter, $\Delta\nu$. Thus water vapor absorption can be expressed as:

$$\alpha_{H_2O}(\zeta) = \alpha_{22}(\zeta) + \alpha_{res}(\zeta) \qquad (4.13)$$

$$\alpha_{22}(\zeta) = K_{22}\,\gamma_{22}\,\nu^2\left[\frac{1}{(22.235-\nu)^2+\Delta\nu^2} + \frac{1}{(22.235+\nu)^2+\Delta\nu^2}\right] \quad (4.14a)$$

$$\alpha_{res}(\zeta) = K_{res}\,\nu^2\,\Delta\nu\,\frac{\rho(\zeta)}{[T_{air}(\zeta)]^{1.5}} \quad \text{nep/km} \quad (4.14b)$$

$$K_{22} = 43.2$$

$$K_{res} = 2.55 \times 10^{-3}$$

$$\gamma_{22}(\zeta) = P(\zeta)\,\rho(\zeta)\left(1 + 0.11\,\frac{\rho(\zeta)\,T_{air}(\zeta)}{P(\zeta)}\right)[T_{air}(\zeta)]^{-3.125}\exp\left[-644/T_{air}(\zeta)\right] \quad (4.14c)$$

$$\Delta\nu = 2.62\left(1 + 0.001\,\frac{\rho(\zeta)\,T_{air}(\zeta)}{P(\zeta)}\right)P(\zeta)/760\,[T_{air}(\zeta)/318]^{-0.625} \quad (4.14d)$$

$\rho(\zeta)$ = water vapor density in gm/m^3 at altitude ζ.

B) The Absorption Coefficient of Cloud and Rain

Ryde and Ryde (1946) were the first to calculate the attenuation of clouds and rain based on Mie's theory (1908), and their result has been the basis for much of the subsequent works. By using Laws and Parsons(1943) drop-size distribution of various precipitation rates, they calculated the theoretical attenuation coefficient of rain directly in terms of eight different precipitation rates with eight wavelengths from 0.3 to 10 cm at 18°C. For temperature different from 18°C, the correction factor is tabulated from 0 to 40°C at 10°C interval.

For non-precipitating clouds with drop radii much less than the wavelength, the familiar Rayleigh scattering equation was used by Goldstein (1951) to calculate cloud attenuation.

Gunn and East (1954) not only reviewed Ryde's development since 1946, but added the backscattering cross section calculation for clouds and rain which has been widely quoted in radar meteorology. The dielectric constant of ice is very much different from water. Consequently they calculated the attenuation of ice and water clouds separately, and the temperature effect was also included.

Medhurst (1965), using Ryde's theoretical approach, re-calculated the attenuation for rain with five precipitation rates and sixteen wavelengths from 0.3 to 15 cm at 20°C. He also collected rain attenuation measurements from 1946 to 1962, and compared with his theoretical result. He used a set of theoretical maximum and minimum attenuations for rain to compare with measurements and concluded that the agreement was not entirely satisfactory. There was a tendency

for measured attenuation to exceed the maximum possible levels predicted by the theory. But recent measurements by Brown and Haroules (1969) at 8 GHz to 15 GHz indicate that there is no tendency for measured attenuations to lie above the theoretical maximum values. Hence theoretical calculations seem to provide a reasonable basis for the prediction of attenuation by rain.

Benoit (1968) interpolated Gunn and East's discrete data with respect to frequency and temperature and have come out with one simple empirical equation very convenient for computation purposes, particularly when the temperature varies continuously with respect to height in the atmosphere.

Following Benoit's result, the absorption coefficient for clouds is expressed in the form

$$\alpha_{cld}(\ell) = M\, \nu^{b}\, exp(a) \qquad (4.15)$$

M = liquid water content of clouds in gm/m^3

ν = propagating frequency in GHz

b = frequency index

b_ω = 1.95 for water cloud

b_i = 1.006 for ice cloud

a = temperature coefficient

$$a_\omega = -6.866\,[1 + 0.0045\,(T_{air}(\ell) - 273)]$$

$$a_i = -8.261\,[1 - 1.767 \times 10^{-2}(T_{air}(\ell) - 273) - 4.374 \times 10^{-4}(T_{air}(\ell) - 273)^2]$$

Figure 4.2 shows Gunn and East's original discrete data and the straight lines were drawn by Benoit using the interpolating equation (4.15).

Presently available absorption coefficients for rain are all expressed in terms of attenuation in db/km. If the scattering effect is ignored, the attenuation is mainly due to absorption and we can use attenuation coefficient to calculate the apparent temperature. Here we use Gunn and East's empirical expression:

$$\alpha_{rain}(\ell) = a\,[p(\ell)]^{b} \qquad (4.16)$$

to relate the attenuation to the precipitation rate. $\alpha_{rain}(\ell)$ is the attenuation in db/km and p is the precipitation rate in mm/hr. The parameters a and b are

frequency dependent constants. Referring to Ippolito (1970), the a and b parameters are obtained with Laws and Parson's distribution at three frequencies:

a = 0.008	b = 1.32	at 8.9 GHz
a = 0.0125	b = 1.25	at 11.1 GHz
a = 0.026	b = 1.18	at 13.9 GHz

Ippolito has shown that the attenuation calculated by this formula is between Medhurst's (1965) theoretical maximum and minimum attenuation.

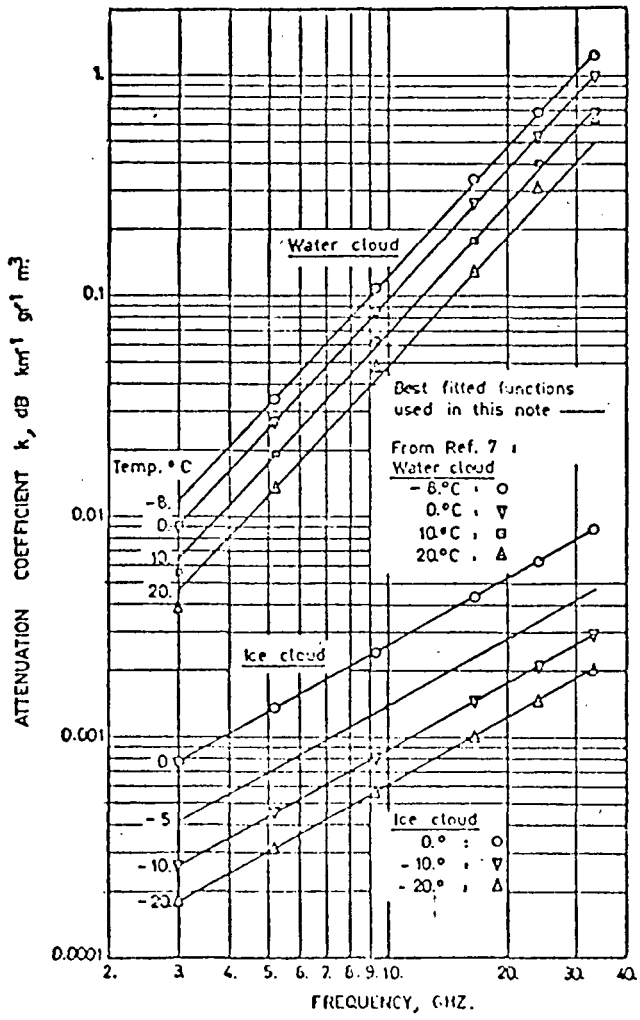

Figure 4.2 Attenuation Coefficient for Clouds.

4.2.3 Apparent Temperature Theory with β_{sc} Included

Under heavy precipitation a large percentage of precipitating particles exhibit diameters comparable to wavelengths at frequencies in the range 10 to 15 GHz. As a consequence scattering cannot be neglected in considering the transfer of radiation through heavy precipitation. The physical effects are clear. The radiation from the surface not only encounters absorption but also scatters in all directions on its upward course. The addition of "collision" on its upward course, as a consequence, attenuates the surface radiation and reflections more effectively. Similar physical process describes the propagation of the inherent radiation of the atmosphere.

To compute the apparent temperature $T_{aj}(z,\theta,\phi)$, the radiative transfer equation presented in the previous section should be employed and is rewritten below

$$\cos\theta \frac{dT_{aj}(z,\theta,\phi)}{dz} + [\alpha(z)+\beta_{sc}(z)]\,T_{aj}(z,\theta,\phi) = \alpha(z)\,T_{air}(z) + \beta_{sc}(z)\int_0^{2\pi}\int_0^{\pi}\gamma(\cos\Theta)\,T_{aj}(z,\theta_s,\phi_s)\sin\theta_s\,d\theta_s\,d\phi_s \qquad j = h \text{ or } v \qquad (4.2)$$

A close form solution of (4.2) such as the solution of the first order differential equation presented in the previous section is unwiedly complicated and impractical. A finite difference method that simulates (4.2) as closely as possible at the net points is employed in this study.

Letting $\mu = \cos\theta$, $\beta_{ex}(z) = \alpha(z) + \beta_{sc}(z)$, $\varpi(z) = \beta_{sc}(z)/\beta_{ex}(z)$

$\tau = \int_z^{\infty} \beta_{ex}(z)\,dz$ (where τ is called the optical depth of the atmosphere).

We may express (4.2) in the form

$$\mu \frac{dT_{aj}(\tau,\mu,\phi)}{d\tau} + T_{aj}(\tau,\mu,\phi) = (1-\varpi(z))\,T_{air}(\tau) + \varpi(\tau)\int_0^{2\pi}\int_{-1}^{1}\gamma(\cos\Theta)\,T_{aj}(\tau,\mu_s,\phi_s)\,d\mu_s\,d\phi_s \qquad j = h \text{ or } v \qquad (4.17)$$

with $$\cos\Theta = \mu\mu_s + \sqrt{1-\mu^2}\sqrt{1-\mu_s^2}\cos(\phi-\phi_s) \qquad (4.18)$$

The direction cosine of μ, μ_s and the azimuthal angles ϕ and ϕ_s is presented below (Figure 4.3).

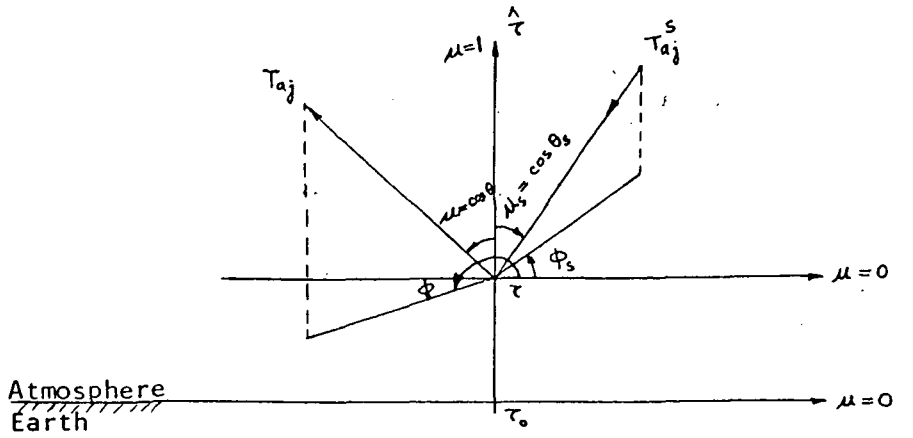

Figure 4.3 The coordinate system using the direction cosine and the optical thickness for expressing the incident and scattering of the polarized apparent temperature.

The scattering characteristics of precipitation represented by the function $\beta_{ex}(\tau)$, $\beta_{sc}(\tau)$, $\varpi(\tau)$, and $\gamma(\cos\Theta)$ in (4.16) are also discussed below.

Equation (4.17) consists of three variables τ, μ, ϕ. To further simplify it, the scattering phase function $\gamma(\cos\Theta)$, can be represented in a finite series of Legendre Polynomials (Shifrin, 1969).

$$\gamma(\cos\Theta) = \sum_{\ell=0}^{N} \gamma_\ell \, P_\ell(\cos\Theta) \tag{4.19}$$

where P_ℓ is the Legendre polynomial of order ℓ. Additional simplification will result when the following iaentity is employed.

$$P_\ell(\cos\Theta) = P_\ell\left[\mu\mu_s + \sqrt{1-\mu^2}\sqrt{1-\mu_s^2}\cos(\phi-\phi_s)\right]$$

$$= P_\ell(\mu)P_\ell(\mu_s) + 2\sum_{m=1}^{\ell}\frac{(\ell-m)!}{(\ell+m)!}P_\ell^m(\mu)P_\ell^m(\mu_s)\cos m(\phi-\phi_s) \tag{4.20}$$

where

$P_\ell^m(\;)$ = associated Legendre polynomial of order ℓ degree m.

We thus have

$$\gamma(\cos\Theta) = \gamma(\mu,\phi;\mu_s,\phi_s)$$

$$= \sum_{\ell=0}^{N}\gamma_\ell\left[P_\ell(\mu)P_\ell(\mu_s) + 2\sum_{m=1}^{\ell}\frac{(\ell-m)!}{(\ell+m)!}P_\ell^m(\mu)P_\ell^m(\mu_s)\cos m(\phi-\phi_s)\right]$$

$$= \sum_{m=0}^{N} A^m \cos m(\phi-\phi_s) \tag{4.21}$$

where $$A^m = (2 - \delta_{0,m}) \left[\sum_{l=m}^{N} \gamma_l^m P_l^m(\mu) P_l^m(\mu_s) \right]$$

$$(l = m, \cdots, N, \quad 0 \le m \le N) \tag{4.22}$$

$$\delta_{0,m} = \begin{cases} 1 & \text{if } m = 0 \\ 0 & \text{otherwise} \end{cases}$$

$$\gamma_l^m = \gamma_l \frac{(l-m)!}{(l+m)!}$$

Equation (4.21) suggests that we expand $T_{aj}(\tau, \mu, \phi)$ in the form

$$T_{aj}(\tau, \mu, \phi) = \sum_{m=0}^{N} T_j^m(\tau, \mu) \cos m\phi \tag{4.23}$$

When equations (4.21) and (4.23) are substituted into equation (4.17), the following independent equations result:

$$\mu \frac{dT_j^m(\tau, \mu)}{d\tau} + T_j^m(\tau, \mu) = \frac{\pi \varpi(\tau)}{2} \int_{-1}^{1} A^m(\mu, \mu_s) T_j^m(\tau, \mu_s) \, d\mu_s + (1 - \omega(\tau)) T_{air}(\tau)$$

$$(m = 0, 1, \cdots, N) \tag{4.24}$$

The boundary conditions for a rough surface bounded below and the atmosphere extended to infinity may be approximated in the form

$$T_j(\tau_0, \mu) = \epsilon_j(\mu) T_g + [1 - \epsilon_j(\mu)] T_j(\tau_0, -\mu) \qquad \mu \ge 0$$

$$T_j(0, \mu) = 0 \qquad \mu \le 0 \tag{4.25}$$

where τ_0 is the total optical depth of the precipitating atmosphere. $\epsilon_j(\mu)$ is the rough surface emissivity and T_g is the surface temperature.

Let us assume (1) the rough surface is isotropic, and since (2) there are no sources above the atmosphere, and (3) the thermal radiation in the medium is also isotropic in nature. Then the solution of equation (4.24) consists of one term (m = 0) only and it becomes a function of τ, μ, and independent of ϕ.

A) Method of Finite Difference for Solving Radiative Transfer Equation

In order to obtain the function $T_j(\tau, \mu)$ numerically, the approximate problem is formulated by confining ourselves to (N =) 5 terms in the expressions shown in eqatuions (4.21) and (4.23) and requiring that equation (4.24) and boundary condition (4.25) be fulfilled at the points $\mu_1, \mu_2, \ldots, \mu_N$ in the interval (0,1) and $\mu_{-1}, \mu_{-2}, \ldots, \mu_{-N}$ in the interval (0,-1). The integrals are here replaced by quadrature summations.

A system of ordinary differential equations of the first order with N boundary conditions at $\tau = 0$, and another N conditions at $\tau = \tau_0$ is obtained for the 2N unknown functions $T_j^i(\tau) = T_j(\mu_i, \tau)$, ($i = 1,2,\ldots,N,-1,-2,\ldots,-N$) of this approximate problem.

We introduce a difference net in τ in such a way that the boundaries of the different substances in the points of discontinuity of the coefficients of equation (4.24) are points of the net. A finite difference system is obtained by integration over each step of the net $(\tau_\ell, \tau_{\ell+1})$ of the system of differential equations for the functions $T_j^i(\tau)$ on the assumption that these functions can be interpolated linearly over the step. For N = 5, the system of equations with the subscript j removed, is represented as follows:

$$\frac{\mu_1}{\tau_\ell}(T_{\ell+1}^1 - T_\ell^1) + \frac{1}{2}(T_{\ell+1}^1 + T_\ell^1) = (1-\omega(\tau_\ell))\,T_{air}(\tau_\ell) + \\ + \frac{\pi\omega(\tau_\ell)}{2}\sum_{i=1}^{5} a_i\left[A(\mu_1,\mu_i)(T_{\ell+1}^i + T_\ell^i) + A(\mu_1,-\mu_i)(T_{\ell+1}^{-i} + T_\ell^{-i})\right]$$

$$\vdots \qquad (4.26)$$

$$\frac{\mu_5}{\tau_\ell}(T_{\ell+1}^5 - T_\ell^5) + \frac{1}{2}(T_{\ell+1}^5 + T_\ell^5) = (1-\omega(\tau_\ell))\,T_{air}(\tau_\ell) + \\ + \frac{\pi\omega(\tau_\ell)}{2}\sum_{i=1}^{5} a_i\left[A(\mu_5,\mu_i)(T_{\ell+1}^i + T_\ell^i) + A(\mu_5,-\mu_i)(T_{\ell+1}^{-i} + T_\ell^{-i})\right]$$

$$\frac{\mu_1}{\tau_\ell}\left(T_\ell^{-1} - T_{\ell+1}^{-1}\right) + \frac{1}{2}\left(T_\ell^{-1} + T_{\ell+1}^{-1}\right) = \left(1 - \omega(\tau_\ell)\right) T_{air}(\tau_\ell) +$$

$$+ \frac{\pi\omega(\tau_\ell)}{2} \sum_{i=1}^{5} a_i \left[A(\mu_1, \mu_i)\left(T_\ell^{-i} + T_{\ell+1}^{-i}\right) + A(\mu_1, -\mu_i)\left(T_\ell^{i} + T_{\ell+1}^{i}\right)\right]$$

$$\vdots \qquad (4.27)$$

$$\frac{\mu_5}{\tau_\ell}\left(T_\ell^{-5} - T_{\ell+1}^{-5}\right) + \frac{1}{2}\left(T_\ell^{-5} + T_{\ell+1}^{-5}\right) = \left(1 - \omega(\tau_\ell)\right) T_{air}(\tau_\ell) +$$

$$+ \frac{\pi\omega(\tau_\ell)}{2} \sum_{i=1}^{5} a_i \left[A(\mu_5, \mu_i)\left(T_\ell^{-i} + T_{\ell+1}^{-i}\right) + A(\mu_5, -\mu_i)\left(T_\ell^{i} + T_{\ell+1}^{i}\right)\right]$$

Note that

$$\int_{-1}^{1} f(\mu)\, d\mu = \int_{0}^{1} \left[f(\mu) + f(-\mu)\right] d\mu$$

$$\cong \sum_{j=1}^{N} a_j \left[f(\mu_j) + f(-\mu_j)\right] \qquad (4.28)$$

$a_1 = 0.11846,\ a_2 = 0.23931,\ a_3 = 0.28444,\ a_4 = 0.23931,\ a_5 = 0.11846$

$\mu_1 = 0.04691,\ \mu_2 = 0.23077,\ \mu_3 = 0.50000,\ \mu_4 = 0.76923,\ \mu_5 = 0.93509$

where a_j's are the weighting factors and μ_j's are elements of the domain of T when a five point Gaussian quadrature integration technique is employed.

Equivalently this can be written in matrix form as:

$$A_\ell T_{\ell+1}^{+} + B_\ell T_\ell^{+} + C_\ell\left(T_{\ell+1}^{-} + T_\ell^{-}\right) = F_\ell^{+}$$

$$C_\ell\left(T_{\ell+1}^{+} + T_\ell^{+}\right) + B_\ell T_{\ell+1}^{-} + A_\ell T_\ell^{-} = F_\ell^{-} \qquad (4.29)$$

with

$$T_\ell^{+} = \begin{bmatrix} T_\ell^{1} \\ \vdots \\ T_\ell^{5} \end{bmatrix}, \quad T_\ell^{-} = \begin{bmatrix} T_\ell^{-1} \\ \vdots \\ T_\ell^{-5} \end{bmatrix}, \quad F_\ell^{+} = F_\ell^{-} = \left(1 - \omega(\tau_\ell)\right) T_{air}(\tau_\ell) \begin{bmatrix} 1 \\ 1 \\ 1 \\ 1 \\ 1 \end{bmatrix}$$

$$A_\ell = [\, a_{ij} \,], \qquad a_{ij} = \left(\frac{\mu_i}{\tau_\ell} + \frac{1}{2}\right)\delta_{ij} - \frac{\pi\,\omega(\tau_\ell)}{2} A(\mu_i, \mu_j)\, a_j$$

$$B_\ell = [\, b_{ij} \,] \qquad b_{ij} = \left(-\frac{\mu_i}{\tau_\ell} + \frac{1}{2}\right)\delta_{ij} - \frac{\pi\,\omega(\tau_\ell)}{2} A(\mu_i, \mu_j)\, a_j \tag{4.30}$$

$$C_\ell = [\, c_{ij} \,] \qquad c_{ij} = -\frac{\pi\,\omega(\tau_\ell)}{2} A(\mu_i, -\mu_j)\, a_j$$

$$\delta_{ij} = \begin{cases} 1, & i = j \\ 0 & \text{otherwise} \end{cases}$$

The boundary conditions of equation (4.25) imply: (a) on the rough surface

$$T^+(\tau_0) = T_g\, \epsilon_j^+ + \{\, [I] - \epsilon_j^+ \,\} \cdot T^-(\tau_0)$$

where

$$\epsilon_j^+ = \begin{bmatrix} \epsilon_j(\mu_i) \\ \vdots \\ \epsilon_j(\mu_s) \end{bmatrix}$$

(b) with no incident radiation above the layer L

$$T^-(0) = [0]$$

(c) an invariance principle is based on the general reflection and emission properties of the layer ,

$$T_\ell^+ = \hat{\sigma}_\ell\, T_\ell^- + \pi_\ell \tag{4.31}$$

with

$$\hat{\sigma}_0 = [I] - \epsilon_j^+ \;, \qquad \pi_0 = T_g\, \epsilon_j^+$$

where [1] is the unit vector, ϵ_j^+ is the emission vector of the rough surface, and $\hat{\sigma}_\ell$, π_ℓ are the reflection and emission vector of the layer (τ_ℓ, τ_0). When equation (4.31) is substituted in (4.28) and solved for $\hat{\sigma}_\ell$, and π_ℓ , we get

$$\hat{\sigma}_{\ell+1} = -\epsilon_\ell^{-1}\left[\, C_\ell - (B_\ell \hat{\sigma}_\ell + C_\ell)(C_\ell \hat{\sigma}_\ell + A_\ell)^{-1} B_\ell \,\right]$$

$$\pi_{\ell+1} = \epsilon_\ell^{-1}\left[\, F_{\ell+1}^+ - B_\ell \pi_\ell - (B_\ell \hat{\sigma}_\ell + C_\ell)(C_\ell \hat{\sigma}_\ell + A_\ell)^{-1}(F_{\ell+1}^- - C_\ell \pi_\ell) \,\right]$$

$$\epsilon_\ell = A_\ell - (B_\ell \hat{\sigma}_\ell + C_\ell)(C_\ell \hat{\sigma}_\ell + A_\ell)^{-1} C_\ell \tag{4.32}$$

It is also known from the transmission properties of the layer that

$$\bar{T}_{\ell-1} = \hat{\gamma}_\ell \, \bar{T}_\ell + \delta_\ell \qquad (4.33)$$

where

$\hat{\gamma}_\ell$ = attenuation coefficient of the layer

δ_ℓ = emission coefficient of the layer

From equations (4.33) and (4.28), the following expressions result

$$\hat{\gamma}_\ell = -\left(C_\ell \hat{\sigma}_\ell + A_\ell \right)^{-1} \left(C_\ell \hat{\sigma}_{\ell+1} + B_\ell \right)$$

$$\delta_\ell = \left(C_\ell \hat{\sigma}_\ell + A_\ell \right)^{-1} \left[F_{\ell+1}^- - C_\ell \left(\pi_{\ell+1} + \pi_\ell \right) \right] \qquad (4.34)$$

The matrix functional equations shown in equations (4.28) to (4.34) which represent the original finite difference equation are applied to solve the integral differential equation with two boundary conditions given in equation (4.25).

Computationally, the coefficients $\hat{\sigma}_\ell$, $\hat{\gamma}_\ell$, π_ℓ, δ_ℓ are first found for $\ell = 0, 1, \ldots, L$, using $\hat{\sigma}_o = [1] - \epsilon_j^+$, $\pi_o = T_g \, \epsilon_j^+$, and the recursive relations given in equations (4.32) and (4.34). These coefficients do not depend on . With these coefficients calculated at every net point, equations (4.31) and (4.33) therefore enable us to find the solutions T_ℓ^+ and T_ℓ^- for all values of ℓ. To increase the accuracy of the numerical computation, the number of nets for μ_i and τ_ℓ can be increased. Under the assumption that the emission induced by scattering contains equal probability for both polarizations, the system of difference equations presented in equations (4.28) through (4.34) is applicable for either horizontal or vertical polarization; the only difference is the surface reflection and emission characteristics, namely $\hat{\sigma}_o = [1] - \epsilon_j^+$, $\pi_o = T_g \, \epsilon_j^+$, where $j = h$ or v .

B) Scattering Characteristics in Precipitation

The microwave scattering characteristics in precipitation consists of the extinction coefficient, the scattering coefficient and the scattering phase function. Although the extinction coefficient has been computed for various precipitation rates in radar applications (Ryde and Ryde, 1946; Gunn and East, 1954; Medhurst, 1965), the scattering coefficient and phase function are still lacking. In what follows these coefficients will be derived first for a single drop and then the result

will be extended to a unit volume of water drops using an appropriate distribution function.

(i) Single Drop Characteristics

It will be assumed that the precipitation particles are spherical in shape so that Mie's theory of scattering by a dielectric sphere is applicable. A detailed analysis of Mie's theory can be found elsewhere (Mie, 1908; Stratton, 1941; Van De Hurst, 1957). Here, only a brief outline is given.

Suppose a plane wave $\underline{E} = \hat{x}\ e^{j(\omega t - kz)}$, with unit strength, time dependence $e^{j\omega t}$, propagation constant k, and polarization in the z direction is incident in the z direction (Figure 4.4), then the scattered electric field, due to a spherical particle situated at the origin, at large distance R is given in the spherical coordinates by

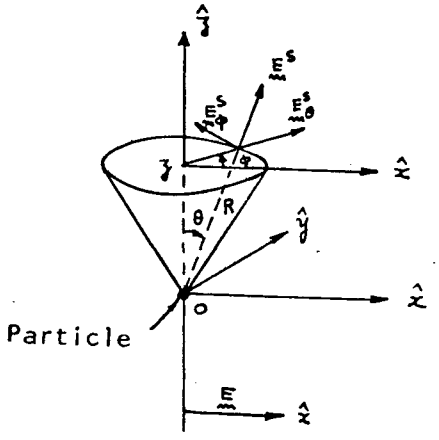

$$E_\theta^s = \frac{-e^{-jkR}}{jkR} A(\theta) \cos\phi \qquad (4.35a)$$

$$E_\phi^s = \frac{e^{-jkR}}{jkR} B(\theta) \sin\phi \qquad (4.35b)$$

Figure 4.4 The scattered electric field due to a spherical particle.

where

$$A(\theta) = \sum_{n=1}^{\infty} \frac{(2n+1)}{n(n+1)} \left[a_n^s \frac{P_n'(\cos\theta)}{\sin\theta} + b_n^s \frac{dP_n'(\cos\theta)}{d\theta} \right] \qquad (4.36a)$$

$$B(\theta) = \sum_{n=1}^{\infty} \frac{(2n+1)}{n(n+1)} \left[a_n^s \frac{dP_n'(\cos\theta)}{d\theta} + b_n^s \frac{P_n'(\cos\theta)}{\sin\theta} \right] \qquad (4.36b)$$

$P_n'(\cos\theta)$ = associate Legendre polynomials

$$a_n^s = \frac{S_n(\rho)\, S_n'(m\rho) - m\, S_n'(\rho)\, S_n(m\rho)}{\Phi_n(\rho)\, S_n'(m\rho) - m\, \Phi_n'(\rho)\, S_n(m\rho)} \tag{4.37a}$$

$$b_n^s = \frac{m\, S_n(\rho)\, S_n'(m\rho) - S_n'(\rho)\, S_n(m\rho)}{m\, \Phi_n(\rho)\, S_n'(m\rho) - \Phi_n'(\rho)\, S_n(m\rho)} \tag{4.37b}$$

$$S_n(x) = \sqrt{\frac{\pi x}{2}}\, J_{n+\frac{1}{2}}(x)$$

$$\Phi_n(x) = S_n(x) + j\, C_n(x)$$

$$C_n(x) = (-1)^n \sqrt{\frac{\pi x}{2}}\, J_{-n-1/2}(x)$$

$J_\nu(x)$ = ν^{th} order Bessel function of the first kind

ρ = normalized radius

$= 2\pi a/\lambda$

λ = wavelength

a = particle radius (in the same unit as λ)

m = square root of the complex dielectric constant of the particle

$= (\epsilon' - j\epsilon'')^{1/2}$

$= \eta(1 - j\chi)$

The prime symbol in (4.37) indicates differentiation of the function with respect to the variable shown in the argument.

The power scattered by the particle into a unit steradian in the direction (θ, ϕ) is

$$i(\theta, \phi) = \frac{1}{k^2}\left[|A(\theta)|^2 \cos^2\phi + |B(\theta)|^2 \sin^2\phi\right] \tag{4.38}$$

For a randomly polarized beam, the scattered power may be obtained by averaging $i(\theta, \phi)$ over ϕ, namely.

$$i(\theta) = \langle i(\theta, \phi)\rangle_\phi = \frac{1}{2k^2}\left[|A(\theta)|^2 + |B(\theta)|^2\right] \tag{4.39}$$

The scattering cross section $q(m, \rho)$ defined as the radio of total power scattered by the particle in all directions to the incident power can be computed by using (4.39) as

$$q(m, \rho) = 2\pi \int_0^\pi i(\theta) \sin\theta\, d\theta \tag{4.40}$$

The scattering coefficient $K_{sc}(m, \rho)$, in turn, defined as the ratio of the scattering cross section to the geometric cross section of the particle, can be computed by using (4.40) and (4.36). It is expressed in the form

$$K_{sc}(m, \rho) = \frac{\sigma(m, \rho)}{\pi a^2} = \frac{2}{\rho^2} \sum_{n=1}^{\infty} (2n+1)\left(|a_n^s|^2 + |b_n^s|^2\right) \tag{4.41}$$

Similarly, the extinction coefficient is expressed as (Van de Hurst, 1957).

$$K_{ex}(m, \rho) = \frac{2}{\rho^2} \sum_{n=1}^{\infty} (2n+1)\, Re\left(a_n^s + b_n^s\right) \tag{4.42}$$

The scattering phase function, $f(\theta)$, is defined as the ratio of the scattered power directed into a unit solid angle in the direction θ to the scattering cross section. It is expressed in the form

$$f(\theta) = \frac{i(\theta)}{\sigma(m, \alpha)} = \frac{|A(\theta)|^2 + |B(\theta)|^2}{2\pi\alpha^2 K_{sc}(m, \rho)} \tag{4.43}$$

From (4.43) it is obvious that

$$2\pi \int_0^{\pi} f(\theta) \sin\theta \, d\theta = 1$$

Equation (4.41) through (4.43) are the formulas from which the scattering characteristics of a single drop can be calculated.

(ii) Unit Volume Characteristics

Under the assumption that many particles of different sizes are randomly distributed in space within a unit volume of precipitation, the macroscopic scattering characteristic can be computed by integrating the single drop characteristics with a known drop size distribution function over the entire size distribution range. The scattering characteristics of precipitation for a unit volume may thus be expressed in the form

$$\beta_{ex} = \pi \int_0^{\infty} a^2 K_{ex}(m, \rho)\, N(a)\, da \tag{4.44}$$

$$\beta_{sc} = \pi \int_0^{\infty} a^2 K_{sc}(m, \rho)\, N(a)\, da \tag{4.45}$$

$$\gamma(\theta) = \frac{\pi}{\beta_{sc}} \int_0^\infty a^2 K_{sc}(m, \rho) f(\theta) N(a) \, da \qquad (4.46)$$

where

β_{ex} = extinction coefficient per unit volume of precipitation in neper/cm

β_{sc} = scattering coefficient per unit volume of precipitation in neper/cm

$\gamma(\theta)$ = scattering phase function per unit volume of precipitation

a = radius of raindrop in cm

$N(a)$ = drop size probability density function in the precipitation

For the case of a Marshall-Palmer distribution, the probability density function is expressed in the form

$$N(a) = 2N_0 \exp(-C_0 a) \qquad (4.47)$$

where $N_0 = 8 \times 10^{-2} \quad cm^{-4}$

$$C_0 = 82 P^{-0.21} \quad cm^{-1}$$

P = precipitation rate in millimeter per hour

(iii) Computed Scattering Characteristics of Precipitation

From the above derived equations, the extinction coefficient, the scattering coefficient, and the albedo of scattering can be computed and are given in Table 4.1 with different frequencies, precipitation rates, and raindrop temperatures. The scattering phase function versus angles are plotted in Figure 4.5 through 4.8.

From Table 4.2, it is shown that extinction and scattering coefficients increase with increasing precipitation rate and frequency. On the other hand a decreasing raindrop temperature will increase the albedo of scattering. For precipitation rate less than 10 mm/hr and microwave frequency below 9 GHz, the scattering effect is negligible since the contribution of the scattering term is less than five percent of the total energy.

From Figure 4.5 through 4.8, it is shown that an increasing precipitation rate at 13.9 and 8.9 GHz will increase the backscattering power. As mentioned before, this scattering phase function can be approximated by a finite series of Legendre polynomials

$$\gamma(\cos\theta) = \sum_{\ell=1}^{N} \gamma_\ell P_\ell(\cos\theta) \qquad (4.19)$$

TABLE 4.2

THE EXTINCTION COEFFICIENT, THE SCATTERING COEFFICIENT, AND THE ALBEDO OF PRECIPITATION

Freq. GHz	Temp. °K / Coefficient / $P_{mm/hr}$	273			283			293		
		$k_m^{-1}\beta_{ex}$	$k_m^{-1}\beta_{sc}$	ω	$k_m^{-1}\beta_{ex}$	$k_m^{-1}\beta_{sc}$	ω	$k_m^{-1}\beta_{ex}$	$k_m^{-1}\beta_{sc}$	ω
8.9	10	.0318	.00147	.046	.0307	.00151	.049	.0288	.00157	.054
	20	.0729	.00426	.058	.0735	.00440	.060	.0723	.00460	.064
	30	.1185	.00792	.067	.1222	.00821	.067	.1230	.00859	.070
	40	.1669	.01229	.074	.1743	.01278	.073	.1774	.01333	.075
11.1	10	.0558	.00372	.067	.0574	.00383	.067	.0582	.00397	.068
	20	.1251	.01070	.086	.1322	.01101	.083	.1380	.01142	.083
	30	.1998	.01977	.099	.2133	.02031	.095	.2251	.02101	.093
	40	.2777	.03042	.110	.2985	.03148	.105	.3158	.03219	.102
13.9	10	.0942	.00949	.101	.0994	.00971	.098	.1051	.00998	.095
	20	.2065	.02684	.130	.2201	.02740	.124	.2350	.02800	.119
	30	.3253	.04881	.150	.3470	.04959	.143	.3708	.05051	.136
	40	.4465	.07339	.164	.4800	.07609	.159	.5080	.07557	.149

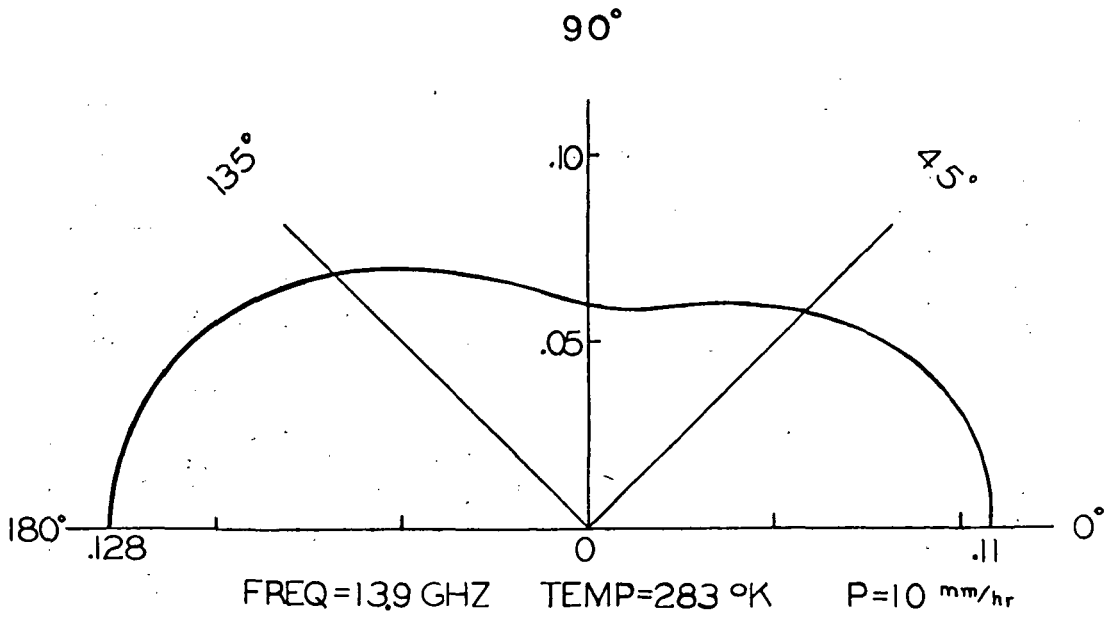

FIGURE 4.5

The computed scattering phase functions of rain.

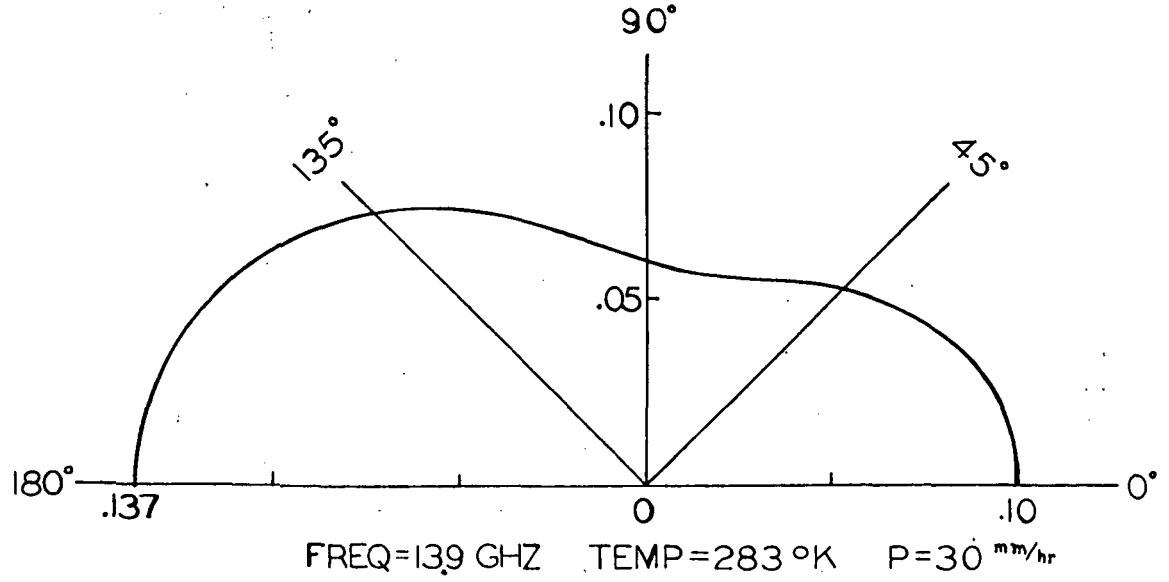

FIGURE 4.6

The computed scattering phase functions of rain.

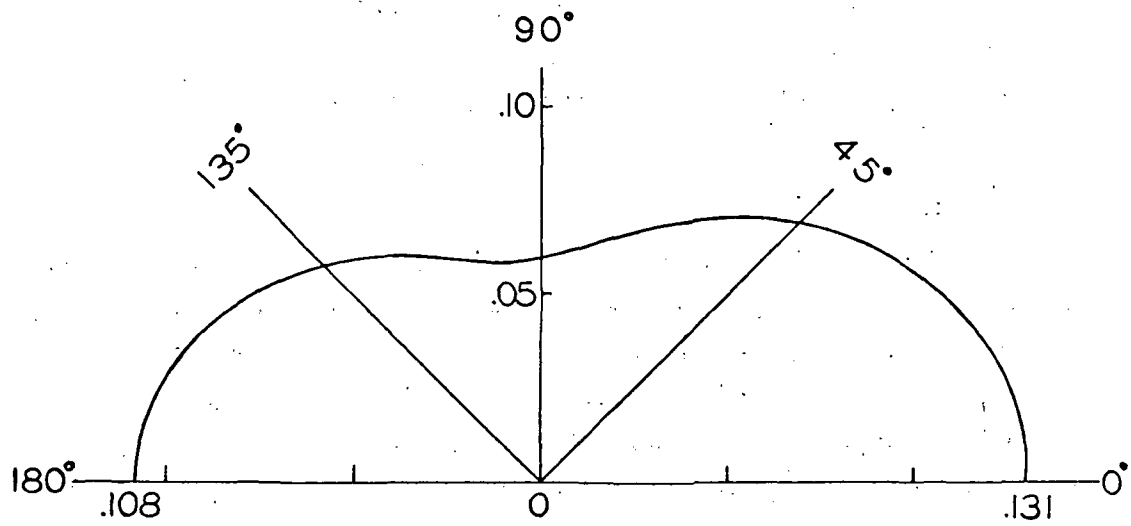

FREQ = 8.9 GHZ TEMP = 283 °K P = 10 mm/hr

FIGURE 4.7

The computed scattering phase functions of rain.

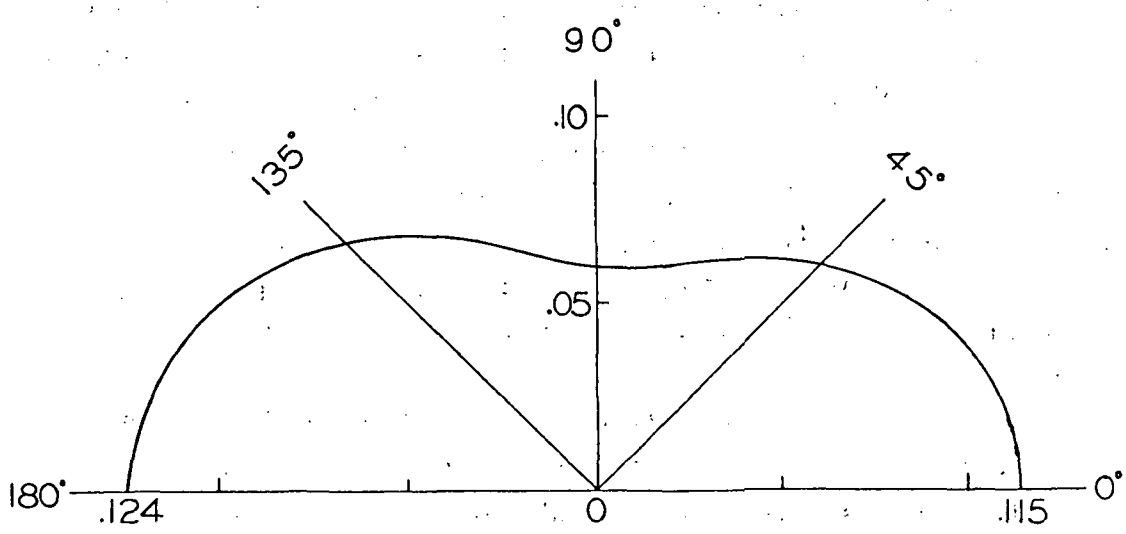

FREQ = 8.9 GHZ TEMP = 283 °K P = 30 mm/hr

FIGURE 4.8

The computed scattering phase functions of rain.

4.3 COMPUTED APPARENT TEMPERATURES OF CLOUDS AND RAIN

4.3.1 Introduction

The theoretical investigation given in the previous two sections described in general the equations to be used for various weather conditions. To compute the downward-looking apparent temperature for a β_{sc} excluded weather condition, it is necessary to assume some values for the parameters in (4.6) and (4.7). As can be seen in (4.6) and (4.7) both sea surface brightness temperature and atmospheric contribution play an important role to the total apparent temperature. Here we employ the results of Chapter III and a sea water temperature of 290°K to calculate the rough sea surface emissivity at 13.9 GHz. Since sea surface roughness characteristics can be related to wind speed over the sea as mentioned in Chapter II, in what follows we also assume a wind speed variation of 5 to 15 m/sec to represent different sea surface roughness.

To compute the apparent temperature due to atmospheric contribution it is necessary to assume the atmospheric temperature profile, $T_{air}(z)$, and the absorption coefficient for a specific weather condition. In this study unless otherwise stated we apply ARDC standard atmosphere for describing atmospheric temperature profile,

. To compute the clear sky absorption coefficient we also employ ARDC standard atmosphere in which the temperature, pressure, and water vapor profile of atmosphere are given by (4.8). The magnitudes of temperature, pressure, and water vapor density at sea level are yet to be specified. In the following, an air temperature of 290°K, a pressure of 760 mmHg and a water vapor density of 7.5 g/m^3 at sea level are assumed.

The presence of clouds and light to moderate rain can be expressed as additional absorption to the already present clear sky absorption and the ARDC standard atmosphere is still applicable. But the spatial distribution of the liquid water content for clouds and the precipitation rate for rain are required to compute the cloud and rain effects. Some realistic clouds and rain models proposed by meteorologists which include the spatial distribution of liquid water content for clouds and precipitation rates for rain are presented below. Subsequent computations of the apparent temperature using these models assumes an observational height of 7 km.

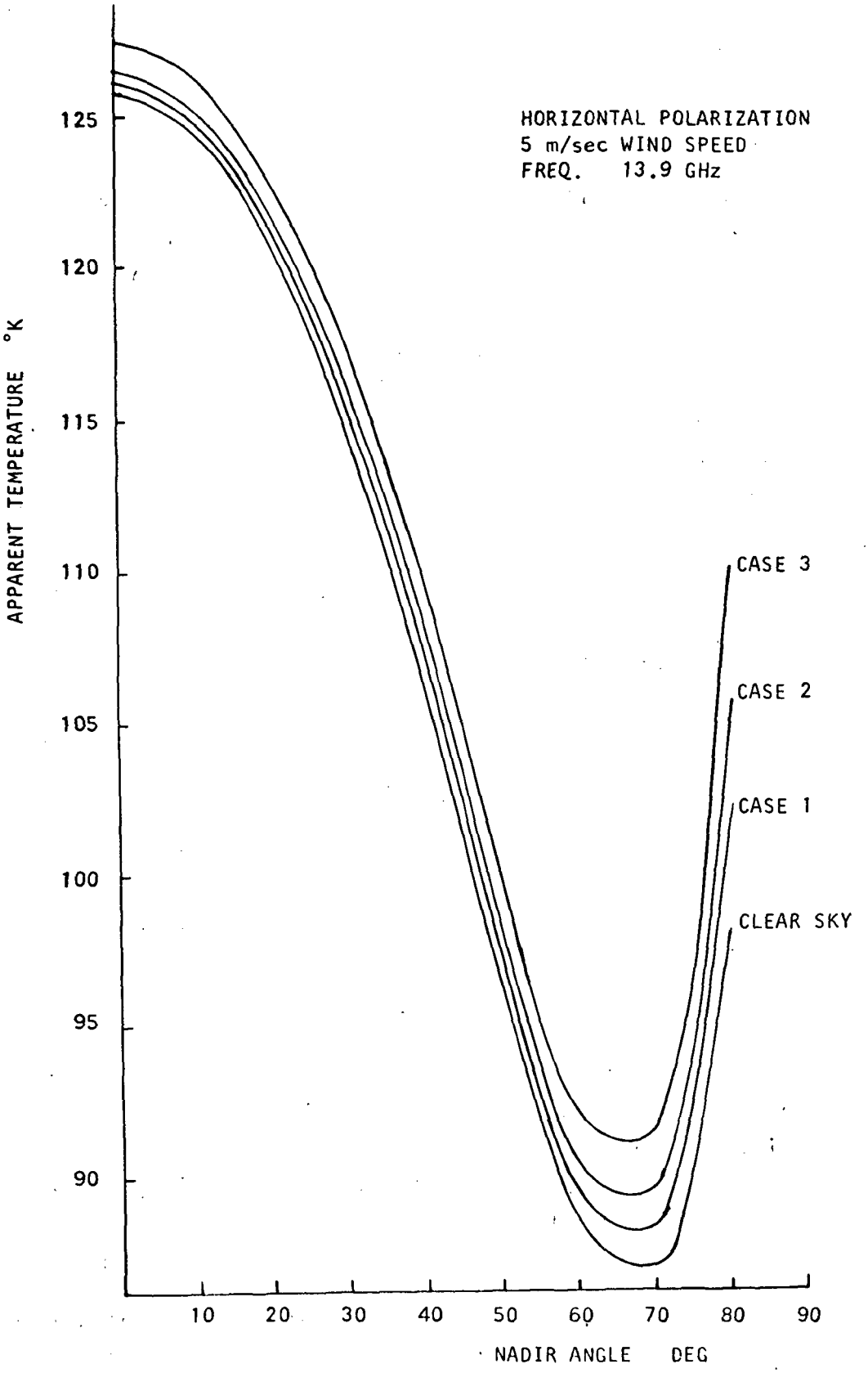

FIG. 4.9 The Computed Apparent Temperature for Observation Through Stratus Clouds

4.3.2 Clouds

According to meteorologist classification (Donn, 1964) there are three basic cloud forms, namely cirrus, cumulus, and stratus. All cloud formations consist of these standard forms, a combination of these forms, or a modification of these forms.

Since cirrus clouds are typically thin layers of ice, their absorption (or emission) are relatively insignificant compared with the other cloud types at microwave frequencies. Hence only stratus and cumulus cloud formations are considered. Usually the liquid water content of the cloud varies with height and attains its maximum near the cloud top. However, for convenience of computation, the average value over the total cloud thickness is employed in the calculations to follow.

(i) Stratus

Stratus clouds are typified by a thin layer of low water content clouds. The apparent temperature versus nadir angle calculation of these cloud conditions are based on Neiburger's models (1949) given in Table 4.3.

TABLE 4.3

Neiburger's Stratus Models

Cases	Altitude Extent (m)	Water Content (gm/m^3)
Case 1	30-580	.35
Case 2	152-520	.25
Case 3	213-490	.20

The results for horizontal polarization at 13.9 GHz and 5 m/sec wind speed are shown in Figure 4.9.

It is evident that stratus do not contribute much to the rise in the apparent temperature compared to the clear sky case.

(ii) Cumulus

Cumulus clouds are prevalent over the ocean for all seasons. To typify their effect Levine's models (1965) for cumulus are employed (See Table 4.4 below).

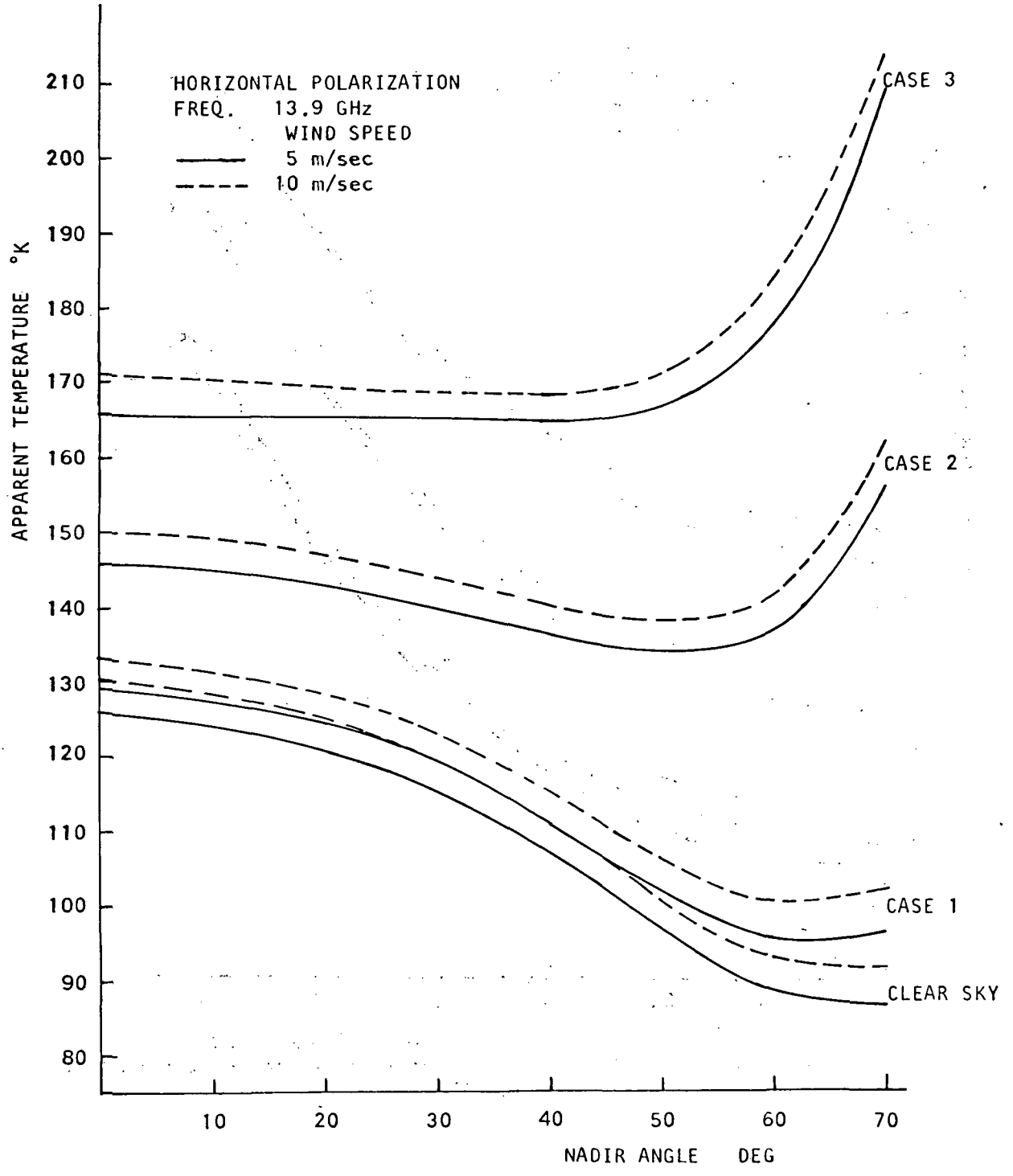

FIG. 4.10 The Computed Apparent Temperature for Observation Through Cumulus Clouds

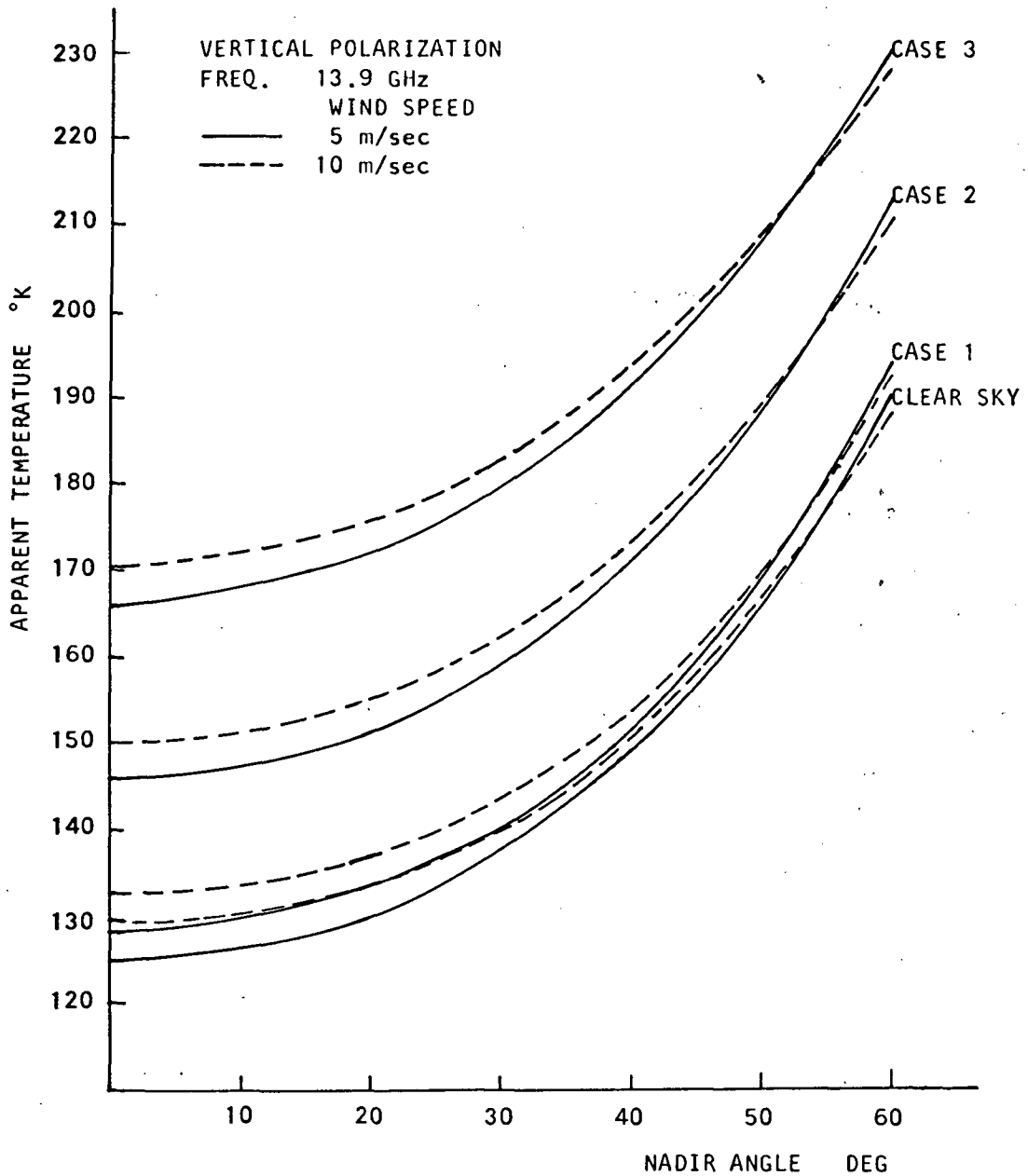

FIG. 4.11 The Computed Apparent Temperature for Observation Through cumulus Clouds

TABLE 4.4

Levine's Cumulus Models

Case	Altitude Extent (m)	Water Content (gm/m^3)
Case 1	457-1068	0.5
Case 2	457-2590	1.0
Case 3	457-3810	1.25

The computed apparent temperature versus nadir angle by using (4.6) and (4.7) for these three cases are shown in Figures 4.10 and 4.11 for horizontal and vertical polarization, respectively. Results are also shown for different surface roughness conditions as well as cloud cases. The result indicates that (1) for the same surface condition the thicker and the higher the water content, the higher the temperature rise with respect to clear sky; (2) at larger nadir angles say around 50 degrees horizontal polarization is more sensitive to the temperature rise as compared to vertical polarization; (3) the rise of apparent temperature due to the increase of surface roughness, namely increasing wind speed, can be detected in all cumulus cases and (4) comparison of the horizontal apparent temperature curves between clear sky and cumulus cloud (Case 1) (Figure 4.10) a qualitative differentiation between surface effect and cloud absorption effect can be made. The cloud absorption temperature increases with increasing nadir angles, while the surface effect causes the same amount of temperature increase over all nadir angles.

(iii) Overcast

Overcast may be considered as a combination of stratus and cumulus clouds. Frequently an overcast condition can be associated with the warm sector preceding a cold front. An overcast may be classified according to its depth and water content.

To study these overcast conditions Porter's models (1969) are employed. A description of these overcast situations is shown in Table 4.5.

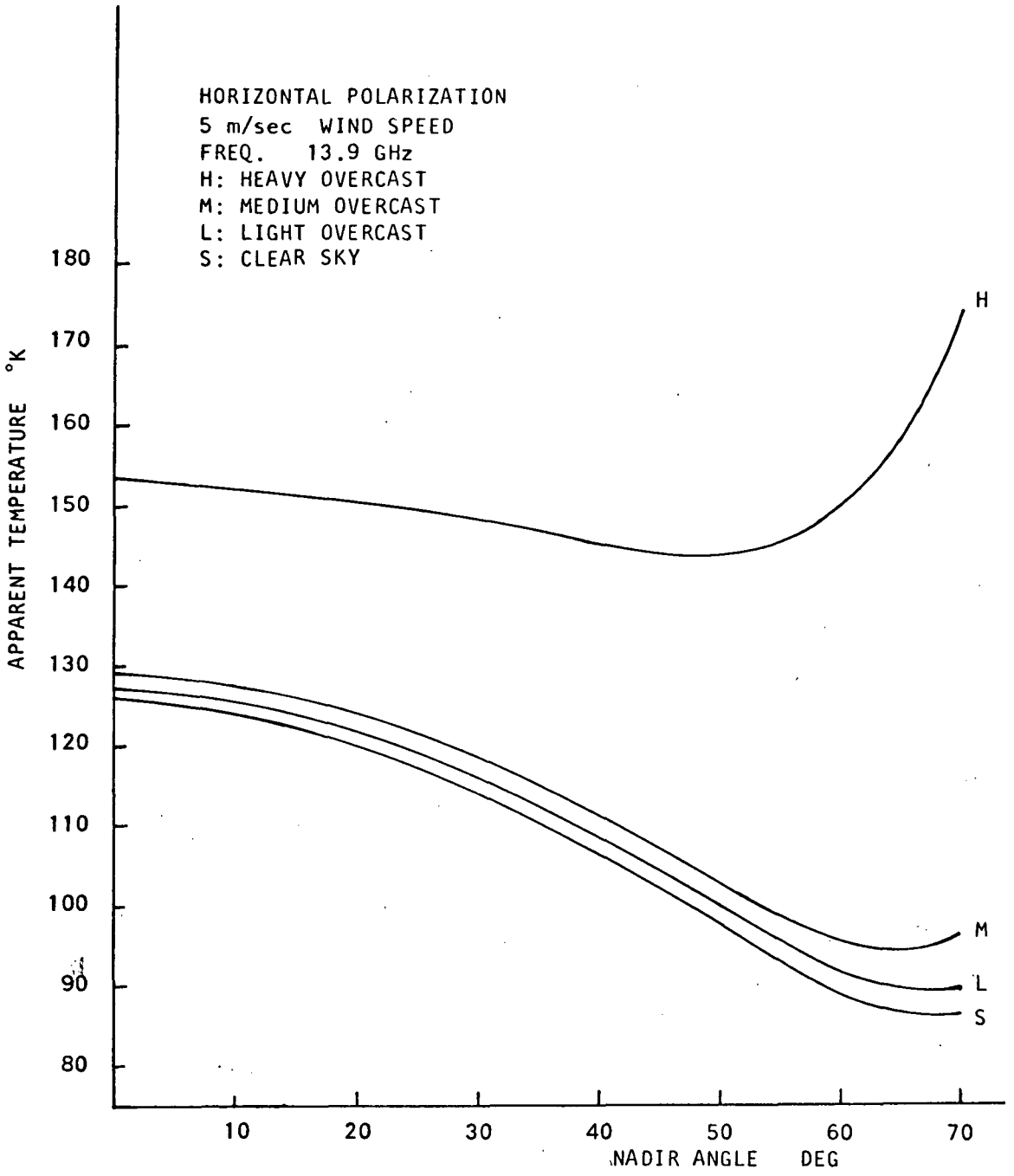

FIG. 4.12 The Computed Apparent Temperature for Overcast Conditions

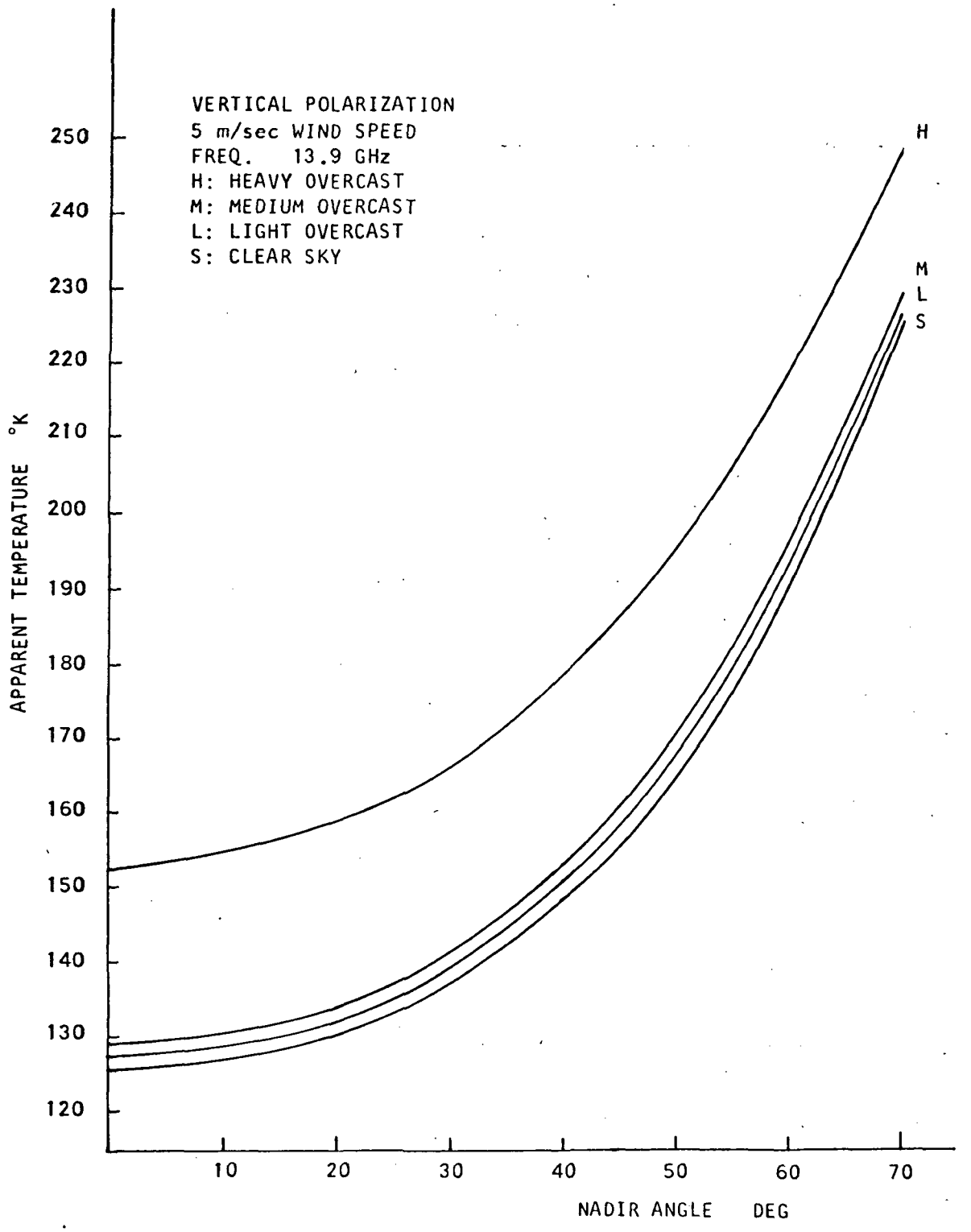

FIG. 4.13 The Computed Apparent Temperature for Overcast Conditions

TABLE 4.5

Porter's Overcast Models

Classification	Altitude Extent (m)	Water Content (gm/m^3)
Light (sun visible)	300-650	0.33
Medium (light sky)	400-900	0.67
Heavy	500-3200	1.00

The apparent temperature characteristic for these overcast conditions are shown in Figures 4.12 and 4.13 for horizontal and vertical polarization with sea surface wind speed of 5 m/sec and microwave frequency of 13.9 GHz. In the figures, the horizontal polarization exhibits an increasing sensitivity with nadir angles under the overcast condition. A $70^{\circ}K$ separation between the heavy overcast and the clear sky condition can be observed at nadir angles in the vicinity of 70 degrees. The response for the vertical polarization on the other hand shows maximum sensitivity to clouds only at nadir.

4.3.3 Light to Moderate Rains

The extent of precipitation over the world at any time is small in comparison to the extent of the non-precipitating regions. The frequency of rain over oceans is known to be even lower than that over land. As a consequence the operation of a combined radiometer-scatterometer will not be impeded often by rain. It is important, however, to estimate the effects of rain on the radiometric observation to attempt to discriminate between precipitating and non-precipitating regions.

The characteristics of precipitation have largely been described over land. No information regarding vertical rainfall distributions has been found for rain over oceans. It is assumed that the rain characteristics over land and sea are similar. In this respect Valley's rain models (1965) are used in computing the apparent microwave temperature. He described several cases, only one case, however, is treated here.

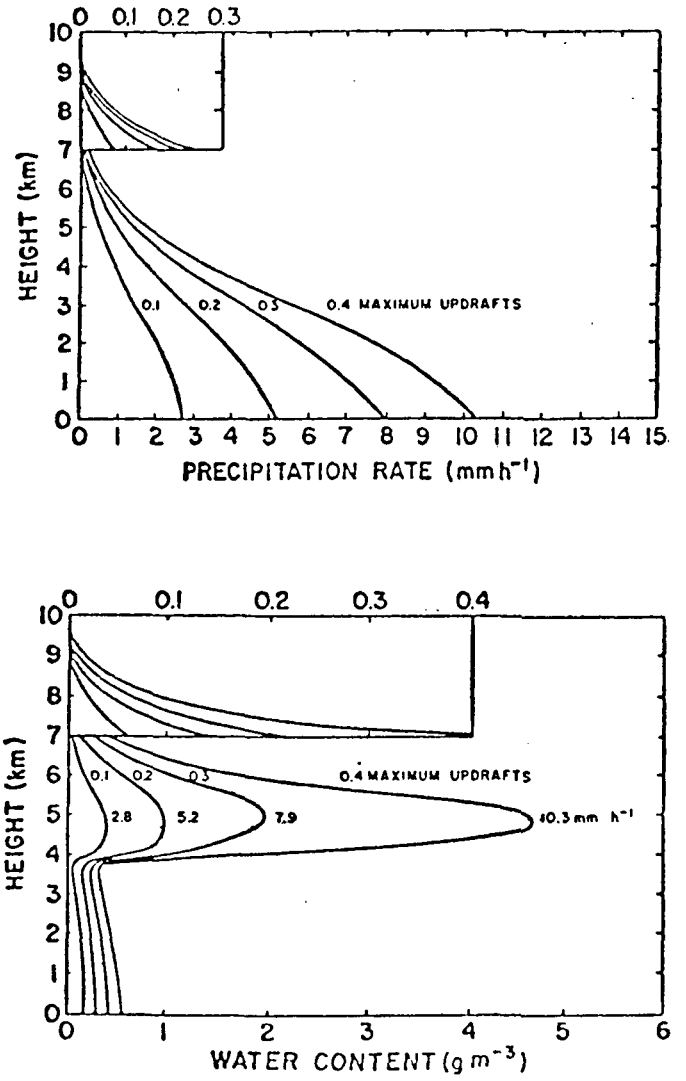

FIG. 4.14 Precipitation and Water Content Distribution for Extensive Showers

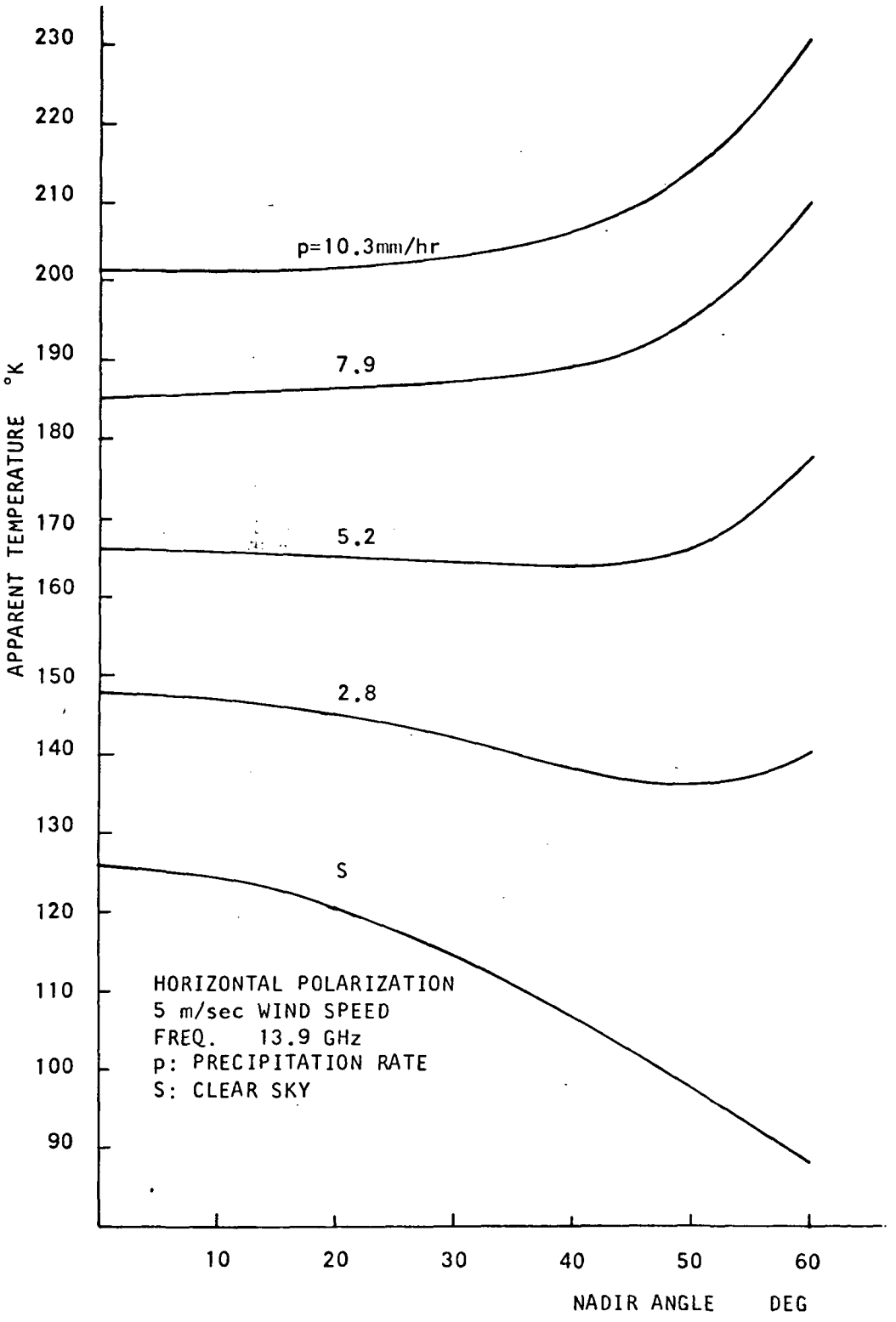

FIG. 4.15 The Computed Apparent Temperature for Observations Through Rain

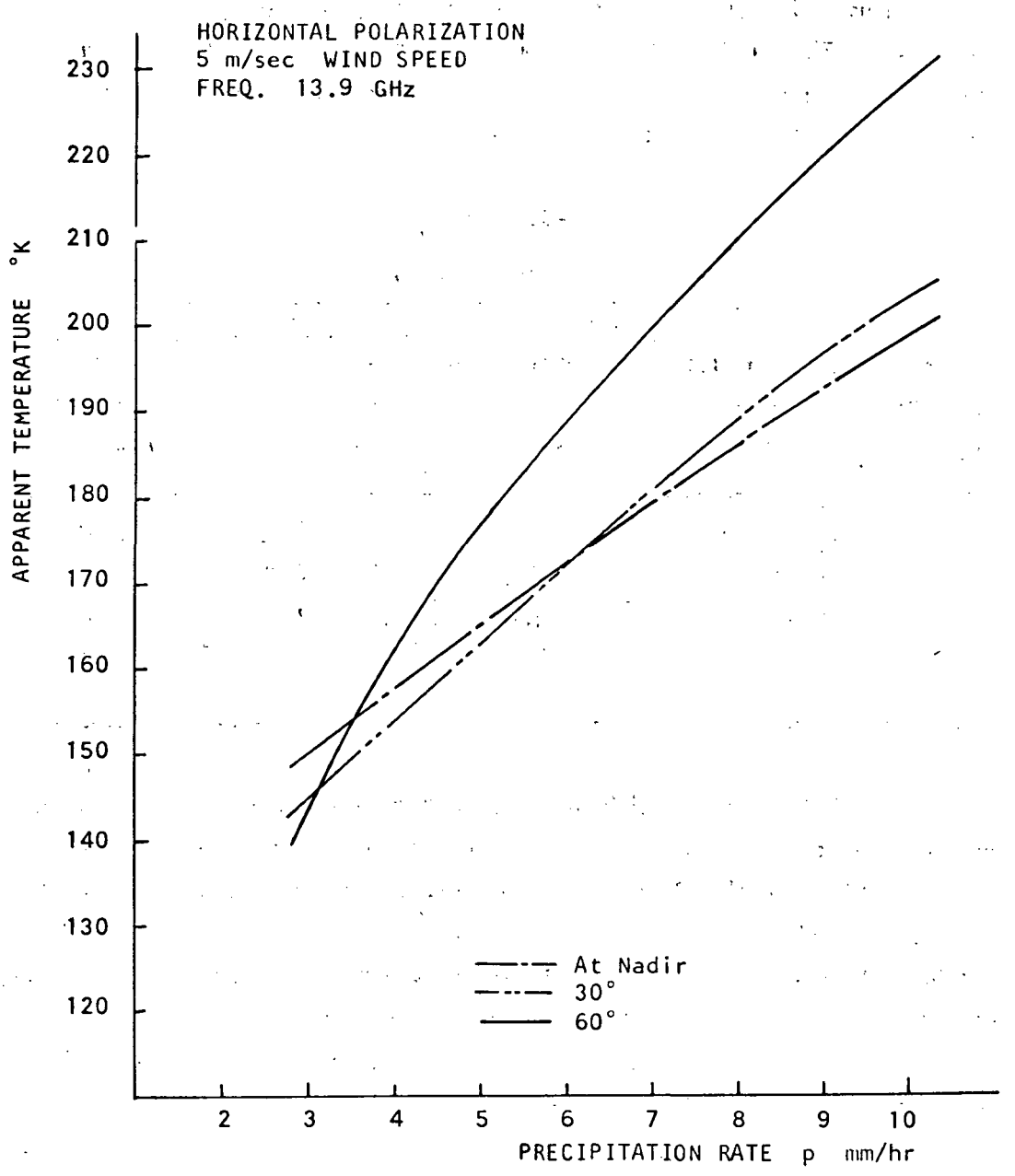

FIG. 4.16 The Computed Apparent Temperature as a Function of Precipitation Rate

This case is representative of summer rain in temperate latitudes and with a slight increase in temperature, of widespread tropical rains as well.

This model typifies widespread uniform precipitation and not showery conditions. The precipitation and cloud characteristics are shown in Figure 4.14 and Table 4.6 respectively. As a result of different updrafts, four different precipitation rates can be described for each case.

TABLE 4.6

Valley's Rain Model

	Rain Parameters		Cloud Parameters	
Updraft Condition (m/sec)	Altitude Extent (m)	Precipitation at z = 0 (mm/hr)	Altitude Extent (m)	Water Content (gm/m^3)
0.4	0-3100	10.3	3100-7000	0.30
0.3	0-3200	7.9	3200-7000	0.25
0.2	0-3300	5.2	3300-7000	0.15
0.1	3-3500	2.8	3500-7000	0.10

The computed apparent temperature characteristics are shown in Figures 4.15 and 4.16. From Figure 4.15 it is evident that the sensitivity to rain is greater at higher angles for small rainfall rates than for larger rainfall rates. In Figure 4.16, an approximately linear correlation of apparent temperature rise with respect to precipitation rate are demonstrated at nadir. From this it may be possible to predict precipitation rate from the measured apparent temperature whenever the surface characteristic is known. It is also clear that the radiometric contributions by rain are notably larger than those of clouds.

4.3.4 Heavy Rain

Based on finite difference method described in earlier sections, computer programs are developed to compute the apparent temperature as observed at altitudes above heavy rain. The results for two uniformly distributed precipitation rates, 10

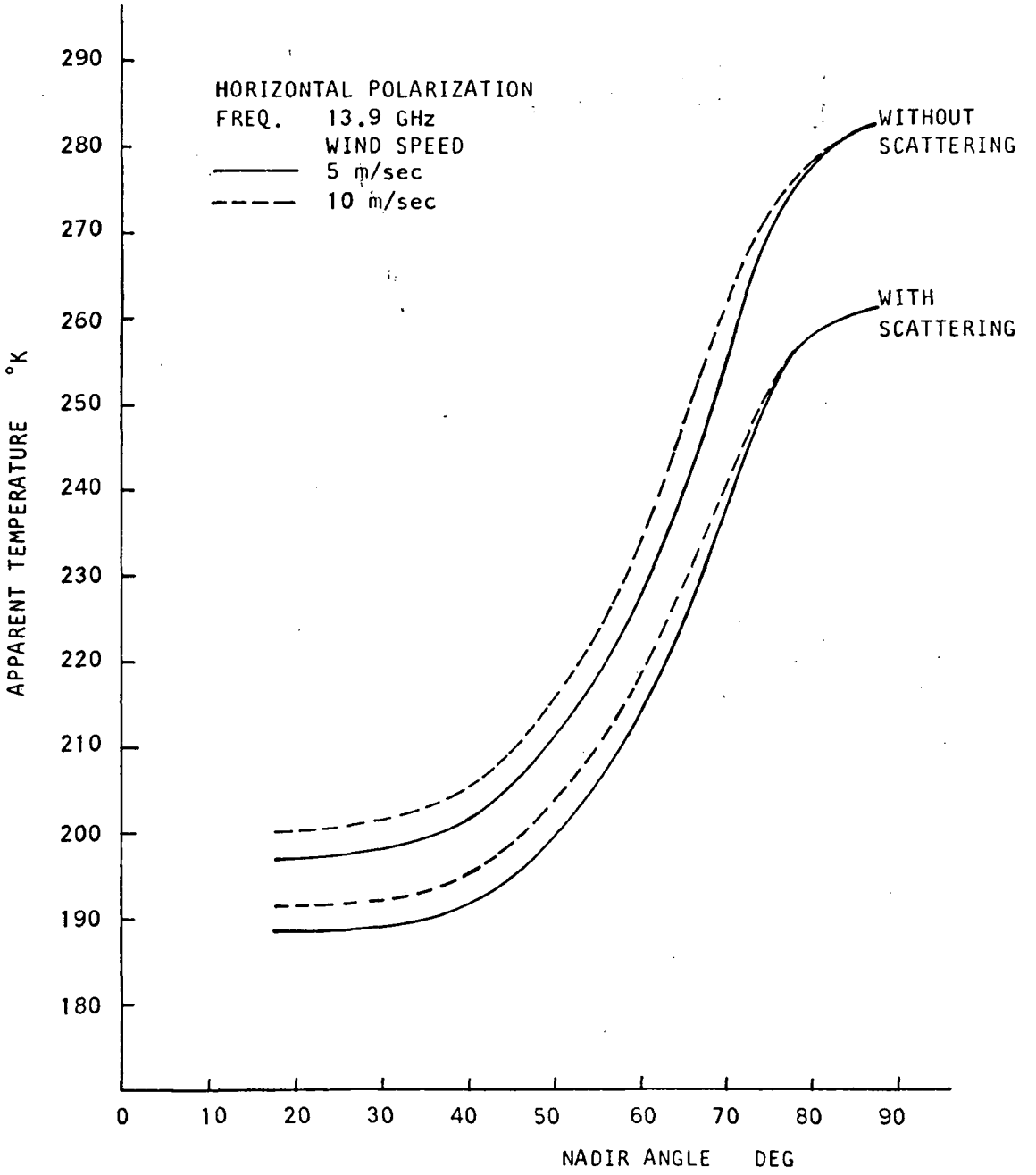

FIG. 4.17 The Computed Apparent Temperature for a Precipitation Rate of 10 mm/hr.

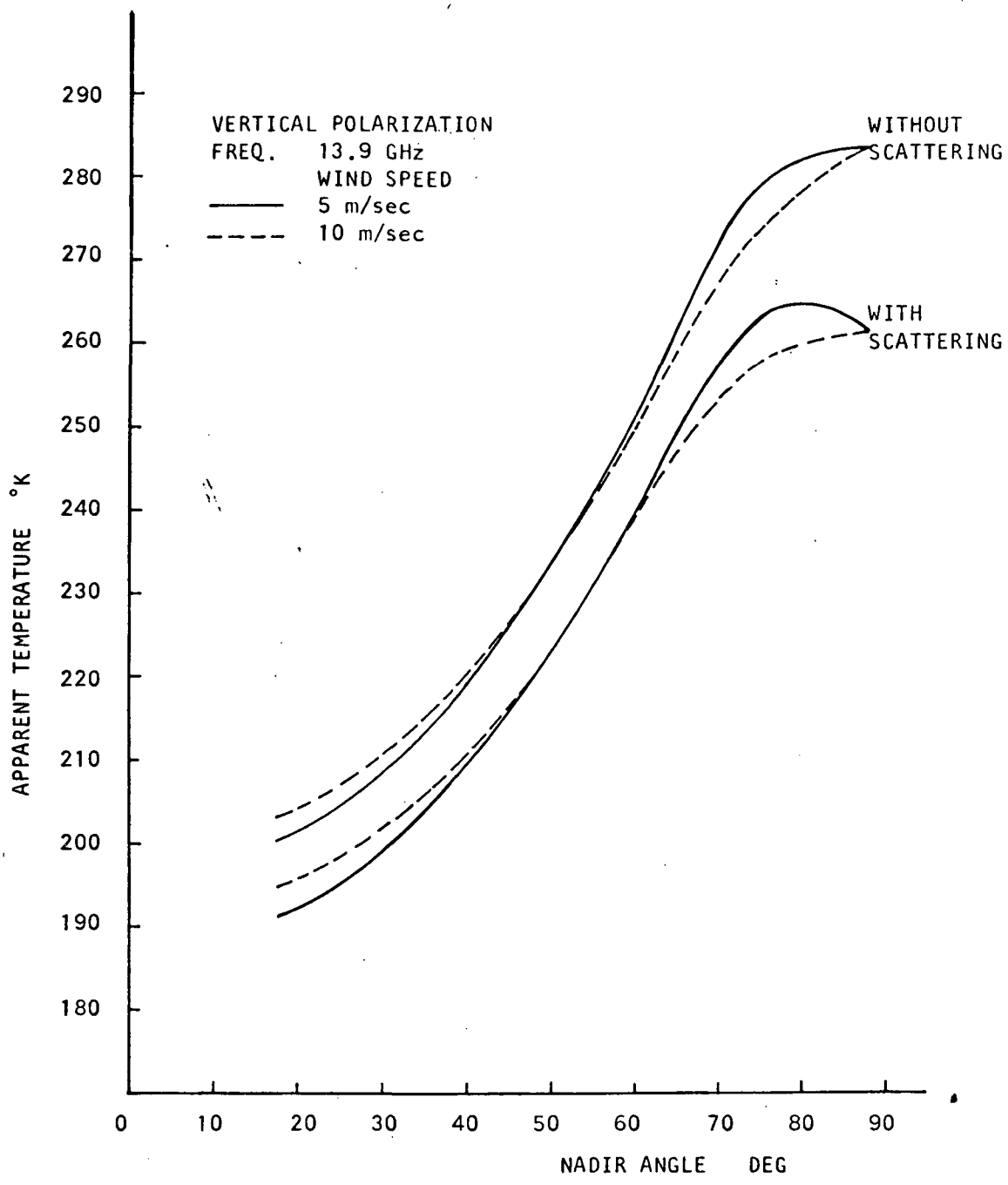

FIG. 4.18 The Computed Apparent Temperature for a Precipitation Rate of 10 mm/hr.

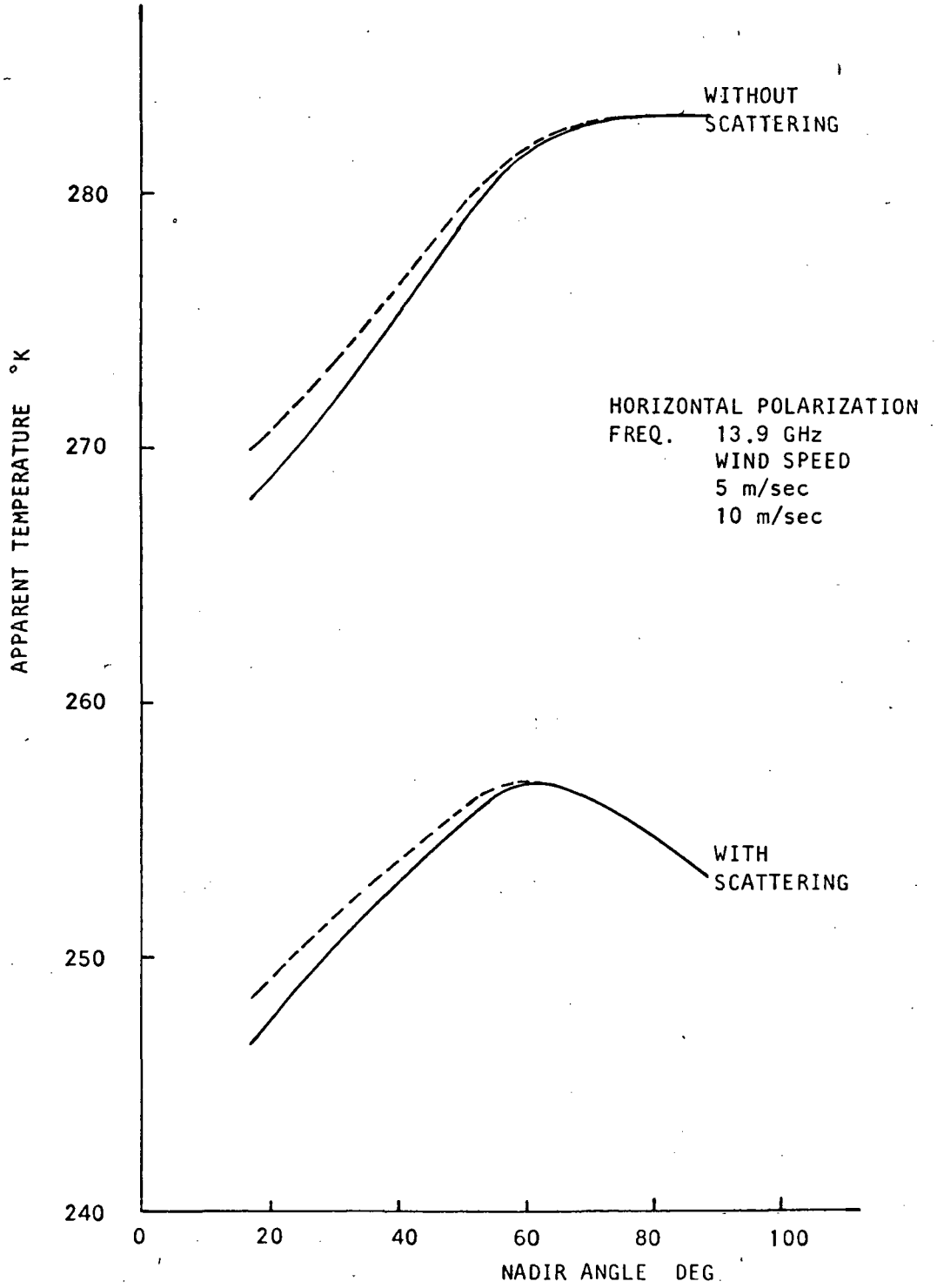

FIG. 4.19 The Computed Apparent Temperature for a Precipitation Rate of 30 mm/hr.

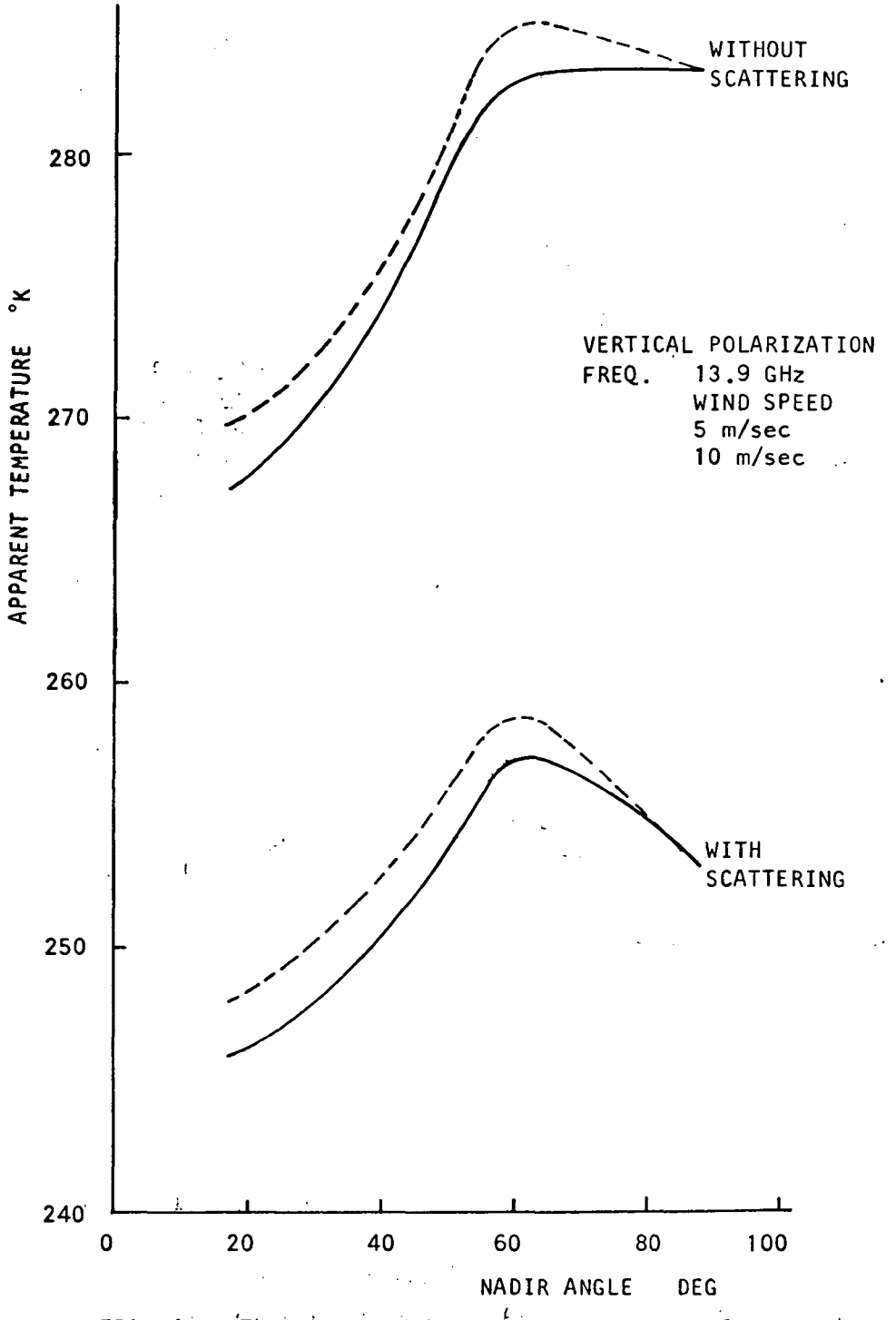

FIG. 4.20 The Computed Apparent Temperature for a Precipitation Rate of 30 mm/hr.

mm/hr and 30 mm/hr, are shown in Figure 4.17 through 4.20 for both horizontal and vertical polarizations.

In the figures both scattering-included and-excluded cases are given for comparison. For scattering-excluded case, we assume the albedo of scattering to be equal to zero in the radiative transfer equation given in (4.33). Since the source function induced by the scattering term is not as effective as the thermal radiation source, a decrease of the computed temperature is clearly evident when the scattering effect is included. At larger nadir angles (greater than 60°) the effect of scattering is seen to increase and causes a larger decrease in the observed apparent temperature. The effect of scattering is most significant as the precipitation rate increases.

4.4 CORRELATION OF EXCESS APPARENT TEMPERATURE WITH ATTENUATION

4.4.1 Introduction

The primary advantage of having a radscat system as opposed to a scatterometer system is that it allows correlation of the excess apparent temperature (i.e., the difference between the total apparent temperature and the surface brightness temperature) with the attenuation, thus providing a correction factor for the scatterometer data. This, in turn, improves the wind speed estimation over the sea when cloud and rain intervene.

Direct numerical computation employing (4.6) to plot the attenuation given by $L(\theta, z)$ versus apparent temperature difference is possible but tedious. In what follows a simplified model is used to investigate the correlation between the excess temperature and atmospheric attenuation.

The apparent temperature for a downward looking radiometer located at an altitude z above the sea surface with nadir angle θ, as derived in section 4.2.2 for non-scattering atmosphere, has the form

$$T_{aj}(\theta, z) = L(\theta, z)\left[\epsilon_j(\theta) T_g + T_{rj}(\theta)\right] + T_{atm}(\theta, z) \qquad (4.6)$$
$$j = h, v$$

where j refer to the state of polarization; $L(\theta, j)$ is the transmittance; $\epsilon_j(\theta) T_g$ is the surface brightness temperature; $\epsilon_j(\theta) T_g$ is the temperature emitted by the atmosphere between the surface and the height j in the direction θ ; $T_{rj}(\theta)$ is the reflected sky temperature. $T_{rj}(\theta)$ is also expressible in the form

$$T_{rj}(\theta) = \frac{1}{4\pi}\int_0^{2\pi}\int_0^{\pi/2} \gamma_j(\theta, \theta_s, \phi_s)\, T_{sky}(\theta_s) \sin\theta_s \, d\theta_s \, d\phi_s \qquad (4.7c)$$

with

$$\epsilon_j(\theta) = 1 - \frac{1}{4\pi}\int_0^{2\pi}\int_0^{\pi/2} \gamma_j(\theta, \theta_s, \phi_s) \sin\theta_s \, d\theta_s \, d\phi_s$$

where , j is either h or v and $\gamma_j(\theta, \theta_s, \phi_s)$ is the surface differential scattering coefficient.

Due to the complexity of $\gamma_j(\theta, \theta_s, \phi_s)$ as derived in Chapter 3 and the integration needed to obtain the reflected sky temperature, the problem can only be evaluated numerically. However, in numerical computation the parameters that affect the apparent temperature cannot be easily visualized. To circumvent this difficulty a simplified model is employed to analyze the correlation of the excess temperature with attenuation.

Let

$$\overline{\rho_j}(\theta) = \frac{1}{4\pi\, T_{sky}(\theta)}\int_0^{2\pi}\int_0^{\pi/2} \gamma_j(\theta, \theta_s, \phi_s)\, T_{sky}(\theta_s) \sin\theta_s \, d\theta_s \, d\phi_s \qquad (4.48a)$$

$$\cong \frac{T_{sky}(\theta)}{4\pi\, T_{sky}(\theta)}\int_0^{2\pi}\int_0^{\pi/2} \gamma_j(\theta, \theta_s, \phi_s) \sin\theta_s \, d\theta_s \, d\phi_s \qquad (4.48b)$$

$$= 1 - \epsilon_j(\theta) \qquad (4.48c)$$

where $\overline{\rho_j}(\theta)$ represents a weighted average sea surface reflectivity with respect to specific sky temperatures. Under many circumstances involving clear sky, stratus, cumulus, overcast and light rain at frequencies below 15 GHz, and nadir angle less than 70 degrees, it is found that $\overline{\rho_j}(\theta)$ is insensitive to $T_{sky}(\theta)$ variation or atmospheric changes. It mainly depends on surface characteristics as can be expressed in terms of (4.48b) or (4.48c) without significant error.

Using (4.48), we can express (4.6) in the form

$$T_{aj}(\theta, z) = L(\theta, z)\left[\epsilon_j(\theta) T_g + \bar{\rho}_j(\theta) T_{sky}(\theta)\right] + T_{atm}(\theta, z) \qquad (4.49)$$

The significant advantage of (4.49) over (4.6) is that the reflected sky temperature $T_{rj}(\theta)$ is now expressed as the product of the effective surface reflectivity $\bar{\rho}_j(\theta)$ $\bar{\rho}_j(\theta)$ and the sky temperature, and that $\bar{\rho}_j(\theta)$ depends only on surface characteristics.

To further simplify the problem, $T_{sky}(\theta)$ can also be written in the form (Peake, 1969)

$$T_{sky}(\theta) = (1.12\, T_{air}(0) - 50)\left(1 - e^{-\tau_0 \sec\theta}\right) \qquad (4.50)$$

where $T_{air}(0)$ is the air temperature at the ground level; and τ_0 is the total optical depth at nadir. The total optical depth τ_0 is given by

$$\tau_0 = \int_0^\infty \alpha(z)\, dz \qquad (4.51)$$

where $\alpha(z)$ is the absorption coefficient of the atmosphere per unit length at altitude z.

Similarly, we can also express $T_{atm}(\theta, z)$ in the form

$$T_{atm}(\theta, z) = (1.12\, T_{air}(0) - 50)\left(1 - e^{-\tau \sec\theta}\right) \qquad (4.52)$$

with

$$\tau = \int_0^z \alpha(z)\, dz \qquad (4.53)$$

and

$$L(\theta, z) = e^{-\tau \sec\theta} \qquad (4.54)$$

By employing (4.49) through (4.54), the correlation of excess temperature with attenuation is presented below.

4.4.2 Analysis

To make the analysis simpler we assume the radiometer to be located high enough that the atmospheric temperature $T_{atm}(\theta, z)$ is about the same as the

sky temperature, i.e.

$$T_{atm}(\theta,\zeta) = T_{sky}(\theta) = (1.12\,T_{air}(0) - 50)(1 - e^{-\tau_0 \sec\theta}) = T_M[1 - L] \tag{4.55}$$

where

$$T_M = 1.12\,T_{air}(0) - 50$$

$$L = e^{-\tau_0 \sec\theta}$$

with ζ so large that we may assume $\tau \cong \tau_0$ without significant error. Using (4.55), we can express (4.49) in the form

$$T_{aj}(\theta) = L\left[\epsilon_j(\theta)\,T_g + \bar{\rho}_j(\theta)\,T_M(1-L)\right] + T_M(1-L) \tag{4.56}$$

When we define the excess apparent temperature, $T_{Ej}(\theta)$, as the difference between the total apparent temperature and the brightness temperature due to sea surface only, we get

$$\begin{aligned} T_{Ej}(\theta) &= T_{aj}(\theta) - \epsilon_j(\theta)\,T_g \\ &= (1-L)\,T_M\left[1 + L\,\bar{\rho}_j(\theta)\right] + L\,\epsilon_j(\theta)\,T_g - \epsilon_j(\theta)\,T_g \\ &= (1-L)\left[T_M\{1 + L\,\bar{\rho}_j(\theta)\} - \epsilon_j(\theta)\,T_g\right] \end{aligned} \tag{4.57}$$

Letting the attenuation factor, A, equal to the inverse of the transmittance, namely

$$A = \frac{1}{L} = e^{\sec\theta\,\tau_0} \geq 1 \tag{4.58}$$

$$\log_e A = \sec\theta\,\tau_0$$

We get

$$T_{Ej}(\theta) = \left(1 - \frac{1}{A}\right)\left[T_M\left(1 + \frac{\bar{\rho}_j(\theta)}{A}\right) - \epsilon_j(\theta)\,T_g\right] \tag{4.59}$$

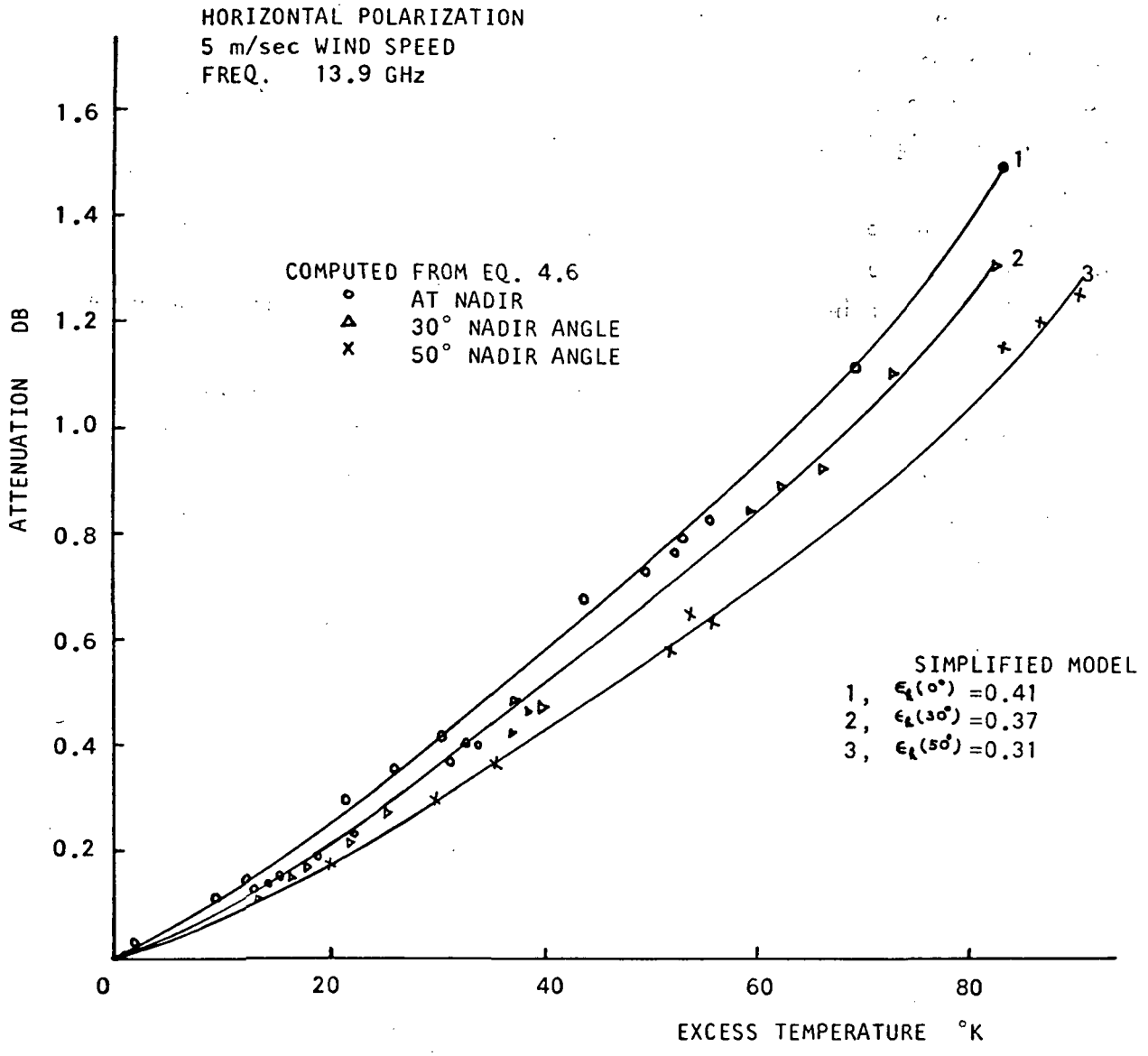

FIG. 4.21 Attenuation as a Function of Excess Temperature for the Conditions Noted

Differentiating $T_{Ej}(\theta)$ with respect to A in (4.59), we get

$$\frac{\partial T_{Ej}(\theta)}{\partial A} = \frac{1}{A^2}\left[\{1 - \bar{P}_j(\theta)\} T_M - \epsilon_j(\theta) T_g + \frac{2}{A} T_M \bar{P}_j(\theta)\right] \quad (4.60)$$

From (4.59) and (4.60) some remarks can be made: (1) For fixed T_g, T_M and $\epsilon_j(\theta)$ (and hence $\bar{P}_j(\theta)$), the larger the attenuation A the larger the excess apparent temperature, $T_{Ej}(\theta)$, and the rate of increase of the excess apparent temperature $T_{Ej}(\theta)$, decrease with the increase of the attenuation A. (2) For a fixed attenuation A and surface temperature T_g, decreasing surface emissivity $\epsilon_j(\theta)$ will increase both the excess apparent temperature and the rate of increase of the excess apparent temperature with respect to attenuation.

The trend of the excess apparent temperature versus attenuation is demonstrated in Figure 4.21.

In Chapter III it has been shown that the surface emissivity decreases with increasing nadir angle. Thus to obtain a better sensitivity of the excess temperature versus attenuation, it is suggested that the radiometer should look at larger nadir angles, say 50 degrees or larger, and operate in horizontal polarization mode.

CHAPTER 5

SUGGESTIONS FOR FUTURE STUDIES

The non-coherent composite surface model is shown to predict scatterometric and radiometric responses of the sea with reasonable accuracy. The use of an isotropic surface model, however, has completely ignored the anisotropic characteristics of the sea surface. The cross wind response, for instance, cannot be distinguished from that of the upwind. Also, the evaluation of the scattering integral by the stationary phase approximation results in a wind speed dependence of the large undulations only through the rms slope of the large structures and not the specific shape of the surface spectrum. It is suggested that future effort for sea scattering theory should accommodate the two dimensional (anisotropic) sea spectrum proposed by oceanographers. This approach may, however, be too involved for microwave emission theory due to the many lengthy numerical integrations required for a number of multiple integrals, but is certainly feasible for radar backscattering with the present computer capabilities.

Theoretical computations of the microwave apparent temperature over the ocean have shown a definite temperature increase due to clouds and rain. However, the cloud and rain models presented are not extensive enough to include all possible conditions. The horizontally non-uniform cloud and rain models that will occur a lot of times should be considered in future studies, although it may further complicate the formulation of the problem. For heavy rain, the solution is based on the uncoupled radiative transfer equation. It may also be extended to a more complicated coupled integral differential equation as given in Stogryn's work.

A simplified model is used to study the parameters that affects the apparent temperature under cloudy and rainy conditions. Good agreement between simplified model and detailed numerical computation for correlating excess temperature with attenuation suggests that the simplified model can also be employed for the sensitivity study of surface parameters such as temperature and salinity of sea water. Further correlations of the excess temperature for detecting a definite rain fall rate in a precipitating atmosphere may also be possible if the related parameters can be estimated properly.

CHAPTER 6

CONCLUSIONS

The investigation in the previous chapters presents a complete microwave apparent temperature theory over the ocean. The model for computing the sea surface emission characteristics is the same as the model for deriving the expressions of differential scattering coefficient, since the surface emissivity depends on the differential scattering coefficient of the sea in an integral form given by Peake. On the other hand, the rise of the apparent temperature over the sea due to clouds or rain depends on its absorption (emission) characteristics, atmospheric temperature profile, and the specific meteorological model used.

A bistatic two scale non-coherent scattering theory extended from Symyonov's paper has been developed to yield the expressions for the differential scattering coefficients. The emission and the backscattering characteristics are then derived from the differential scattering coefficients in the standard way. The theory assumed Gaussian surface height distributions and Gaussian correlation functions for both scales of roughness.

The emission and the scattering characteristics are shown to be dependent on the rms slope of the large undulations m, the standard deviation of the small irregularities σ_1, and the correlation length of the small irregularities ℓ. The wind dependence of the first two parameters is associated with m through slick sea measurements by Cox and Munk, and the σ_1 through the high frequency sea spectrum. The parameter ℓ is associated with the shape of the high frequency sea spectrum and can be reasonably chosen by fitting the sea spectrum BK^{-4} to the assumed Gaussian spectrum. It is noted that the emission characteristics for horizontal polarization is a sensitive measure of σ_1. Thus, σ_1 is established by fitting the emission characteristic to measured data for different wind speeds. The parameters chosen in this way are then used to compute the vertically polarized emission characteristic. Good agreement with measured data and better agreement than single surface model are demonstrated.

The same set of surface parameters at each wind speed is then used to compute the backscatter characteristics. The results except for level are shown to

agree reasonably over all angles with NRL backscatter data under similar wind conditions. Comparison of these characteristics with a single parameter surface model demonstrated better results.

These findings have proven that the validity of the assumed scattering model is better demonstrated when both the predicted backscatter and the emission characteristics are compared with measurements. They have further shown that the measured emission and scattering characteristics with the aid of a reasonable composite surface theory may aid the oceanographer in identifying the wind dependence of the sea spectrum.

Numerical technique has been applied to solve the radiative transfer equation and to determine the cloud and rain effects on the observed apparent temperature when looking downward over the ocean. For large rainfall rates the effects of scattering are found to be significant and are incorporated into the radiative transfer equation.

It is shown that stratus, cumulus, overcast, and rain all contribute significantly to the observed temperature. Larger sensitivities to clouds and rain are observed for horizontally polarized apparent temperature at large nadir angles than for vertically polarized apparent temperature.

Aside from roughness detections, the apparent temperature of a radiometer can be used to infer sea water temperature when surface roughness parameters is being measured by a scatterometer.

The rise of apparent temperature has been found to correlate with the atmospheric attenuation. This result is useful for correcting scatterometric observations. It may also be used to differentiate between a precipitating and a non-precipitating atmosphere when the surface condition is known.

BIBLIOGRAPHY

Artmen, J.O., and J.P. Gordon, "Absorption of Microwave by Oxygen in the Millimeter Region," Physical Review, vol. 96, pp. 1237-1245, December 1954.

Aufm Kampe, H.J. and Weickmann, "Visibility and Liquid Water Content in Clouds in the Free Atmosphere," Jour. of Meteor., vol. 7, no. 1, February 1950.

Aukland, J.C., P.C. Caruso, and W.H. Conway, "Remote Sensing of the Sea Conditions with Microwave Radiometer Systems," Proc. 6th Symp. on Remote Sensing of Environment, University of Michigan, Ann Arbor, October 1969.

Barrett, A. H. and V.K. Chung, "A Method for the Determination of High-Altitude Water-Vapor Abundance from Ground-Based Microwave Observations," JGR, vol. 67, no. 11, 1962, pp. 4259.

Barrick, D.E. and W.H. Peake, "Scattering from Surfaces with Different Roughness Scales: Analysis and Interpretation," Res. Rep. BAT-197A-10-3, Battelle Memorial Institute, Columbus Laboratories, Nov. 1, 1967.

Bass, F.G., I.M. Fuks, A.I. Kalmykov, I.E. Ostrovsky and A.D. Rosenberg, "Very High Frequency Radiowave Scattering by a Disturbed Sea Surface," IEEE Trans. Ant. Prop., vol. AP-16, no. 5, pp. 560-568, September 1968.

Beckmann, P. and A. Spizzichino, The Scattering of Electromagnetic Waves From Rough Surfaces, New York, Macmillan, 1963.

Benoit, A., "Signal Attenuation Due to Neutral Oxygen and Water Vapor, Rain and Cloud," Microwave Journal, vol 11, no. 11, pp. 73-80, November 1968.

Bradley, G.A., "Remote Sensing of Ocean Winds Using a Radar Scatterometer," Ph. D. Thesis, University of Kansas Center for Research, Inc., September 1971.

Capurro, L.R.A., "Oceanography Using Remote Sensors," Report no. AD 682 939, Texas A & M University, January 15, 1969.

Cardone, V.J., "Specification of the Wind Distribution in the Marine Boundary Layer for Wave Forecasting," Ph. D. Thesis, New York University, Geophysical Science Laboratory, Technical Report 69-1, December 1969.

Chan, H.L. and A.K. Fung, "Backscattering from a Two-Scale Rough Surface with Application ro Radar Sea Returns," University of Kansas Center for Research, Inc., CRES Technical Report 186-4, August 1971.

Chandrase Khar, S., Radiative Transfer, Oxford Press, pp. 149-150, 1950.

Chia, R.C., "The Theory of Radar Scatter from the Ocean," University of Kansas Center for Research, Inc., CRES Technical Report 112-1, October 1968.

Chu, C.M. and S.W. Churchill, "Representation of the Angular Distribution of Radiation Scattered by a Spherical Particle," Journ. of Opt. Soc. of Am., vol. 45, no. 11, pp. 958-962, November 1955.

Claassen, J. P., A.K. Fung, and S. Wu, "Toward RADSCAT Measurements Over the Sea and Their Interpretation-Final Report," University of Kansas Center for Research, Inc., CRES Technical Report 186-6, Contract NAS 1-10048, September 1971.

Claassen, J.P. and H. S. Fung, "The Wind Response of NRL Scatterometric Observations at X-band," University of Kansas Center for Research, Inc., CRES Technical Report 186-5, March 1972. (Available upon Request)

Cole, K.S. and R.H. Cole, "Dispersion and Absorption in Dielectrics," Jour. Chemical Physics, vol. 9, 1941, p. 341.

Conaway, J., "Microwave Radiometric Observations of Sea State in March 1966," Microwave Observations of the Ocean Surface, Naval Oceanographic Office, SP-152, pp. 67-74, June 1969.

Cox, C. and W. Munk, "Statistics of the Sea Surface Derived from Sun Glitter," Journal of Marine Research, vol. 13, no. 2, pp. 198-227, February 1954.

Crane, R.K., "Propagation Phenomena Affecting Satellite Communication Systems Operating in the Centimeter and Millimeter Wavelength Bands," Proceedings of IEEE, vol. 59, no. 2, pp. 173-188, February 1971.

Daley, J.C., J.T. Ransome, Jr., and J.A. Burkett, "Radar Sea Return-JOSS I," Navel Research Laboratory, Report no. 7268, May 1971.

Davenport, W.B. Jr., and W.J. Rost, Random Signals and Noise, McGraw-Hill Co., New York, 1958.

Debye, P., "Polar Molecules," New York; The Chemical Catalog Co., Inc. 1929.

Deirmendjian, D., "Complete Microwave Scattering and Extinction Properties of Polydispersed Cloud and Rain Elements," The RAND Corporation Report R-422-PR, December 1963.

De Lorenzo, J.D. and E.S. Cassedy, "A Study of the Mechanism of Sea Surface Scattering," IEEE Transactions, vol. AP-14, no. 5, pp. 611-620, September 1966.

Donn, W.L., "Meteorology," 3rd ed., McGraw-Hill, New York, p. 107.

Droppleman, J.D., "Apparent Microwave Emissivity of Sea Foam," Journal of Geophysical Research, vol. 75, no. 3, pp. 696-698, January 1970.

Eckart, C., "The Scattering of Sound From the Sea Surface, J. Acoust. Soc. Am., vol. 25, 1953, pp. 566-570.

Edgerton, A.T., "Engineering Applications of Microwave Radiometry," Proc. 5th Symp. on Remote Sensing of Environment, University of Michigan, Ann Arbor, p. 711, April 1968.

Fletcher, N.H., The Physics of Rainclouds, Cambridge University Press, 1966.

Fung, A.K., "Theory of Cross Polarized Power Returned from a Random Surface," Appl. Sci. Res., vol. 18, pp. 50-60, August 1967.

Fung, A.K. and H.L. Chan, "Backscattering of Waves Composite Rough Surfaces," IEEE Transactions, vol. AP-17, no. 5, pp. 550-597, September 1969.

Fung, A.K. and F.T. Ulaby, "The Apparent Surface Temperature at Microwave Frequencies," Fall URSI Meeting, Austin, Texas, December 8-10, 1969.

Fuks, I.M., "Theory of Radio Wave Scattering at a Rough Sea Surface," Soviet Radio Physics, vol. 9, no. 5, pp. 513-519, 1969.

Germogenova, T.A., "The Nature of the Solution of the Transfer Equation for a Plane Layer," USSR Computational Mathematics and Mathematical Physics, vol. 1, 3-4, pp. 1168-1186, 1962.

Goldstein, H., "Attenuation by Condensed Water, Propagation of Short Radio Waves," McGraw-Hill Book Co., New York, pp. 671-692, 1951.

Grant, E.H., T.J. Buchanun and H.F. Cook, "Dielectric Behavior of Water at Microwave Frequencies," J. Chemical Physics, vol. 26, January 1957.

Guinard, N.W. and J.C. Daley, "An Experimental Study of Sea Clutter Model," Proceedings of the IEEE, vol. 58, no. 4, pp. 543-550, April 1970.

Gunn, K.L.S. and T.W.R. East, "The Microwave Properties of Precipitation Particles," Quarterly Journal of the Royal Meteorological Society, vol. 80, no. 346, pp. 522-545, October 1954.

Hamilton, P.M., "Vertical Profiles of Total Precipitation in Shower Situations," QJRMS, 92, 1966, p. 346.

Haroules, G.G. and W.E. Browne III, "The Simultaneous Investigation of Attenuation and Emission by the Earth's Atmosphere at Wavelength from 4 Centimeters to 8 Millimeters," Journal of Geophysical Research, vol. 74, no. 18, pp. 4453-4471, August 1969.

Hasted, J.B., D.M. Ritson and C.H. Collie, "Dielectric Properties of Aqueous Ionic Solution," Parts I and II, Jour. of Chemical Physics, vol. 16, no. 1, January 1948.

Hasted, J.B., and G.W. Roderick, "Dielectric Properties of Aqueons and Alcoholic Electrolytic Solutions," Jour. of Chemical Physics, vol. 29, July 1958.

Hill, R.M. and W. Gordy, "Temperature Dependence at the Line Breadth of Oxygen," Physical Review, vol. 91, p. 222, July 1953.

Hogg, D.C., "Millimeter-Wave Communication through the Atmosphere," Science, vol. 159, no. 3810, pp. 39-46, January 5, 1968.

Hollinger, J.P., "Passive Microwave Measurements of the Sea Surface," Journal of Geophysical Research, vol. 75, no. 27, pp. 5209-5213, September 1970.

Hollinger, J.P., "Passive Microwave Measurements of Sea Surface Roughness," IEEE Transactions, vol. GE-9, no. 3, pp. 165-169, July 1971.

Hollinger, J.P., "Remote Passive Microwave Sensing of the Ocean Surface," in 7th International Symposium on Remote Sensing of Environment, May 17-21, 1971, Univ. of Michigan, Ann Arbor, p. 1807, 1971.

Holzer, W., "Atmospheric Attenuation in Satellite Communications," The Microwave Journal, vol. 8, no. 3, March 1965, pp. 119-125.

Hyatt, H.A., "Analysis of Measurements of Microwave Emission from the Earth's Surface and Atmosphere," Report # PB 176 239, Space Sciences Department, Douglas Aircraft Co., June 1967.

Ippolito, L.J., "Effects of Precipitation on 15.3 and 31.65 GHz Earth-Space Transmissions with the ATS-V Satellite," Proceedings of IEEE, vol. 59, no. 2, pp. 189-205, February 1971.

Katzin, M., "On the Mechanism of Radar Sea Clutter," Proceedings of IRE, vol. 45, pp. 44-54, January 1957.

Katzin, M., "Sea Clutter at High Depression Angles with Applications to the Ground Clutter Problem," 1959 Radar Return Symposium Part 1, U.S. Naval Ordnance Test Station and the University of New Mexico, AD no. 244 937, May 1959.

Kerr, D.E., Propagation of Short Radio Waves, MIT Series, 13, McGraw-Hill Co., New York, 1951.

Kinsman, B., Wind Waves, Their Generation and Propagation on the Ocean Surfaces, Prentice-Hall, Inc., Englewood, 1965.

Kreiss, W.T., "Meteorological Observations with Passive Microwave Systems," Ph. D. Dissertation, The Department of Atmospheric Sciences, University of Washington, Seattle, Washington, 1968.

Lane, J.A. and J.A. Saxton, "Dielectric Dispersion in Pure Polar Liquids at Very High Radio Frequencies," Part III: The Effect of Electrolytes in Solution, Proc. Roy. Soc. Am., vol. 213, 1952, pp. 531-545.

Laws, J.O. and D.A. Parsons, "The Relation of Drop Size to Intensity," Trans. Am. Geographers Union, p. 452, 1943.

Levine, J., "The Dynamics of Cumulus Connection in the Trade Winds-A Combined Observational and Theoretical Study," Woods Hole Oceanographic Institution, Ref. no. 65-43, August 1965.

Lynch, R.J. and R.J. Wagner, "Rough -Surface Scattering: Shadowing, Multiple Scatter, and Energy Conservation," J. Math. Physics, September 1970.

Malkus, J.S., "Some Results of a Trade-Cumulus Cloud Investigation," Jour. of Meteor., vol. 11, no. 3, June 1954.

Marshall, J.S. and W. Mck. Palmer, "The Distribution of Raindrops with Size," Journal of Meteor., vol. 5, pp. 165-168, 1948.

Mason, B.J., The Physics of Clouds, second edition, Cambridge, Oxford Press, 1971.

McLelland, H.J., Elements of Physical Oceanography, Pergamon Press, New York, 1965, p. 150.

Medhurst, R.G., "Rainfall Attenuation of Centimeter Waves: Comparison of the Theory and Measurement," IEEE Trans. on Antenna and Propagation, vol. AP-13, pp. 550-564, July 1965.

Meeks, M.L. and A.E. Lilley, "The Microwave Spectrum of Oxygen in the Earth's Atmosphere," JGR, vol. 68, no. 6, pp. 1683-1703, March 1963.

Mie, G., "Beitrage Zur Optik truber Medien, Speziell Kolloidah Metallosungen," Ann. Phys., vol. 25, pp. 345-377, 1908.

Moore, R.K. and W.J. Pierson, Jr., "Worldwide Oceanic Wind and Wave Predictions Using a Satellite Radar Radiometer," Journal of Hydronautics, vol. 5, no. 2, pp. 52-60, February 1971.

Moore, R.K. and F.T. Ulaby, "The Radar Radiometer," Proceedings of the IEEE, vol. 57, no. 4, no. 4, pp. 587-590, April 1969.

National Academy of Sciences, Ocean Wave Spectra, proceedings of conference sponsored by U.S. Navy Oceanographic Office and Division of Earth Sciences, National Research Council, Easton, Md., 1-4 May 1961.

Neumann G. and W.J. Pierson, Jr., Principles of Physical Oceanography, Prentice-Hall, Inc., Englewood Cliffs, N.J., 1966.

Neiburger, M., "Reflection, Absorption and Transmission of Insolation by Stratus Clouds," Journal of Meteorology, vol. 6, no. 2, pp. , April 1949.

Nordberg, W., J. Conaway, and P. Thaddens, "Microwave Observations of Sea State from Aircraft," Report no. X-620-68-414, Goddard Space Flight Center, Greenbelt, Maryland, November 1968.

Nordberg, W., J. Conaway and P. Thaddeus, "Microwave Observations of Sea State from Aircraft," Quarterly Journal of the Royal Meteorological Society, vol. 95, pp. 408-413, 1969.

Nordberg, W., J. Conaway, D.B. Ross, and T. Wilheit, Measurements of Microwave Emission from a Foam-Covered, Wind Driven Sea, Jour. Atmos. Sci., 28, p. 429-435, 1971.

Paris, J.F., "Microwave Radiometry and its Applications to Marine Meteorology and Oceanography," Report Department of Oceanography, Texas A & M University (Project 286-13), College Station, Texas, January 1969.

Parkins, B.E., "Scattering from the Time Varying Surface of the Ocean," Jour. of the Acoustic Soc. of Am., vol. 42, no. 6, pp. 1262-1267, December 1967.

Peake, W.H., "Interaction of Electromagnetic Waves with Some Natural Surfaces," IRE Transactions on Antennas and Propagation (special suppl.), vol. AP-7, pp. 5324-5329, December 1959.

Peake, W.H., R.L. Riegler, and C.H. Schults, "The Mutual Interpretation of Active and Passive Microwave Sensor Outputs," Proc. 4th Symp. on Remote Sensing of Environment, University of Michigan, Ann Arbor, 771 pp., April 1966.

Phillips. O.M., "The Dynamics of the Upper Ocean," Cambridge University Press, London, p. 120, 1966.

Pierson, W.J., and L. Moskowitz, "A Proposed Spectral Form for Fully Developed Wind Seas Based on the Similarity of S.A. Kitaigorodski," Jour. Geophys. Res., vol. 69, 1964, pp. 5181-5190.

Pierson, W.J., Jr., "The Integration of Remote Sensing Data into Global Weather Prediction, Wave Forecasting, and Ocean Circulation Computer Based Systems," New York University, Hydrology and Oceanography, Third Annual Earth Resources Review, vol. 3, December 1970.

Pierson, W.J., Jr., "A Proposed Vector Wave Number Spectrum for a Study of Radar Sea Return," Microwave Observations of the Sea, Naval Oceanographic Office, SP-152, pp. 251-282.

Pierson, W.J., Jr., F.C. Jackson, R.A. Stacy, and E. Mehr, "Research on the Problem of the Radar Return from a Wind Roughened Sea," AAFE Principal Investigator's Review, pp. 83-113, October 5-6, 1971.

Porter, R.A., "An Analytical Study of Measured Radiometric Data, vol. 1," Radiometric Technology, Inc., JPL Contract 952397, NASA Accession no. N 70-20193, December 1969.

Porter, R.A., "An Analysis of Airborne Microwave Radiometric Data—Final Report," Goddard Space Flight Center, Contract NAS5-11685, February 1970.

Porter, R.A. and F.J. Wentz, III, "Microwave Radiometric Study of Ocean Surface Characteristics," Final Report, Contract I-35140, Radiometric Technology, Inc., Wakefield, Massachusetts, July 1971.

Rice, S.O., "Reflection of Electromagnetic Waves from Slightly Rough Surfaces," Communications in Pure and Applied Mathematics, vol. 4, pp. 361-378, February 1951.

Rooth, C. and G. Williams, "Microwave Radiometry of the Ocean," University of Miami, Quarterly Reports, May and August 1970.

Ross, D.B., V.J. Cardone, J.W. Conaway, Jr., "Laser and Microwave Observation of Sea-Surface Condition for Fetch Limited 17-25 m/s Winds," IEEE Transactions, vol. GE-8, no. 4, pp. 326-336, October 1970.

Ryde, J.W., and D. Ryde, "Attenuation of Centimeters Waves by Rain, Hail and Clouds," Report no. 8516, General Electric Company Research Labs, Wembley, England, August 1944.

Saxton, J.A. and J.A. Lane, "Electrical Properties of Sea Water," Wireless Engr., vol. 29, p. 269, October 1952.

Semyonov, B., "Approximate Computation of Scattering of Electromagnetic Waves by Rough Surface Contours," Radio Engineering and Electronic Phys., vol. 11, pp. 1179-1187, 1966.

Shifrin, K.S., "Transfer of Microwave Radiation in the Atmosphere," Transactions of the Main Geophysical Observatory (USSR), NASA N69-31851-31868, July 1969.

Silver, S., Microwave Antenna Theory and Design, MIT Series, 12, McGraw-Hill Book Co., New York, 1947.

Singer, S.F. and F.G. Williams, Jr., "Microwave Detection of Precipitation over the Surface of the Ocean," Jour. of Geophysical Research, vol. 73, no. 11, pp. 3324-3327, May 1968.

Sirounian, V.A., "Passive Microwave Radiometry of Sea State," Report DAC-60786, Douglas Aircraft Company, September 1967.

Skelnik, M.I., Radar Handbook, McGraw-Hill Book Co., New York, 1970.

Sobolev, V.V., A Treatise of Radiative Transfer, D. Van Nostrand Co., Inc., New York, 1963.

Spyers-Duran, P.A., "Comparative Measurements of Cloud Liquid Water Using Heated Wire and Cloud Replicating Devices," Jour. of Appl. Meteor., vol. 7, pp. 674-678, August 1968.

Staelin, D.H., "Measurements and Interpretation of the Microwave Spectrum of the Terrestrial Atmosphere near 1-centimeter Wavelength," JGR, vol. 71, no. 12, pp. 2875-2881, June 1966.

Stilwell, D., Jr., "Directional Energy of Sea Waves from Photographs," Jour. Geophys, Res., vol. 79, no. 8, pp. 1974-1986, August 1969.

Stogryn, A., "Effect of Scattering by Precipitation on Apparent Sky Temperature in the Microwave Region," Space General Corporation, Report SGC 613 TM-1, El Monte, California, 1964.

Stogryn, A., "The Apparent Temperature of the Sea at Microwave Frequencies," IEEE Trans. on Antennas and Propagation, vol. AP-15, pp. 278-286, March 1967.

Stogryn, A., "The Emissivity of Sea Foam at Microwave Frequencies," Technical Report for Contracr NAS1-10633, Microwave Division, Aerojet-General Corp., El Monte, Cal., April 30, 1971.

Stratton, J.A., Electromagnetic Theory, McGraw-Hill Book Co., New York, 1941.

Strickland, J.I., "Attenuation, Emission, and Backscatter by Precipitation," USNC/URSI Meeting, Columbus, Ohio, September 15, 1970.

Strong, A.E., "Mapping Sea-Surface Roughness Using Microwave Radiometry," Jour. of Geophysical Research, vol. 76, no. 36, pp. 8647-8648, December 20, 1971.

Sutherland, A.J., "Spectral Measurements and Growth Rates of Wind-Generated Water Waves," Stanford University, Dept. of Civil Engineering, Technical Report 84, August 1967.

Sverdrup, H.V., M.W. Johnson and R.H. Fleming, "The Oceans, Their Physics, Chemistry, and General Biology," Prentice-Hall, Englewood Cliffs, N.J., 1942.

Ulaby, F.T., A.K. Fung, and S. Wu, "The Apparent Temperature and Emissivity of Natural Surfaces at Microwave Frequencies," CRES Technical Report 133-12, University of Kansas, Lawrence, 1970.

United States Standard Atmosphere, Washington, D.C., December 1962.

Valenzuela, G.R., "Depolarization of Em Waves by Slightly Rough Surfaces," IEEE Transactions, vol. AP-15, no. 4, pp. 552-557, July 1967.

Valenzuela, G.R., "Backscattering of Electromagnetic Waves from a Tilted Slightly Rough Surface," Radio Science, vol. 3, no. 11, pp. 1057-1066, November November 1968.

Valenzuela, G.R., "The Effective Reflection Coefficients in Forward Scatter from a Dielectric Slightly Rough Surface," IEEE Proceedings, vol. 58, no. 8, p. 1279, 1970.

Valenzuela, G.R., M.B. Laing and J.C. Daley, "Ocean Spectra for High Frequency Waves from Airborne Radar Measurements," Jour. of Marine Research, vol. 29, no. 2, May 1971.

Valley, S.L., Handbook of Geophysics and Space Environment, McGraw-Hill Book Co., New York, 1965.

Van De Hulst, H.C., Light Scattering by Small Particles, John Wiley & Sons, Inc., New York, 1957.

Van Vleck, J.H. and V.F. Weisskopf, "On the Shape of Collision Broadened Lines," Reviews of Modern Physics, vol. 17, 1945.

Van Vleck, J.H., "The Absorption of Microwaves by Oxygen," Physical Review, vol. 71, no. 7, pp. 413-424, April 1947.

Van Vleck, J.H., "The Absorption of Microwaves by Uncondensed Water Vapor," Physical Review, vol. 71, no. 7, pp. 425-432, April 1947.

Volchok, V.A. and M.M. Chesnyak, "Transfer of Microwave Radiation in Clouds and Precipitation," NASA Report N69-31851-868, pp. 90-107, July 1969.

Williams, G., "Microwave Radiometry of the Ocean and the Possibility of Marine Wind Velocity Determination from Satellite Observations," Jour. Geophys, Res., 74 (18), 4591, 1969.

Wright, J.W., "Backscattering from Capillary Waves with Application to Sea Clutter," IEEE Transactions, vol. AP-16, no. 2, pp. 217-223, March 1968.

Wu. S., "The Meteorological Effects on Microwave Apparent Temperatures Looking Downward over a Smooth Sea," University of Kansas Center for Research, Inc., CRES Technical Report 186-1, NASA Contract NASA 1-10048, October 1970.

Wu, T. S. and A. K. Fung, "A Non-Coherent Model for Microwave Emission and Backscattering from the Sea," JGR, vol. 77, no. 30, pp. 5917-5929, October 20, 1972.

APPENDIX
FORTRAN IV COMPUTER PROGRAMS

A list of FORTRAN IV computer programs and a brief description of the input and output format are presented in this appendix. The equations and formulas shown in the programs are based on the derivations given in the main text with some modification. The tabulated results and the figures of the main text are computed by applying these programs.

A-1 A computer program for computing the sea water dielectric constant and the plane sea surface emissivity.

In this program the input cards are punched in data-card format with different frequency FR(I), temperature TEMP(I) and salinity SALI(I). The output for the computed dielectric constant is tabulated with respect to temperature and salinity. A different frequency results in a different table. The output for the computed plane sea surface emissivity is tabulated with respect to nadir angle at a ten degree interval for both horizontal and vertical polarizations at one frequency, one temperature and one salinity. For multiple frequency, temperature or salinity input, the output of the computed emissivity is printed out sequentially with preassigned sequence until all values are printed out.

A-2 A computer program for computing the surface emissivity due to small scale differential scattering coefficient.

This program is written for computing the surface emissivity due to small scale roughness. From this program the contribution of the small scale roughness to the overall emissivity can be estimated. The inputs are punched in constant-card format. The first three constant-cards contain the information on surface roughness parameters, i.e. the rms slope of the large scale sea surface, and the correlation distance and the standard deviation of small scale roughness. On the second two constant-cards are the real and the imaginary parts of the dielectric constant. The output of the computed surface emissivity is printed out versus nadir angle at a ten degree interval for both horizontal and vertical polarization. To compute a different surface condition either due to surface roughness or dielectric properties it is required to change the input card.

A-3 A computer program for computing the modified Fresnel reflection coefficient.

In this program the inputs are punched in constant-card format. The first two constant-cards contain the correlation distance and the standard deviation of small scale roughness. On the second two constant-cards are the real and the imaginary parts of the dielectric constant. The output of the computed results are printed out versus nadir angle at a fifteen degree interval for both horizontal and vertical polarizations. In this program Romberg integration is being employed.

A-4 A computer program for computing the two-scale rough surface emissivity.

The computed results of the last two programs and the differential scattering coefficient due to the large scale roughness have been employed in this program for computing the two-scale rough surface emissivity. Due to the complexity of multiple integration and the averaging procedure only one case is computed in one program time. The inputs are all punched in constant-card format. The first three cards contain the surface roughness parameters. The second two cards contain the real and the imaginary parts of the dielectric constant. The output of the computed surface emissivity is printed out versus nadir angle at a ten degree interval for both horizontal and vertical polarizations.

A-5 A computer program for computing two scale backscattering cross-section.

In this program the input is punched in data-card and constant-card format. The data-card contains the surface parameters i.e. the large and the small scale roughness. The two constant-cards contain the real and the imaginary part of the dielectric constant. The output of the computed backscattering cross-section is printed out versus nadir angle at a ten degree interval for both horizontal and vertical polarizations.

A-6 A computer program for computing the clear sky and cloudy sky apparent temperatures.

In this program the input data contains three parts. The first part is in read-card format that reads in the required surface emissivity and averaged surface reflectivity. The surface emissivity data are obtained from previous computer

program. The second part of the input is in data-card format. It specifies the standard atmospheric conditions such as the temperature, the water vapor and the pressure at the sea level. The last part of the input data is in read-card format that reads in various cloud conditions, i.e. the cloud thickness and liquid water contents. The output of the computed apparent temperature is printed out versus nadir angle at a ten degree interval for both horizontal and vertical polarizations. Each cloud condition is printed out in one tabulated form.

A-7 A computer program for computing the apparent temperature of light to moderate rain.

The input and output format in this program is the same as the above clear and cloudy sky apparent temperature program. The only difference is in the third part of the input cards. In this program various rain cases are employed instead of cloud conditions.

A-8 A computer program for computing the scattering characteristics of rain.

In this program all the input data are punched in read-card format. The first card contains the number of integrations and the differential increment needed in the integrations to obtain good accuracy. The second card contains the number of frequencies, temperatures, precipitation rates and angles that are required in the computation. The last three cards contain the values of the frequencies, the rain drop temperatures, and the precipitation rates. The output is headed by the title of the problem. For a specific case with one frequency, one temperature and one precipitation rate, the output of the computed results is printed out in two parts. The first part contains the extinction coefficient, the scattering coefficient, and the albedo of scattering. The second part contains the scattering phase function at nineteen different angles at a ten degree interval. For different precipitation rates, temperatures and frequencies, the format of the printed output will repeat as above.

A-9 A computer program for computing the apparent temperature of heavy rain.

This program contains many matrix operations. The matrix inversion subroutine is obtained from computer subprogram library. Hence we only use a call

statement to call in this subroutine. The input data are punched in read-card format. The first card specifies the surface emissivity and reflectivity. The second card specifies the scattering characteristics of rain and the values are obtained from the above program outputs.

The output of the computed results are printed out with respect to nadir angle and increment layer. In this program we assume thirty increment layers for total rain thickness and five nadir angles. Hence, the printed output will contain one hundred and fifty net points. For different precipitation rates and surface conditions that include the change of polarization, it is necessary to change the input card and re-run the program to obtain the computed results.

A-1. A computer program for computing the sea water dielectric constant and the plane sea surface emissivity.

```
$       IDENT   2523,W3 WU SHIH TSENG
$       OPTION  FORTRAN,ERCNT/15/
$       FORTRAN NDECK
        DIMENSION EP(10,6,6),EPP(10,6,6),FR(10),TEMP(6),SALI(6)
        DIMENSION EMH(10,6,10),EMV(10,6,10),TBH(10,6,10),TBV(10,6,10)
        DATA (FR(I),I=1,10)/1.228,1.41,4.455,8.36,8.91,9.3,13.9,15.8,17.4
       1,19.34/
        DATA (TEMP(I),I=1,6)/276.,28Y.,284.,288.,292.,296./
        DATA (SALI(I),I=1,6)/32.,33.,34.,35.,36.,37./
        DO 70 I=1,10
        FQ=FR(I)
        DO 70 J=1,6
        TG=TEMP(J)
        DO 70 K=1,6
        S=SALI(K)
        CALL DIELCO(FQ,TG,S,E1,E2)
        EP(I,J,K)=E1
        EPP(I,J,K)=E2
    70  CONTINUE
        DO 71 I=1,10
        WRITE (6,72)   FR(I)
    72  FORMAT(1H1,//45X,5HFREQ=,F8.4,4H GHZ,//)
        WRITE(6,73) (TEMP(J),J=1,6)
    73  FORMAT(11X,6(5HTEMP=,F5.1,2H K,4X)//)
        WRITE(6,22)
    22  FORMAT(3X,4HSALI,6(4X,2HE1,6X,2HE2,2X)//)
        WRITE(6,74) (SALI(K),(EP(I,J,K),EPP(I,J,K),J=1,6),K=1,6)
    74  FORMAT(    13(3XF5.2)//)
    71  CONTINUE
         PI = ATAN(1.)*4.
        PI10=PI/18.0
        L=4
        DO 8 I=1,10
        DO 8 J=1,6
        DO 8 K=1,10
        E1=EP(I,J,L)
        E2=EPP(I,J,L)
        THETA1=FLOAT(K-1)*PI10
        CES=COS(THETA1)
        SEN=SIN(THETA1)
        COS2=CES*CES
        SIN2=SEN*SEN
        F1=E1-SIN2
        B=(F1*F1+E2*E2)**0.25
        GAMA0=0.5*ATAN(E2/F1)
        F2=CES*COS(GAMA0)
        F=1.0/(COS2+2.0*B*F2+B*B)
        EMH(I,J,K)=4.*B*F2*F
        GAMA2=ATAN(E2/E1)
        G=CES*(F1*F1+E2*E2)**0.5
```

```
      RG=R*G*COS(GAMA2-GAMA0)
      R4=1.0/(R*R+G*G+2.0*RG)
      EMV(I,J,K)=4.*RG*R4
      TBH(I,J,K)=TEMP(J)*EMH(I,J,K)
      TBV(I,J,K)=TEMP(J)*EMV(I,J,K)
    8 CONTINUE
      WRITE(6,21)
   21 FORMAT(1H1,50HTHIS IS TO CALCULATE THE EMISSIVITY OF SEA SURFACE,)
      DO 11 I=1,10
      WRITE(6,18) (EMH(I,5,K),K=1,10),(EMV(I,5,K),K=1,10)
   18 FORMAT(10(4XF 6.4)//)
   11 CONTINUE
      DO 12 J=1,6
      WRITE(6,19) (EMH(I,J,1),I=1,10),(TBH(I,J,1),I=1,10)
   19 FORMAT(10(2XF8.2)//)
   12 CONTINUE
      STOP
      END
$      FORTRAN NDECK
      SUBROUTINE DIELCO(FQ,TG,S,E1,E2)
      PIN2=ATAN(1.)/25.
      DAM=30./FQ
      SWN=S/58.45
      TC=TG-273.
      ES=87.8-15.3*SWN-0.363*TC
      DMS=3.38-0.11*TC+0.00147*TC*TC+0.0173*TC*SWN -0.52*SWN
      THEG=5.*SWN+0.12*TC*SWN+0.04*TC
      DN=1.+PIN2*(DMS/DAM)**0.98
      DD=2.*DN-1.+(DMS/DAM)**1.96
      E1=4.8+(ES-4.8)*DN/DD
      E2=18.*THEG/FQ+(ES-4.8)*(DMS/DAM)**0.98/DD
      RETURN
      END
$      EXECUTE
$      LIMITS  10,20000,,10000
$      ENDJOB
***EOF
```

A-2. A computer program for computing the surface emissivity, $\epsilon_j(\theta)$ due to small scale differential scattering coefficient $\langle \gamma_j'(\theta, \theta_s, \phi_s) \rangle$.

```
$       IDENT   2526. WU SHIH-TSENG
$       OPTION  FORTRAN,FRONT/15/
$       FORTRAN NODECK
        DIMENSION A(61,61),P(61),E(61),REFH(9),REFV(9),TAH(9),TAV(9)
       1,CO(9)
        COMMON /ZZ/VCO,THEI,THES,PHIS
        COMMON /XX/E1,E2
        DATA (CO(I),I=1,4)/4.,6.,7.,8./
        PI=ATAN(1.)*4.
        PI10=PI/18.
        TG=291.
        KY=61
        KP=70
        KXP=2*KP-1
        CALL COEFFS(A,P,E,PI,KP,KXP,FCTRI,KY)
        E1=49.
        E2=35.
        DO 4 II=1,1
        CKT=CO(II)
        E12=(E1-1.)**2+E2*E2
        DO 2 K=1,8
        THEI=PI10*FLOAT(K-1)
        STI=SIN(THEI)
        CTI=COS(THEI)
        CALL REFCO(CTI,DLI,DRI,R2I,BI,QI)
        SUMH=0.0
        SUMV=0.0
        DO 3 L=1,KXP
        THES=(PI+P(L))*.25
        STS=SIN(THES)
        CTS=COS(THES)
        CALL REFCO(CTS,DLS,DRS,R2S,BS,QS)
        DO 3 M=1,KXP
        PHIS=E(M)
        AH=0.0
        AV=0.0
        VCO=0.12
        DO 12 I2=1,2
        PHIN=PI/4.
        DO 11 I=1,2
        CALL ANGLE(PHIN,CTI,STI,SPI,CPI,CTS,STS,SPS,CPS)
        IF(CTI.LT.1.E-3.OR.CTS.LT.1.E-3) GO TO 24
        CPSI=(CPS*CPI+SPS*SPI)
        CPS2=CPSI*CPSI
        SPS2=1.-CPS2
        QT=STI**2-2.*STI*STS*CPSI+STS**2
        PMR=.04*CKT*E12*EXP(-.25*CKT*QT)*CTI*CTS**2
        VN1=(E1*STI*STS-CPSI*(BI*BS-QI*QS))**2
        VN2=(CPSI*(BI*QS+BS*QI)-E2*STI*STS)**2
        AH=(CPS2/DRS+SPS2*R2S/DLS)/DRI*PMR+AH
        AV=((VN1+VN2)/DLS+SPS2*R2I/DRS)/DLI*PMR+AV
```

```
   24 CONTINUE
   11 PHIN=-PHIN
   12 VCO=-VCO
      SUMH=SUMH+.25*AH*SIN(THES)*A(L,M)
      SUMV=SUMV+.25*AV*SIN(THES)*A(L,M)
    3 CONTINUE
      REFV(  K)=SUMV*.0625/PI*FCTR1
      REFH(  K)=SUMH*.0625/PI*FCTR1
      TAH(  K)=TG*REFH(  K)
      TAV(  K)=TG*REFV(  K)
    2 CONTINUE
      WRITE(6,5) REFH,REFV,TAH,TAV
    5 FORMAT(1H0,9(2XE11.4)//)
    4 CONTINUE
      STOP
      END
      SUBROUTINE REFCO(U,DRL2,DRB2,B2,P,Q)
      COMMON /XX/E1,E2
      PHI2=ATAN(E2/E1)
      G=U*(E1*E1+E2*E2)**.5
      EU=E1-1.+U*U
      PHI0=.5*ATAN(E2/EU)
      B=(EU*EU+E2*E2)**.25
      P=B*COS(PHI0)
      Q=B*SIN(PHI0)
      B2=B*B
      DRB2=U*U+2.*U*B*COS(PHI0)+B2
      DRL2=G*G+2.*G*B*COS(PHI2-PHI0)+B2
      RETURN
      END
$       FORTRAN NDECK
      SUBROUTINE ANGLE(A,S,T,U,V,W,X,Y,Z)
      COMMON /ZZ/VCO,THE1,THES,PHIS
      B=SQRT(1.+VCO*VCO)
      S=(COS(THE1)+VCO*SIN(THE1)*COS(A))/B
      T=SQRT(1.-S*S)
      U=-SIN(A)*SIN(THE1)/T
      V=SQRT(1.-U*U)
      W=(COS(THES)-VCO*SIN(THES)*COS(A-PHIS))/B
      X=SQRT(1.-W*W)
      Y=SIN(PHIS-A)*SIN(THES)/X
      Z=SQRT(1.-Y*Y)
      RETURN
      END
```

```
      SUBROUTINE COEFFS(A,P,E,PI,K,KX,FCTR1,KY)
      DIMENSION A(KY,KY),P(KY),E(KY)
      H=PI
      C=K-1
      DO 1 J=2,KX,2
      A(J,K)=-32.0
    1 A(J,K-1)=1000.0
      DO 2 J=3,KX,2
      A(J,K)=14.0
    2 A(J,K-1)=-64.0
      A(1,K)=7.0
      A(KX,K)=7.0
      A(1,K-1)=-32.0
      A(KX,K-1)=-32.0
      DO 11 I=1,KX
      DO 11 J=3,K,2
      L=K-J
      A(I,L+1)=2.0*A(I,K)
      IF (L.EQ.0) GO TO 11
      A(I,L)=A(I,K-1)
   11 CONTINUE
      FCTR1=4.0*H*H/(900.0*C*C)
      Q=H/C
      E(1)=0.0
      P(1)=-H
      DO 5 I=2,K
      E(I)=E(I-1)+Q
    5 P(I)=P(I-1)+Q
      K1=K+1
      DO 6 I=K1,KX
    6 P(I)=P(I-1)+Q
      J1=2
      DO 15 I=K1,KY
      DO 14 J=1,KX
   14 A(J,I)=A(J,J1)
      E(I)=-E(J1)
   15 J1=J1+1
      RETURN
      END
$      EXECUTE
$      LIMITS  10,48000,,10000
$      ENDJOB
***EOF
```

A-3. A computer program for computing the modified Fresnel reflection coefficient.

```
$       IDENT   2523,W3WU SHIH TSENG
$       OPTION  FORTRAN,FRCNT/15/
$       FORTRAN NDECK
      DIMENSION F(5),SH(9),SHI(9) ,SHJ(9),T(9,9),SV(9),SVI(9),SVJ(9)
      COMMON SC,SS,CP2,SP2,E1,E2,ST2
      EXTERNAL FH1,FH2,FV1,FEXP,FV2
      DATA (F(J),J=1,5)/7.,32.,12.,32.,7./
      E1=54.
      E2=38.5
      PI=ATAN(1.)*4.
      DO 5 I=1,3
      THI=(FLOAT(I)+5.5)*PI/18.
      ST2=SIN(THI)**2
      SN2=2.*SIN(THI)
      SHI(I)=0.0
      SHJ(I)=0.0
      SVI(I)=0.0
      SVJ(I)=0.0
      DO 6 J=1,5
      PHI=FLOAT(J-1)*PI/16.
      SC=SN2*COS(PHI)
      SS=SN2*SIN(PHI)
      CP2=COS(PHI)**2
      SP2=SIN(2.*PHI)
      AT1=0.0
      AT2=0.0
      AT3=0.0
      AT4=0.0
      A=0.0
      DO 7 L=1,4
      B=A+1.0
      CALL TROMB(8,A,B,FH1,FEXP,T,5,9)
      T1=T(5,5)
      CALL TROMB(8,A,B,FH2,FEXP,T,5,9)
      T2=T(5,5)
      CALL TROMB(8,A,B,FV1,FEXP,T,5,9)
      T3=T(5,5)
      CALL TROMB(8,A,B,FV2,FEXP,T,5,9)
      T4=T(5,5)
      WRITE(6,2) A,B,T1,T2,THI,PHI,T3,T4
      AT1=AT1+T1
      AT2=AT2+T2
      AT3=AT3+T3
      AT4=AT4+T4
    7 A=B
      SHI(I)=SHI(I)+AT1*F(J)/90.
      SHJ(I)=SHJ(I)+AT2*F(J)/90.
      SVI(I)=SVI(I)+AT3*F(J)/90.
      SVJ(I)=SVJ(I)+AT4*F(J)/90.
    6 CONTINUE
```

```
      SH(I)=EXP(-ST2)/PI*(SHI(I)+SHJ(I))
      SV(I)=EXP(-ST2)/PI*(SVI(I)+SVJ(I))
    5 CONTINUE
      WRITE(6,2) SH,SHI,SHJ,SV,SVI,SVJ
    2 FORMAT(9(2XE11.4)//)
      STOP
      END
$      FORTRAN NDECK
      FUNCTION FEXP(X)
      FEXP=EXP(-X*X)*X

      RETURN
      END
$      FORTRAN NDECK
      FUNCTION FH1(X)
      COMMON SC,SS,CP2,SP2,E1,E2,ST2
      S2=SQRT(2.)
      Y=SC*X
      P=Y/S2
      Z=SS*X
      Q=Z/S2
      COSHP= (EXP(P)+EXP(-P))/2.
      EP=EXP(Y)+EXP(-Z)+2.*COSHP  *EXP(-Q)
      IF(X.LE.1.0) B=SQRT(1.-X*X)
      IF(X.GT.1.0) B=0.0
      ER=REAL(CSQRT(E1-ST2-(0.0,1.0)*E2))
      CR=REAL(CSQRT(E1-X*X-(0.0,1.0)*E2))
      FH1=EP*(B+ER-CR)
      RETURN
      END
$      FORTRAN NDECK
      FUNCTION FH2(X)
      COMPLEX B,C
      COMMON SC,SS,CP2,SP2,E1,E2,ST2
      S2=SQRT(2.)
      Y=SC*X
      Z=SS*X
      P=Y/S2
      Q=Z/S2
      COSHP= (EXP(P)+EXP(-P))/2.
      SINHP= (EXP(P)-EXP(-P))/2.
      EP=EXP(Y)*(1.-CP2)+CP2*EXP(-Z)+EXP(-Q)*(COSHP  +SP2*SINHP  )
      IF(X.LE.1.0) B=SQRT(1.-X*X)
      IF(X.GT.1.0) B=(0.0,1.0)*SQRT(X*X-1.0)
      C=CSQRT(E1-X*X-(0.0,1.0)*E2)
      FH2=REAL((C-B)/(X*X+B*C))*X*X*EP
      RETURN
      END
```

```
$       FORTRAN NDECK
        FUNCTION FV1(X)
        COMPLEX B,C,ECS,CMB
        COMMON SC,SS,CP2,SP2,E1,E2,ST2
        S2=SQRT(2.)
        CT2=1.-ST2
        ECS=(E1-(0.0,1.0)*E2)/((E1+1.)*CT2-1.-(0.0,1.0)*E2*CT2)
        Y=SC*X
        P=Y/S2
        Z=SS*X
        Q=Z/S2
        COSHP= (EXP(P)+EXP(-P))/2.
        EP=EXP(Y)+EXP(-Z)+2.*COSHP   *EXP(-Q)
        IF(X.LE.1.0) B=SQRT(1.-X*X)
        IF(X.GT.1.0) B=(0.0,1.0)*SQRT(X*X-1.0)
        C=CSQRT(E1-X*X-(0.0,1.0)*E2)
        CMB=ECS*(CSQRT(E1-ST2-(0.0,1.0)*E2)-B*C*ST2*(C-B)/(X*X+B*C))
        FV1=REAL(B+CMB-C)*EP
        RETURN
        END
$       FORTRAN NDECK
        FUNCTION FV2(X)
        COMPLEX B,C,ECS,CMB,SEL,SEQ,CFV
        COMMON SC,SS,CP2,SP2,E1,E2,ST2
        S2=SQRT(2.)
        ST1=SQRT(ST2)
        CT2=1.-ST2
        SEL=ST2/(E1-(0.0,1.0)*E2)
        ECS=CT2-SEL
        Y=SC*X
        Z=SS*X
        P=Y/S2
        Q=Z/S2
        COSHP= (EXP(P)+EXP(-P))/2.
        SINHP= (EXP(P)-EXP(-P))/2.
        CP1=SQRT(CP2)*(EXP(Y)+S2*EXP(-Q)*SINHP)
        SP1=SQRT(1.-CP2)*(EXP(-Z)+S2*EXP(-Q)*COSHP)
        EP=EXP(Y)*CP2+(1.-CP2)*EXP(-Z)+EXP(-Q)*(COSHP-SP2*SINHP)
        IF(X.LE.1.0) B=SQRT(1.-X*X)
        IF(X.GT.1.0) B=(0.0,1.0)*SQRT(X*X-1.0)
        C=CSQRT(E1-X*X-(0.0,1.0)*E2)
        SEQ=CSQRT(E1-ST2-(0.0,1.0)*E2)
        CMB=X/(X*X+B*C)
        CFV=CMB*((C-B)*(1.-SEL)*X*EP-2.*ST1*SEQ*(CP1-SP1))/ECS
        FV2=REAL(CFV)
        RETURN
        END
```

```
$       FORTRAN NDECK
        SUBROUTINE TROMB(NMAX,A,B,F, G,T,JMAX,NRC)
        DIMENSION T(NRC,NRC)
        H=B-A
        T(1,1)=(F(A)*G(A)+F(B)*G(B))*H/2.
        DO 2 N=1,NMAX
        T(N+1,1)=0.0
        FR=H/2.0**N
        IMAX=2**N-1
        DO 1 I=1,IMAX,2
      1 T(N+1,1)=T(N+1,1)+F(FLOAT(I)*FR+A)*G(FLOAT(I)*FR+A)
      2 T(N+1,1)=T(N,1)/2.0+H*T(N+1,1)/2.0**N
        DO 3 J=2,JMAX
        NXMJP2=NMAX-J+2
        FORJM1=4.0**(J-1)
        DO 3 N=1,NXMJP2
      3 T(N,J)=(FORJM1*T(N+1,J-1)-T(N,J-1))/(FORJM1-1.0)
        RETURN
        END
$       EXECUTE
$       LIMITS  10,10000,,10000
$       ENDJOB
***EOF
```

A-4. A computer program for computing the two-scale rough surface emissivity $\epsilon_j(\theta)$.

```
$       IDENT   2523,W3,STEVE WU
$       OPTION  FORTRAN,FRCNT/15/
$       FORTRAN NDECK
      DIMENSION A( 61, 61),P(061),E(061),TATM(09),ATZ(09),TREF(10,3,9)
     1,CES1(061),CES2(061),CES3(061),CES4(061),CES5(061),CES6(061)
     2,SEN1(061),SEN2(061),SEN3(061),SEN4(061),SEN5(061),SEN6(061)
     3,VEL(3),EMIS(10,3,5),TARS(10,3,5),TMES(10,3,5),TSKY(09)
     4,CES7(61),CES8(061),CES9(061),CES0(061),SEN7(061),SEN8(061)
     5,SEN0(61),SEN9(061),AP(61,61),PP(61),EP(61)
      COMMON PI,PI360,E1,E2,CES,SEN,EUI,E12,ES,EC,PE,QE,TM,S20
      DATA (VEL(K),K=1,2)/15.0,20.00/
       PI = ATAN(1.)*4.
      PI10=PI/18.0
      PI360=2.0*PI
      PI90=PI/2.0
      PI45=PI90/2.
      PI22=PI45/2.
      SLOP1=.25
      SLOP2=.125
      SLOP3=.0625
      SLOP0=.1875
      TG=291.
      TM=1.12*TG-50.
      S20=.01921
      E1=58.6
      E2=36.6
      EUI=(E1-1.)**2+E2*E2
      E12=E1*E1+E2*E2
      PHI0=.5*ATAN(E2/E1)
      ES=SQRT(E12)
      RQ=SQRT(ES)
      PE=RQ*COS(PHI0)
      EC=PE*ES
      QE=RQ*SIN(PHI0)
      KY=61
      KYP=61
      K=10
      KP=20
      KX=2*K-1
      KXP=2*KP-1
      CALL COEFFS(A ,P ,E ,PI,K ,KX ,FCTR1,KY )
      CALL COEFFS(AP,PP,EP,PI,KP,KXP,FCTR2,KYP)
      CALL SORT(P,0.,PI90,SLOP1,PI,CES1,SEN1,KX ,KY )
      CALL SORT(P,PI45,PI90,SLOP2,PI,CES2,SEN2,KX,KY)
      CALL SORT(PP,0.0,PI45,SLOP2,PI,CES3,SEN3,KXP,KYP)
      CALL SORT(P,PI90,PI,SLOP1,PI,CES8,SEN8,KX,KY)
      CALL SORT(P, 0.0,PI22,SLOP3,PI,CES9,SEN9,KX,KY)
      CALL SORT(P,PI22,PI90,SLOP0,PI,CES0,SEN0,KX,KY)
      DO 90 K=1,9
      THETA1= FLOAT(K-1)*PI10
```

```
      CES=COS(THETA1)
      SEN=SIN(THETA1)
      X1=THETA1-PI22
      IF (X1.LT.0.0) X1=0.0
      X2=THETA1+PI22
      IF (X2.GT.PI90) X2=PI90
      SLOP4=X1/PI360
      SLOP5=(PI90-X2)/PI360
      SLOP6=(X2-X1)/PI360
      CALL SORT(E ,0.0,X1,SLOP4,PI,CES4,SEN4,KX ,KY )
      CALL SORT(E ,X2,PI90,SLOP5,PI,CES5,SEN5,KX ,KY )
      CALL SORT(E,X1,X2,SLOP6,PI,CES6,SEN6,KX,KY)
      CALL SORT(EP,X1,X2,  SLOP6,PI,CES7,SEN7,KXP,KYP)
      DO 90 N=1,2
      DO 90 KK=1,2
      CO=.004+0.78E-3*VEL(KK)
      FF2=SLOP1*SLOP4
      P1=PINT(P11,SLOP4,CES4,SEN4,CES1,SEN1,CO,N, FF2,A ,KX ,KY )
      FF2=SLOP1*SLOP5
      P2=PINT(P22,SLOP5,CES5,SEN5,CES1,SEN1,CO,N, FF2,A ,KX ,KY )
      FF2=SLOP2*SLOP6
      P3=PINT(P33,SLOP6,CES6,SEN6,CES2,SEN2,CO,N, FF2,A,KX,KY)
      FF2=SLOP2*SLOP6
      P4=PINT(P44,SLOP6,CES7,SEN7,CES3,SEN3,CO,N, FF2,AP,KXP,KYP)
      FF2=SLOP1*SLOP3
      P5=PINT(P55,SLOP3,CES9,SEN9,CES8,SEN8,CO,N,FF2,A,KX,KY)
      FF2=SLOP1*SLOP0
      P6=PINT(P66,SLOP0,CES0,SEN0,CES8,SEN8,CO,N,FF2,A,KX,KY)
      WRITE(6,7) P1,P2,P3,P4,P5,P6
    7 FORMAT(6(5XE11.4)//)
      TINT=(P1+P2+P3+P5+P6)/PI360*FCTR1+P4*FCTR2/PI360
      TARS(K,N,KK)=(1.-TINT)*TG
      TREF(K,N,KK)=((P11+P22+P33+P55+P66)*FCTR1+P44*FCTR2)/PI360
     1/(TM*(1.-EXP(-S20/CES)))
      TMES(K,N,KK)=ATZ(K)*(TARS(K,N,KK)+TREF(K,N,KK))+TATM(K)
   90 EMIS(K,N,KK)=1.-TINT
      DO 15 N=1,2
      DO 14 L=1,2
   14 WRITE(6,5) (EMIS(K,N,L),K=1,9),(TARS(K,N,L),K=1,9)
     1,(TREF(K,N,L),K=1,9),(TMES(K,N,L),K=1,9)
    5 FORMAT(1H0,9(2XF11.4)//)
      EMIS(10,N,L)=0.0
      TREF(10,N,L)=1.0
   15 CONTINUE
      WRITE(43,20) (((EMIS(K,N,L),K=1,10),N=1,2),L=1,2)
     1,            (((TREF(K,N,L),K=1,10),N=1,2),L=1,2)
   20 FORMAT(10(F8.4))
       STOP
       END
```

```
$       FORTRAN NDECK
        SUBROUTINE SORT(E,Z1,Z2,SLOP,PI,CES,SEN,KX,KY)
        DIMENSION E(KY),CES(KY),SEN(KY)
        IF (SLOP.EQ.0.0) GO TO 20
        DO 17 I=1,KX
        X=E(I)
        ANG=Z1+(X+PI)*SLOP
        CES(I)=COS(ANG)
   17   SEN(I)=SIN(ANG)
   20   RETURN
        END

        SUBROUTINE COEFFS(A,P,E,PI,K,KX,FCTR1,KY)
        DIMENSION A(KY,KY),P(KY),E(KY)
        H=PI
        C=K-1
        DO 1 J=2,KX,2
        A(J,K)=-32.0
    1   A(J,K-1)=1000.0
        DO 2 J=3,KX,2
        A(J,K)=14.0
    2   A(J,K-1)=-64.0
        A(1,K)=7.0
        A(KX,K)=7.0
        A(1,K-1)=-32.0
        A(KX,K-1)=-32.0
        DO 11 I=1,KX
        DO 11 J=3,K,2
        L=K-J
        A(I,L+1)=2.0*A(I,K)
        IF (L.EQ.0) GO TO 11
        A(I,L)=A(I,K-1)
   11   CONTINUE
        FCTR1=4.0*H*H/(900.0*C*C)
        D=H/C
        E(1)=0.0
        P(1)=-H
        DO 5 I=2,K
        E(I)=E(I-1)+D
    5   P(I)=P(I-1)+D
        K1=K+1
        DO 6 I=K1,KX
    6   P(I)=P(I-1)+D
        J1=2
        DO 15 I=K1,KX
        DO 14 J=1,KX
   14   A(J,I)=A(J,J1)
        E(I)=-E(J1)
   15   J1=J1+1
        RETURN
        END
```

```
$       FORTRAN NDECK
      FUNCTION PINT(Q,SLOP,CTH2,STH2,CPH2,SPH2,C0,N,F2,A,KX,KY)
      DIMENSION A(KY,KY1),CTH2(KY1),STH2(KY1),CPH2(KY1),SPH2(KY1)
      COMMON PI,PI360,E1,E2,CES,SEN,EUI,E12,ES,EC,PE,QE,TM,S20
      Q=0.0
      PINT=0.0
      IF (SLOP.EQ.0.0) GO TO 20
      IF(C0.LT..016) TTT=1.754*BS(63.0)
      IF(C0.GE..016) TTT=1.754*BS(95.0)
      DR1=ES+2.*PE*CES+CES*CES
      DL1=ES+2.*EC*CES+CES*CES*E12
      DO 17 I=1,KX
      CT1=CTH2(I)
      TSKY=TM*(1.-EXP(-S20/CT1))
      ST1=STH2(I)
      V3=CES+CT1
      VP=2.*V3**2*C0
      VZ2=V3*V3
      DRS=ES+2.*PE*CT1+CT1*CT1
      DLS=ES+2.*EC*CT1+CT1*CT1*E12
      DO 17 M=1,KX
      SP1=SPH2(M)
      CP1=CPH2(M)
      V1=ST1*SP1
      V2=ST1*CP1-SEN
      VXY=V1*V1+V2*V2
      V4=ST1*CES*CP1+SEN*CT1
      R1=V4*V4+V1*V1
      U2=1.0+CES*CT1-SEN*ST1*CP1
      UU=U2*U2
      U=SQRT(U2/2.0)
      IF(N.EQ.3) GO TO 14
      RH2=1.-4.*PE*U/(ES+2.*PE*U+U*U)
      RV2=1.-4.*EC*U/(ES+2.*EC*U+U*U*E12)
      RH2=RH2*(1.-8.*U*TTT*FRCH(U))
      RV2=RV2*(1.-8.*U*TTT*FRCV(U))
   14 CONTINUE
      IF(N.EQ.1) FH2=(RH2*V4*V4+RV2*V1*V1)/R1
      IF(N.EQ.2) FH2=(RV2*V4*V4+RH2*V1*V1)/R1
      IF(N.EQ.3) FH2=1.0
      GAMA=4.*UU*    FH2*EXP(-VXY/VP)/(CES*VP*VZ2)
      SPS2=SP1*SP1
      CPS2=CP1*CP1
      QT=SEN**2-2.*SEN*ST1*CP1+ST1**2
      PMR=4.*TTT*EXP(-QT)*CES*CT1**2*EUI*4.
      IF(N.EQ.2) GO TO 15
      IF(N.EQ.3) GO TO 16
      GAMA=GAMA+PMR*(CPS2/DRS+SPS2*ES/DLS)/DR1
      GO TO 18
   15 VN1=(E1*SEN*ST1-CP1*(PE*PE-QE*Q))**2
      VN2=(2.*CP1*PE*QE-E2*SEN*ST1)**2
      GAMA=GAMA+PMR*((VN1+VN2)/DLS+SPS2*ES/DRS)/DL1
```

```
      GO TO 18
   16 CONTINUE
   18 CONTINUE
      PTINT=GAMA*ST1*F2*A(M,I)
      Q=Q+PTINT*TSKY
      PINT=PINT+PTINT
   17 CONTINUE
   20 RETURN
      END
$      FORTRAN NDECK
      FUNCTION BS(X)
      BS=4.05E-3*(1.247+0.0268*X+6.03E-5*X*X)**2
      RETURN
      END
$      FORTRAN NDECK
      FUNCTION FRCV(X)
      IF(X.GT.1.0 .OR.X.LT.1.E-8) FRCV=0.0
      IF(X.LE.1.0.AND.X.GT.0.5) FRCV=1./(8.57*X-4.4*X*X-2.243)
      IF(X.LE.0.5.AND.X.GT.0.173) FRCV=1./(0.8*X+2.81*X*X-0.14)
      IF(X.LE.0.173) FRCV=1./(11.1*X-55.3*X*X-0.184)
      RETURN
      END
$      FORTRAN NDECK
      FUNCTION FRCH(X)
      IF(X.GT.1.0.OR.X.LT.1.E-8) GO TO 1
      FRCH=0.2245*X**2.5+0.2944
      GO TO 2
    1 FRCH=0.0
    2 CONTINUE
      RETURN
      END
$      EXECUTE
$      LIMITS  10,20000,,10000
```

A-5. A computer program for computing two scale backscattering cross-section, $\sigma^{o}_{Dj}(\theta)$.

```
$       IDENT   2523,W3 WU SHIH TSENG
$       OPTION  FORTRAN,FRCNT/15/
$       FORTRAN NDECK
        DIMENSION CT(3),RMS(3),ARH(9,3),ARV(9,3),STGR(9,3),TCAH(9,3),
       1TCAV(9,3),ATH(9,3),ATV(9,3)
        DATA  (RMS(J),CT(J),J=1,3)/.10,.13,.12,.17,.15,.20/
        E1=48.3
        E2=34.9
        CALL REFCO(1.,Z1,Z2,Z3,Z4,Z5)
        RFS=1.-4.*Z4/Z2
        DO 2 K=1,9
        THEI=PI10*FLOAT(K-1)
        VN1=(E2*(2.-CS2))**2
        VN2=(E1*(2.-CS2)-1.+CS2)**2
        DO 2 M=1,3
        CMF=16.*CT(M)*CS4*EXP(-4.*(1.-CS2))*CT(M)
        G2=RMS(M)**2
        VCO=2.*G2*CS2
        STGR(K,M)=RFS/(VCO*CS2)*EXP(-(1.-CS2)/VCO)*(1.-4.*CT(M)**2)
    2   CONTINUE
        DO 4 J=1,3
        VN=RMS(J)/SQRT(2.)
        VD=SQRT(1.+RMS(J)**2)
        DO 4 K=1,9
        THEI=PI10*FLOAT(K-1)
        RH=0.0
        RV=0.0
        FA=1.0
        DO 12 I2=1,2
        CXP=(COS(THEI)+FA*SIN(THEI)*VN)/VD
        CS4=CS2*CS2
        COMF=8.*CT(J)**2*CS4*EXP(-4.*(1.-CS2))
        RH=RH+COMF*RH2
        RV=RV+COMF*(VN1+VN2)*E12/DRL2**2
   12   FA=-1.0
        ARH(K,J)=RH
        ARV(K,J)=RV
        ATH(K,J)=ARH(K,J)+STGR(K,J)
        ATV(K,J)=ARV(K,J)+STGR(K,J)
    4   CONTINUE
        WRITE(6,24) STGR,ATH,ATV,ARH,ARV,TCAH,TCAV
   24   FORMAT(9(2XF11.4)//)
$       EXECUTE
$       LIMITS  10,20000,,10000
$       ENDJOB
***EOF
```

A-6. A computer program for computing the clear sky and cloudy sky apparent temperatures.

```
$       IDENT   2523,W3,WU SHIH TSENG
$       OPTION  FORTRAN,FRCNT/15/
$       FORTRAN NOFCK
$       INCODE  IBMF
        DIMENSION EMIS(10,2,4),RFCO(10,2,4),TMES(10,2,4),C(100),
       1CBT(10),CTP(10),CLDM(10),AZ(300),TZ(300),Z(300),ATZ(10),TSKY(10),
       2 TATM(10),ATTN(10),CSPF(10)
        PI=ATAN(1.)*4.
        PII0=PI/18.
        FR=13.9
        TG=291.
        H=7.0
        PN=.23026
        AIC=-4.374*1.E-4
        BIC=-1.767*1.E-2
        READ(5,3) (((EMIS(K,N,KK),K=1,10),N=1,2),KK=1,4)
       1,          (((RFCO(K,N,KK),K=1,10),N=1,2),KK=1,4)
     3 FORMAT(10(F8.4))
        CALL ATMEF(TG,7.5,760.,13.9,H ,TATM,ATZ,S20,TSKY,AZ,TZ,Z)
        DO 90 K=1,10
        DO  90 N=1,2
        DO 90 KK=1,4
        TMES(K,N,KK)=ATZ(K)*(TG*EMIS(K,N,KK)+RFCO(K,N,KK)*TSKY(K))+TATM(K)
    90 CONTINUE
        WRITE(6,55) EMIS,RFCO,TMES
    55 FORMAT(10(2XE11.4)//)
        DO  8 M=1,10
        READ(5,123) CBT(M),CTP(M),CLDM(M),CSPF(M)
   123 FORMAT(4(F10.4))
        WRITE(6,18) CBT(M),CTP(M),CLDM(M),CSPF(M)
    18 FORMAT(1H0,4(10X,F10.4)//)
        KB=(CBT(M)+50.)/100.+1.0
        KT=(CTP(M)-50.)/100.+1.0
        CM=CLDM(M)
        IF (CM.LT.0.001) GO TO 16
        DO 11 I=KB,KT
        C(I)=0.0
        U=TZ(I)-273.
        IF((U+8.).LT.0.01) GO TO 27
        CK=PN*FR**1.95*EXP(-6.866*(1.+.0045*U))
        GO TO 26
    27 CK=PN*FR**1.006*EXP(-8.261*(1.+BIC*U+AIC*U*U))
    26 C(I)=CM*CK*CSPF(M)
        WRITE(6,7) S(I),TZ(I),C(I),AZ(I)
     7 FORMAT(10X,4(10X,E12.4))
        AZ(I)=AZ(I)+C(I)
    11 CONTINUE
    16 CONTINUE
C       THIS IS TO CALCULATE TRANSMITTANCE, TATM, TSKY
        JJ = 10.*H
```

```
      AT = 0.0
      DO 20 J=1,JJ
      AT = AT+0.1*AZ(J)
20    CONTINUE
      WRITE(6,603)
603   FORMAT(1H0,3X,7HDEGREES,08X,13HTRANSMITTANCE,10X,11HT/ATMOSPHER,
     115X,5HT/SKY/)
      DO 30 K=1,10
      THETA1=FLOAT(K-1)*PI10
      IF(K.EQ.10) THETA1=8.95*PI10
      CES=COS(THETA1)
      ATZ(K)=EXP(-1./CES*AT)
      ATTN(K)=10.*ALOG10(ATZ(K))
      S1 = 0.0
      DO 40 I=1,JJ
      S2 = 0.0
      DO 50 J=1,JJ
      S2 = S2+0.1*AZ(J)
50    CONTINUE
      S3=EXP(-1./CES*S2)
      S1=S1+0.1*S3*TZ(I)*AZ(I)
40    CONTINUE
      TATM(K)=1./CES*S1
      S4=0.0
      DO 70 I=1,300
      S5=0.0
      DO 80 IJ=1,I
      S5=S5+0.1*AZ(IJ)
   80 CONTINUE
      S6=EXP(-1./CES*S5)
      S4=S4+0.1*S6*TZ(I)*AZ(I)
   70 CONTINUE
      TSKY(K)=1./CES*S4
      K3=(K-1)*10
      WRITE(6,4) K3,ATZ(K),TATM(K),TSKY(K) ,ATTN(K)
    4 FORMAT(5X,I5,4(5X,E16.8)/)
30    CONTINUE
      DO 15 I=KB,KT
      AZ(I)=AZ(I)-C(I)
   15 CONTINUE
C     THIS IS TO CALCULATE EMIS,TREF,TMES
      WRITE(6,605)
605   FORMAT(1H0,16X,7HDEGREES,12X,11HEMMISSIVITY,13X,11HT/REFLECTED
     1,15X,10HT/MEASURED /)
      DO 44 K=1,10
      DO 44 N=1,2
      DO 44 KK=1,4
      TMES(K,N,KK)=ATZ(K)*(TG*EMIS(K,N,KK)+RFCO(K,N,KK)*TSKY(K))+TATM(K)
   44 CONTINUE
      WRITE(6,56) TMES
   56 FORMAT(10(2XF6.2)//)
    8 CONTINUE
      STOP
      END
```

```
$       FORTRAN NOFCK
$       INCODE  IBMF
        SUBROUTINE ATMEF(TG,DNG,PG,FR,H,TATM,ATZ,S20,TSKY,AZ,TZ,Z)
        DIMENSION AZ(300),TZ(300),Z(300) ,TATM(10),ATZ(10),TSKY(10),
       1TTSUP(10)
        REAL LWO,LWW,LWOS,LWWS
          DATA PSEA,TSEA,DNSEA,CK22,CK60,CK118,CKRES,F22,F60,F118/760.,
       1 290.,1.,32.4,362.6,5.23,2.55E-3,22.235,60.,118.75/
        PI10=ATAN(1.)/4.5
        JJ=10.*H
        TM=1.12*TG-50.
        FRS=FR*FR
        SM22 = (ABS(FR-F22))**2
        SP22 = (FR+F22)**2
        SM60 = (ABS(FR-F60))**2
        SP60 = (FR+F60)**2
        SM118 = (ABS(FR-F118))**2
        SP118 = (FR+F118) **2
        S20 = 0.0
        WRITE (6,12)
     12 FORMAT (1HI,28HATTEN. COEF. H NEPER POR KM ,//)
        DO 10 I=1,300
        XI = I
        Z(I) =(100.*XI-50.)*1.E-3
        IF (I.GT.109) GO TO 23
        TZ(I) = TG-71.*Z(I)/11.
        GO TO 24
     23 TZ(I) =217.
     24 CONTINUE
        DNZ=DNG*EXP(-Z(I)/2.205)
        PZ = PG*EXP(-0.143*Z(I))
        PA=1013.25*PZ*1./760.
        LWO = 1.5*((TSEA/TZ(I))**0.5)*PZ/PSEA
        LWW=2.58E-3*(1.+.0147*DNZ*TZ(I)/PA)*PA*((318./TZ(I))**.625)
        GO = 0.21*PZ*LWO*FRS/(TZ(I)*TZ(I)*TZ(I))
        GW=1.*EXP(-644./TZ(I))*FRS*PA*DNZ*(1.+.0147*DNZ*TZ(I)/PA)/(TZ(I)
       1  **3.125)
        LWWS = LWW*LWW
        LWOS = LWO*LWO
        A22 = CK22*GW*(1./(SM22+LWWS)+1./(SP22+LWWS))
        A60 = CK60*GO*(1./(SM60+LWOS)+1.0/(SP60+LWOS)+1.0/(FRS+LWOS))
        A118 = CK118*GO*(1.0/(SM118+LWOS)+1.0/(SP118+LWOS))
        ARES=CKRES*DNZ*FRS*LWW/(TZ(I)**1.5)
        AZ(I)=      A22+A60+A118+ARES
        S20=S20+AZ(I)*.1
        IF(I.EQ.JJ) AT=S20
        WRITE (6,11) TZ(I),AZ(I),Z(I),S20
     10 CONTINUE
        WRITE(6,11) H,AT,S20,TM
     11 FORMAT (1H0,4(10XE11.4)/)
        WRITE(6,13)
     13 FORMAT(1H0,32HTRANS. TATM. TSKY VERSUS ANGLES ,)
```

```
      DO 30 K=1,10
      THE=FLOAT(K-1)*PI10
      IF(K.EQ.10) THE=8.95*PI10
      SEC=1./COS(THE)
      TSKY(K)=TM*(1.-EXP(-SEC*S20))
      ATZ(K)=EXP(-AT*SEC)
      S1=0.0
      DO 40 I=1,JJ
      S2=0.0
      DO 50 J=I,JJ
   50 S2=S2+.1*AZ(J)
   40 S1=S1+.1*TZ(I)*AZ(I)*EXP(-S2*SEC)
      TATM(K)=SEC*S1
      S3=0.0
      DO 60 I=JJ,300
      S4=0.0
      DO 70 J=JJ,I
   70 S4=S4+.1*AZ(J)
   60 S3=S3+.1*TZ(I)*AZ(I)*EXP(-S4*SEC)
      TSUP(K)=SEC*S3
      K3=(K-1)*10
   30 WRITE(6,14) K3,ATZ(K),TATM(K),TSKY(K),TSUP(K)
   14 FORMAT(5X,I5,4(10XE11.4)//)
      RETURN
      END

$      EXECUTE
$      LIMITS  10,20000,,10000
```

A-7. A computer program for computing the apparent temperatures of light to moderate rain.

```
$       IDENT   2523,W3,STEVE WU
$       OPTION  FORTRAN,ERCNT/15/
$       FORTRAN NDECK
$       INCODE  IBMF
        REAL LWO,LWW,LWOS,LWWS,LWV,LWVS,LAM
      DIMENSION C(300),H(10),RFCO(10,2,4),EMIS(10,2,4),TMES(10,2,4),
     1R(300),ATTN(10),FQ(10),Z(300),AZ(300),F(7),TZ(300),ATZ(10),
     2TATM(10),TSKY(10)
      COMMON F
       NAMELIST /LIST1/ TG,DNG,PG
         DATA PSEA,TSEA,DNSEA,CK22,CK60,CK118,CKRES,F22,F60,F118/760.,
     1 291.,1.,32.4,362.6,5.23,2.55E-3,22.235,60.,118.75/
      CK183=8.6E-3
      F183=183.3
      PN=.23026
      AIC=-4.374*1.E-4
      BIC=-1.767*1.E-2
      A890=.008
      A111=.0125
      A139=.026
      B890=1.32
      B111=1.26
      B139=1.18
       PI = ATAN(1.)*4.
      PI10=PI/18.0
      E1=58.6
      E2=36.6
      READ(5,13) (((EMIS(I,J,K),I=1,10),J=1,2),K=1,4)
     1,          (((RFCO(I,J,K),I=1,10),J=1,2),K=1,4)
   13 FORMAT(10(F8.4))
       READ(5,LIST1)
       WRITE(6,LIST1)
    1  FORMAT(3E16.8)
      READ(5,102) (H(J),J=1,3)
  102 FORMAT(3F10.4)
      READ(5,59) NF,NM
   59 FORMAT(2I5)
      READ (5,239) (FQ(J),J=1,NF)
  239 FORMAT (10F8.2)
      DO 8 L=1,1
      WRITE(6,4) L,FQ(L)
    4 FORMAT(1H0,3X,13HFREQUENCY FQ(,I1,2H)=,F8.4,3HGHZ//)
      FR=FQ(L)
C      THIS IS TO CALCULATE THE SKY ABSORPTION COEFF.
       FRS = FR*FR
       S20 = 0.0
       DO 10 I=1,300
       XI = I
       Z(I) =(100.*XI-50.)*1.E-3
       IF (I.GT.150) GO TO 23
```

```
      TZ(I)=TSEA-71.*Z(I)/11.
      IF (TZ(I).LT.217.) TZ(I)=217.
      GO TO 24
   23 TZ(I) =217.
   24 CONTINUE
      DNZ=DNG*EXP(-Z(I)/2.2)
      PZ = PG*EXP(-0.143*Z(I))
      PA=1013.25*PZ*1./760.
      LWO = 1.5*((TSEA/TZ(I))**0.5)*PZ/PSEA
     LWW=2.58E-3*(1.+.0147*DNZ*TZ(I)/PA)*PA*((318./TZ(I))**.625)
     LWV=3.0*(PZ/760.)*(290./TZ(I))**0.5
     GV=DNZ*FRS*LWV*((290./TZ(I))**2)/3.0
      GO = 0.21*PZ*LWO*FRS/(TZ(I)*TZ(I)*TZ(I))
      GW=1.*EXP(-644./TZ(I))*FRS*PA*DNZ*(1.+.0147*DNZ*TZ(I)/PA)/(TZ(I)
     1  **3.125)
      LWWS = LWW*LWW
      LWOS = LWO*LWO
     LWVS=LWV*LWV
      SM22 = (ABS(FR-F22))**2
      SP22 = (FR+F22)**2
      SM60 = (ABS(FR-F60))**2
      SP60 = (FR+F60)**2
      SM118 = (ABS(FR-F118))**2
      SP118 = (FR+F118) **2
      SM183 = (ABS(FR-F183))**2
      SP183 = (FR+F183) **2
      A22 = CK22*GW*(1./(SM22+LWWS)+1./(SP22+LWWS))
      A60 = CK60*GO*(1./(SM60+LWOS)+1.0/(SP60+LWOS)+1.0/(FRS+LWOS))
      A118 = CK118*GO*(1.0/(SM118+LWOS)+1.0/(SP118+LWOS))
      A183 = CK183*GV*(1.0/(SM183+LWVS)+1.0/(SP183+LWVS))
      ARES=CKRES*DNZ*FRS*LWW/(TZ(I)**1.5)
      AZ(I)= A183+A22+A60+A118+ARES
10    CONTINUE
      DO  8 M=1,NM
      READ(5,17) F,CM
   17 FORMAT(8F10.6)
      KR=60
      KR=5
      KT=70
      DO 91 I=1,KR
      ZU=Z(I)
      IF (FR.EQ.13.9)  R(I)=PN*A139*P( ZU)**B139
      IF (FR.EQ. 8.9)  R(I)=PN*A890*P( ZU)**B890
      IF (FR.EQ.11.1)  R(I)=PN*A111*P( ZU)**B111
   91 CONTINUE
      DO 11 I=KR,KT
      U=TZ(I)-273.
      IF((U+8.).LT.0.01) GO TO 27
      CK=PN*FR**1.95*EXP(-6.866*(1.+.0045*U))
      GO TO 26
   27 CK=PN*FR**1.006*EXP(-8.761*(1.+BIC*U+AIC*U*U))
   26 C(I)=CM*CK
```

```
   11 CONTINUE
      DO 16 I=1,KT
      WRITE(6,2) Z(I),TZ(I),R(I),C(I),AZ(I)
    2 FORMAT(10X,5(10X,E12.4))
   16 AZ(I)=AZ(I)+R(I)+C(I)
C      THIS IS TO CALCULATE TRANSMITTANCE, TATM, TSKY
      DO 101 IH=1,1
      H=H(IH)
       JJ = 10.*H
       AT = 0.0
       DO 20 J=1,JJ
       AT = AT+0.1*AZ(J)
20     CONTINUE
       WRITE(6,603)
603    FORMAT(1H0,3X,7HDEGREES,08X,13HTRANSMITTANCE,10X,11HT/ATMOSPHER,
     115X,5HT/SKY/)
      DO 30 K=1,10
      THETA1=FLOAT(K-1)*PI10
      IF(K.EQ.10)  THETA1=8.95*PI10
      CES=COS(THETA1)
      ATZ(K)=EXP(-1./CES*AT)
      ATTN(K)=10.*ALOG10(ATZ(K))
       S1 = 0.0
       DO 40 I=1,JJ
       S2 = 0.0
       DO 50 J=I,JJ
       S2 = S2+0.1*AZ(J)
50     CONTINUE
      S3=EXP(-1./CES*S2)
       S1=S1+0.1*S3*TZ(I)*AZ(I)
40     CONTINUE
      TATM(K)=1./CES*S1
      S4=0.0
      DO 70 I=1,300
      S5=0.0
      DO 80 IJ=1,I
      S5=S5+0.1*AZ(IJ)
   80 CONTINUE
      S6=EXP(-1./CES*S5)
      S4=S4+0.1*S6*TZ(I)*AZ(I)
   70 CONTINUE
      TSKY(K)=1./CES*S4
      K3=(K-1)*10
      WRITE(6,3) K3,ATZ(K),TATM(K),TSKY(K) ,ATTN(K)
3      FORMAT(5X,I5,4(5X,E16.8)/)
30     CONTINUE
C     THIS IS TO CALCULATE EMIS,TREF,TMES
      WRITE(6,605)
605    FORMAT(1H0,16X,7HDEGREES,12X,11HEMMISSIVITY,13X,11HT/REFLECTED
     1,15X,10HT/MEASURED /)
      DO 44 K=1,10
      DO 44 N=1,2
```

```
      DO 44 KK=1,4
      TMES(K,N,KK)=ATZ(K)*(EMIS(K,N,KK)*TG+RFCO(K,N,KK)* TSKY(K))+
     1TATM(K)
   44 CONTINUE
      WRITE(6,71) TMES
   71 FORMAT(10(5XF6.2)//)
  101 CONTINUE
      DO 93 I=1,KR
      AZ(I)=AZ(I)-R(I)
      R(I)=0.0
   93 CONTINUE
      DO 15 I=KR,KT
      AZ(I)=AZ(I)-C(I)
      C(I)=0.0
   15 CONTINUE
    8 CONTINUE
      STOP
      END
$      FORTRAN NDECK
$      INCODE  IBMF
      FUNCTION P( ZU)
      COMMON F
      DIMENSION F(7),D(7,7)
      I=1
      DO 21 J=1,6
   21 D(I,J)=F(J+1)-F(J)
      DO 22 I=2,6
      NI=7-I
      DO 22 J=1,NI
   22 D(I,J)=D(I-1,J+1)-D(I-1,J)
      C=ZU
      P=F(1)+  D(1,1)*ZU
      DO 26 I=2,6
      C=C*(ZU-FLOAT(I-1))/FLOAT(I)
   26 P=P+C*D(I,1)
      RETURN
      END
$      EXECUTE
$      LIMITS  10,20000,,10000
$      INCODE  IBMF
```

A-8. A computer program for computing the scattering characteristics of rain.

```
$       IDENT   2523, WU SHIH-TSENG
$       OPTION  FORTRAN,FRCNT/15/
$       FORTRAN NDECK
C       THE PROGRAM IS DESIGNED  TO CALCULATE THE SCAT.CHARAT. OF PRECIPITA
        REAL LAM
        DIMENSION AMX(100),BMX(100), SX(301),SS(301),SH(301,19),SP(301)
        DIMENSION FQ(10),TR(10),PR(10)
        DIMENSION ANX(100),BNX(100)
        COMPLEX ANX,BNX
        COMPLEX R,RI,AMX,BMX
        PI = ATAN(1.)*4.
        WRITE(6,111)
  111   FORMAT(1HI,50HTHE SCATTERING CHARACTERISTICS OF PRECIPITATIONS  ,)
        READ(5,11) NI,ND,DX
   11   FORMAT(2I5,F10.4)
        IF(DX.LE.0.0) GO TO 41
        NL=5*NI
        NA=NL*ND+1
        WRITE(6,12) DX,NI,ND,NA
   12   FORMAT(1H0,20HBASIC INTERVAL    DX=,F10.4,//1X,
       1 20HINTEGRATED TIMES NI=,I3,//1X,20HCHANGE OF INTRVL ND=,I2,//1X,
       2 20HTOTAL INT. PTS    NA=,I5,//)
        READ(5,21) NF,NT,NP,NK
   21   FORMAT(4I5)
        READ(5,22) (FQ(J),J=1,NF)
        READ(5,22) (TR(J),J=1,NT)
        READ(5,22) (PR(J),J=1,NP)
   22   FORMAT(10F8.4)
        DO 8 I1=1,NF
        FR=FQ(I1)
        LAM=30./FR
        DK=2.*PI/LAM
        DPK=.08*PI/DK**3*2.0
        DO 8 I2=1,NT
        TW=TR(I2)
        RI=R(TW,LAM)
        DO 8 I3=1,NP
        P=PR(I3)
        WRITE(6,1) P,TW,FR
    1   FORMAT(1H0,3H P=,F10.4,10X,3HTW=,F10.4,10X,3HFR=,F10.4)
        DP=82.0/(DK*P**.21)
        L=1
        X=0.0
        DXX=0.0
        DO 16 LL=1,ND
        DXX=DXX+DX
        DO 16 NN=1,NL
        L=L+1
        X=X+DXX
        EXA=2.*DPK*EXP(-DP*X)*DXX
```

```
      CALL COEFABI(X,RI,AMX,BMX,SMX,SMS,N)
      IF(SMX) 41,74,74
   74 CONTINUE
      IF(SMS) 41,24,24
   24 SX(L)=SMX*EXA
      SS(L)=SMS*EXA
      IF (NK.EQ.0) GO TO 31
      DO 26 K=1,NK
      THE=PI/18.*FLOAT(K-1)
        CALL      COEFPT(N,AMX,BMX,THE,PI,SPT,STP)
      IF(SPT) 41,75,75
   75 CONTINUE
      IF(STP) 41,25,25
   25 SH(L,K)=(SPT+STP)*EXA
   26 CONTINUE
   31 CONTINUE
   16 CONTINUE
      S1=S(ND,NI,DP,SX,NA)
      S2=S(ND,NI,DP,SS,NA)
      S4=S2/S1
      WRITE(6,15) S1,S2,S4
   15 FORMAT(1H0,20HEXTINCT. COEF  BEX= ,E16.8//1X,
     1 20HSCATTERING COEF BSC=,E16.8//1X,20HALBEDO OF  SCAT.  W=,F10.4/)
      IF (NK.EQ.0) GO TO 32
      WRITE(6,66)
   66 FORMAT(10X,15HSCAT. ANGLES    ,5X,10HMAGNITUDE ,//)
      DO 17 K=1,NK
      BET=FLOAT(K-1)*10.
      DO 18 LN=2,NA
      SP(LN)=SH(LN,K)
   18 CONTINUE
      S3=S(ND,NI,DP,SP,NA)/S2
      WRITE(6,14) BET,S3
   14 FORMAT(2(10XF10.4)//)
   17 CONTINUE
   32 CONTINUE
    8 CONTINUE
      GO TO 43
   41 WRITE(6,42)
   42 FORMAT(1H0,38HINCORRECT  INPUT OR CALCULATED RESULTS ,)
   43 STOP
      END
$     FORTRAN NDECK
C     THE FUNCTION INTEGRATES  SCAT.CHARACT. BY COMPOSITE RULES
      FUNCTION S(ND,NI,DP,PZ,NA)
      DIMENSION F(6),PZ(NA)
      J=1
      S=0.0
      CHA=1.0
      F(6)=0.0
      DO 17 LL=1,ND
      DO 23 II=1,NI
      F(1)=F(6)
      DO 16 L=2,6
```

```
      J=J+1
   16 F(L)=PZ(J)
   23 S=S+(19.*(F(1)+F(6))+75.*(F(2)+F(5))+50.*(F(3)+F(4)))*5./288.
      ABC=FLOAT(LL+1)/FLOAT(LL)
      CBA=CBA/ABC
   17 F(6)=ABC*F(6)
      S=S+F(6)*CBA/DP
      RETURN
      END
$      FORTRAN NDECK
C     THE SUBROUTINE CALCULATES  THE MIE,EXTINCT.AND SCAT. COEF
      SUBROUTINE COEFAB(X,RI,AMX,BMX,SMX,SMS,N)
      COMPLEX  Y, RI,AY,AY0,WXN1,WX0,WX,AAX,BAX,AMX,BMX,CAX,BDX
      DIMENSION AY(100),WX(100),AMX(100),BMX(100)
      Y=X*RI
      YR=REAL(Y)
      YI=-AIMAG(Y)
      YN1=SIN(YR)*COS(YR)
      YL=2.*YI
      YN2=(EXP(YL)-EXP(-YL))*.25
      YD=SIN(YR)*SIN(YR)-0.5+0.25*( EXP(YL)+EXP(-YL))
      AY0=(YN1+(0.,1.)*YN2)/YD
      AY(1)=-1./Y+1./(1./Y-AY0)
      WX0=SIN(X)+(0.,1.)*COS(X)
      WXN1=COS(X)-(0.,1.)*SIN(X)
      WX(1)=WX0/X-WXN1
      WX( 2)=3.*WX(1)/X-WX0
      CAX=AY(1)/RI+1./X
      BDX=RI*AY(1)+1./X
      AMX(1)=(CAX*REAL(WX(1))-REAL(WX0))/(CAX*WX(1)-WX0)
      BMX(1)=(BDX*REAL(WX(1))-REAL(WX0))/(BDX*WX(1)-WX0)
      ACR=1.0E-06*CABS(AMX(1))
      BCR=1.0E-06*CABS(BMX(1))
      IF(ACR.LT.1.0E-06) ACR=1.0E-06
      IF(BCR.LT.1.0E-06) BCR=1.0E-06
      SMX=0.0
      SMS=0.0
      DO  3 I=1,50
      IF (I.EQ.1) GO TO 9
      IF (I.EQ.2) GO TO 2
      AI=2*I-1
      WX(I)=AI*WX(I-1)/X-WX(I-2)
    2 AI=I
      AY(I)= -AI/Y+1./(AI/Y-AY(I-1))
      AAX=AY(I)/RI+AI/X
      BAX=RI*AY(I)+AI/X
      AMX(I)=(AAX*REAL(WX(I))-REAL(WX(I-1)))/(AAX*WX(I)-WX(I-1))
      BMX(I)=(BAX*REAL(WX(I))-REAL(WX(I-1)))/(BAX*WX(I)-WX(I-1))
      IF(REAL(AMX(I)+BMX(I)).LE.1.E-10) GO TO 6
    9 CONTINUE
      AI=2*I+1
      SMX=SMX+AI*REAL( AMX(I)+BMX(I))
      SMS=SMS+AI*(CABS(AMX(I))**2+CABS(BMX(I))**2)
      AMA=CABS(AMX(I))
      BMA=CABS(BMX(I))
      IF(AMA.LE.ACR.AND.BMA.LE.BCR) GO TO 6
    3 CONTINUE
      -
```

```
      END
$      FORTRAN NDECK
C     THE SUBROUTINE CALCULATES  THE CHARAC.CURVES OF SCAT.VS.ANGLES
      SUBROUTINE COEFPT(N,AMX,BMX,THE,PI,SPT,STP)
      COMPLEX AMX,BMX,CPT,CTP
      DIMENSION AMX(100),BMX(100),CPT(100),CTP(100) ,PHI(100),TAU(100)
      PHI(1)=1.0
      PHI(2)=3.0*COS(THE)
      TAU(1)=COS(THE)
      TAU(2)=3.0*COS(2.*THE)
      SN2=SIN(THE)*SIN(THE)
      CPT=(0.0,0.0)
      CTP=(0.0,0.0)
      DO 3 I=1,N
      IF (I.LE.2) GO TO 9
      AI=2*I-1
      BI=I-1
      PHI(I)=(TAU(1)*AI*PHI(I-1)-PHI(I-2))/BI
      TAU(I)=TAU(1)*(PHI(I)-PHI(I-2))-AI*SN2*PHI(I-1)*TAU(I-2)
    9 CONTINUE
      CI=FLOAT(2*I+1)/FLOAT(I*(I+1))
      CPT=CPT+CI*(AMX(I)*PHI(I)+BMX(I)*TAU(I))
      CTP=CTP+CI*(AMX(I)*TAU(I)+BMX(I)*PHI(I))
    3 CONTINUE
      SPT=CABS(CPT)*CABS(CPT)/(4.*PI)
      STP=CABS(CTP)*CABS(CTP)/(4.*PI)
      RETURN
      END
$      FORTRAN NDECK
C     THE FUNCTION CALCULATES THE INDEX OF REFRACTION OF WATER
      FUNCTION R(TR,RAM)
      COMPLEX  E,R
      REAL    RAM,E0,EINF,DLAM
      EINF = 5.5
      DT=TR-273.
      E0 = 87.74-0.4008*DT+9.398*1.E-4*DT*DT+1.41*1.E-6*DT*DT*DT
      DLAM=3.33-0.1122*DT+1.8*1.E-3*DT*DT-8.3*1.E-6*DT*DT*DT
      E=(E0-EINF)*(1.,0.)/((1.,0.)+(0.,1.)*(DLAM/RAM))+EINF
      R=CSQRT(E)
      RETURN
      END
$      EXECUTE
$      LIMITS  10,20000,,10000
```

A-9. A computer program for computing the apparent temperature of heavy rain.

```
$       IDENT   2526,WU,SHIH
$       OPTION  FORTRAN,FRONT/15/
$       FORTRAN NDECK
        DIMENSION A(5,5),B(5,5),C(5,5),Q(5,5),P(5,1),CQ(5,5),BQ(5,5),
       1CA(5,5),BC(5,5),RA(5,5),RB(5,5),X(5),Y(5),L(5),M(5),Z(5,30),
       2RD(5,5),RE(5,5),RF(5,5),PC(5,1),RC(5,5),CC(5,5),CR(5,5),CB(5,5),
       3PP(5,1),CP(5,1),FP(5,1),DD(5,1),QL(5,5,30),PHLO(5),  GL(5,5,30),
       4DL(5,30),PL(5,30),PHP(5,30),PHPO(5),PLO(5),QLO(5,5),PHL(5,30),
       5          F(5,1),BP(5,1),FB(5,1),CP(5,1),FC(5,1),PA(5,1),PB(5,1)
        COMMON U(5),W(5)
        READ(5,51) U,W
   51   FORMAT(5F10.8)
        WRITE(6,1) U,W
    1   FORMAT(5(5XF16.8)//)
        DO 13 LL=1,2
        READ(5,5) ABD,P0,P1,P2,TAU,TW,TG
    5   FORMAT(7F10.5)
        WRITE(6,5) ABD,P0,P1,P2,TAU,TW,TG
        CALL ABCF(ABD,P0,P1,P2,TAU,TW,A,B,C,F,I)
        WRITE(6,1) A,B,C,F
        DO 13 IL=1,4
        READ(5,52) Q,P
   52   FORMAT(5F10.5)
        WRITE(6,1) Q,P
        DO 11 I=1,5
        P(I,1)=P(I,1)*TG
        PLO(I)  =P(I,1)
        DO 11 J=1,5
        QLO(I,J)=Q(I,J)
   11   CONTINUE
        IJ=1
    2   CALL  MPRD(B,Q,BQ,5,5,5)
        CALL  MADD(BQ,C,BC,5,5)
        CALL  MPRD(C,Q,CQ,5,5,5)
        CALL  MADD(CQ,A,CA,5,5)
        CALL MINV(CA,5,D,L,M)
        CALL  MPRD(BC,CA,RA,5,5,5)
        CALL  MPRD(RA, B,RB,5,5,5)
        CALL MSUB(RB, C,RC,5,5)
        CALL MPRD(RA,C,RD,5,5,5)
        CALL MSUB( A,RD,RE,5,5)
        CALL MINV(RE,5,D,L,M)
        CALL MPRD(RE,RC,RF,5,5,5)
        CALL MPRD(B,P,BP,5,5,1)
        CALL MSUB(F,BP,FB,5,1)
        CALL MPRD(C,P,CP,5,5,1)
        CALL MSUB(F,CP,FC,5,1)
        CALL MPRD(RA,FC,PA,5,5,1)
        CALL MSUB(FB,PA,PB,5,1)
        CALL MPRD(RE,PB,PC,5,5,1)
        CALL MPRD( C,RF,CR,5,5,5)
        CALL MADD(CR, B,CB,5,5)
```

```
      CALL MPRD(CA,CR,CC,5,5,5)
      CALL MADD(PC, P,PP,5,1)
      CALL MPRD( C,PP,CT,5,5,1)
      CALL MSUB( F,CT,FP,5,1)
      CALL MPRD(CA,FP,DD,5,5,1)
      DO 4 I=1,5
      DL(I,  IJ)=DD(I,1)
      PL(I,  IJ)=PC(I,1)

      DO 9 J=1,5
      QL(I,J,IJ)=RF(I,J)
      GL(I,J,IJ)=CC(I,J)*(-1.)
      Q(I,J)=RF(I,J)
    9 CONTINUE
      P(I,1)=PC(I,1)
    4 CONTINUE
      IJ=IJ+1
      IF(IJ-30) 2,2,3
    3 CONTINUE
      DO 6 I=1,5
      PHL(I,  30)=0.0
      DO 7 JJ=1,30
      K=31-JJ
      IF(K.EQ.1) GO TO 12
      Z(I,K)=0.0
      DO 31 J=1,5
   31 Z(I,K)=Z(I,K)+GL(I,J,K)*PHL(J,K)
      PHL(I,K-1)=Z(I,K)+DL(I,K)
   12 CONTINUE
      Z(I,K)=0.0
      DO 32 J=1,5
   32 Z(I,K)=Z(I,K)+QL(I,J,K)*PHL(J,K)
      PHP(I,K)=Z(I,K)+PL(I,K)
    7 CONTINUE
      X(I)=0.0
      DO 33 J=1,5
   33 X(I)=X(I)+GL(I,J,1)*PHL(J,1)
      PHLO(I)=X(I)+DL(I,1)
      Y(I)=0.0
      DO 34 J=1,5
   34 Y(I)=Y(I)+QLO(I,J)*PHLO(J)
      PHPO(I)=Y(I)+PLO(I)
    6 CONTINUE
      WRITE(6,1) PHPO,PHP,PHLO    ,PHL
   13 CONTINUE
      STOP
      END
       FORTRAN NDECK
      SUBROUTINE ABCF(ABD,P0,P1,P2,TAU,TW,A,B,C,F,K)
       DIMENSION A(5,5),B(5,5),C(5,5),F(5,1)
      COMMON U(5),W(5)
      DO 2 I=1,5
      IF(K.GE.2) TW=0.0
      F(I,1)=(1.-ABD)*TW
      DO 2 J=1,5
      COF=-.5*ABD*W(J)
      GO TO (1),22,33),K
```

```
   11 PI=.5*(3.*U(I)*U(I)-1.)
      PJ=.5*(3.*U(J)*U(J)-1.)
      A(I,J)=          COF*(P0+P1*U(I)*U(J)+P2*PI*PJ)
      B(I,J)=          COF*(P0+P1*U(I)*U(J)+P2*PI*PJ)
      C(I,J)=          COF*(P0-P1*U(I)*U(J)+P2*PI*PJ)
      GO TO 44
   22 PI1=SQRT(1.-U(I)*U(I))
      PJ1=SQRT(1.-U(J)*U(J))
      PI2=3.*U(I)*PI1
      PJ2=3.*U(J)*PJ1
      A(I,J)=COF*(P1*PI1*PJ1+P2/3.*PI2*PJ2)
      B(I,J)=COF*(P1*PI1*PJ1+P2/3.*PI2*PJ2)
      C(I,J)=COF*(P1*PI1*PJ1-P2/3.*PI2*PJ2)
      GO TO 44
   33 PI3=3.*(1.-U(I)*U(I))
      PJ3=3.*(1.-U(J)*U(J))
      A(I,J)=P2/12.*PI3*PJ3*COF
      B(I,J)=P2/12.*PI3*PJ3*COF
      C(I,J)=P2/12.*PI3*PJ3*COF
   44 CONTINUE
      IF(J.EQ.I) GO TO 3
      GO TO 2
    3 CONTINUE
      A(I,J)=.5+U(J)/TAU+A(I,J)
      B(I,J)=.5-U(J)/TAU+B(I,J)
    2 CONTINUE
      RETURN
      END

      SUBROUTINE MSUB(A,B,R,N,M)
      DIMENSION A(N,M),B(N,M),R(N,M)
      DO 1 I=1,N
      DO 1 J=1,M
    1 R(I,J)=A(I,J)-B(I,J)
      RETURN
      END

      SUBROUTINE MADD(A,B,R,N,M)
      DIMENSION A(N,M),B(N,M),R(N,M)
      DO 1 I=1,N
      DO 1 J=1,M
    1 R(I,J)=A(I,J)+B(I,J)
      RETURN
      END

      SUBROUTINE MPRD(A,B,R,N,M,L)
      DIMENSION A(N,M),B(M,L),R(N,L)
      DO 1 I=1,N
      DO 1 K=1,L
      R(I,K)=0.0
      DO 1 J=1,M
    1 R(I,K)=R(I,K)+A(I,J)*B(J,K)
      RETURN
      END
$     EXECUTE
$     LIMITS  10,30000,,10000
```

NATIONAL AERONAUTICS AND SPACE ADMINISTRATION
WASHINGTON, D.C. 20546

OFFICIAL BUSINESS
PENALTY FOR PRIVATE USE $300

SPECIAL FOURTH-CLASS RATE BOOK

POSTAGE AND FEES PAID
NATIONAL AERONAUTICS AND SPACE ADMINISTRATION
451

U.S. MAIL

POSTMASTER: If Undeliverable (Section 158 Postal Manual) Do Not Return

"The aeronautical and space activities of the United States shall be conducted so as to contribute . . . to the expansion of human knowledge of phenomena in the atmosphere and space. The Administration shall provide for the widest practicable and appropriate dissemination of information concerning its activities and the results thereof."

—NATIONAL AERONAUTICS AND SPACE ACT OF 1958

NASA SCIENTIFIC AND TECHNICAL PUBLICATIONS

TECHNICAL REPORTS: Scientific and technical information considered important, complete, and a lasting contribution to existing knowledge.

TECHNICAL NOTES: Information less broad in scope but nevertheless of importance as a contribution to existing knowledge.

TECHNICAL MEMORANDUMS: Information receiving limited distribution because of preliminary data, security classification, or other reasons. Also includes conference proceedings with either limited or unlimited distribution.

CONTRACTOR REPORTS: Scientific and technical information generated under a NASA contract or grant and considered an important contribution to existing knowledge.

TECHNICAL TRANSLATIONS: Information published in a foreign language considered to merit NASA distribution in English.

SPECIAL PUBLICATIONS: Information derived from or of value to NASA activities. Publications include final reports of major projects, monographs, data compilations, handbooks, sourcebooks, and special bibliographies.

TECHNOLOGY UTILIZATION PUBLICATIONS: Information on technology used by NASA that may be of particular interest in commercial and other non-aerospace applications. Publications include Tech Briefs, Technology Utilization Reports and Technology Surveys.

Details on the availability of these publications may be obtained from:

SCIENTIFIC AND TECHNICAL INFORMATION OFFICE

NATIONAL AERONAUTICS AND SPACE ADMINISTRATION

Washington, D.C. 20546